PMU-BASED STATE ESTIMATION FOR REAL-TIME MONITORING OF ACTIVE DISTRIBUTION SYSTEMS

by

Krit Kongurai

A thesis submitted in partial fulfillment
of the requirements for the degree of

Master of Science
in
Electrical Engineering

at the Delft University of Technology,
to be defended publicly on December 8, 2021 at 13:00

Student number:	5123658		
Thesis committee:	Dr.ir. M. (Marjan) Popov,	TU Delft,	Committee Chair
	Dr.ir. M. (Milos) Cvetkovic,	TU Delft,	Committee Member
	Ir. N.K. (Nidarshan) Veera Kumar,	TU Delft,	Committee Member
	Dr.ir. M. (Mohamad) Ghaffarian Niasar,	TU Delft,	External Member

This thesis is confidential and cannot be made public until June 30, 2023.

TU Delft Delft University of Technology

ACKNOWLEDGEMENTS

Firstly, I would like to sincerely thank my supervisor, Prof. Marjan Popov, for providing invaluable support, trust, and patience and for giving me the golden opportunity to do this project. Secondly, I cannot express enough thanks to Nidarshan Veera Kumar, my daily supervisor, for his continued support and positive encouragement since the first day we met. I would not achieve this thesis without their supports.

In addition, I would like to express my special gratitude to Dr. Dragan Cetenovic from the University of Manchester for his exceptional guidance and feedback. I have learned so much about state estimation and how to tailor the idea and the way of thinking in the academic field.

My sincere thanks also go to Prof. Somsak Panyakeow, Prof. Somboon Sangwongwanich, and Dr. Aniwat Tandaechanurat, the lecturers from Chulalongkorn University. Their advice and encouragement have enlightened and guided me so far in my life.

I would like to express my special thanks to the Electricity Generating Authority of Thailand (EGAT) for providing me the full financial support and extraordinary opportunity for my post-graduate study.

Most importantly, I am extremely grateful to my girlfriend and my family for their unconditional love, care, and understanding. Their encouragement and being by my side are much appreciated every time I face problems. Their mental supports are the main force help me complete this journey.

Krit Kongurai

ABSTRACT

State estimation (SE) is a crucial tool for power system state monitoring since the control center requires a process to deal with a large number of imprecise measurements. Several SE methods have been applied and developed for the electric power system in the transmission level in the past several decades. Meanwhile, SE for the distribution level remained in the background for a long time since the distribution networks were mainly radial with uni-directional power flows, making classical monitoring and control functions sufficient. Recently, due to the liberalization of the energy market, growing penetration of distributed generation, mainly renewable energy sources, and distributed energy resources such as electric vehicles, the distribution system has been gradually changing from passive into active grids. This requires more sophisticated monitoring and control of the distribution network via a distribution management system (DMS) to ensure optimal integration and maximize the grid hosting capacity. Since one of the key functions of DMS for real-time operation is the SE procedure, this calls for the following: (i) development of SE techniques for the distribution level, so-called distribution system state estimation (DSSE); (ii) more deployment of time-synchronized devices like phasor measurement units (PMU) that can directly measure and acquire accurate and time-aligned phasors with typical refresh rates up to 20-60 times per second.

Two types of DSSE algorithms were developed and implemented on the real-life 50 kV ring distribution grid composed of PMU devices by using the real-time simulation platform. The first is a static approach. The problem is formulated as a WLS problem to be solved based on the iterative Newton method, known as static state estimation (SSE). The second is a dynamic approach, which is more advanced, known as the forecasting-aided state estimation (FASE). It is one of the particular applications of the dynamic state estimation (DSE) concept based on the quasi-steady-state operating conditions. The dynamic formulation is solved using the extended Kalman filter (EKF) technique. This research aims to implement distribution system state estimation (DSSE) algorithms coupled with the auxiliary function, the so-called anomaly detection discrimination and identification (ADDI), into the distribution network. Both normal and abnormal operation scenarios of the power system are simulated to validate the algorithms.

The results reveal that the FASE is superior to the SSE algorithm in terms of estimation accuracy and computational time under normal operating conditions. However, under abnormal conditions, if there is no ADDI module, the performances of both algorithms are degraded significantly due to erroneous measurements. The FASE algorithm loses the system states' trajectory when sudden load change occurs. These issues point out the necessity of using the ADDI module against possible disturbances in real-life networks. In the end, the results show that the proposed FASE algorithm coupled with the ADDI module can accurately estimate the states under both normal and abnormal operations. One significant contribution is that the proposed algorithm can perform adequately fast so that it can process every high-speed measurement from PMU devices.

CONTENTS

LIST OF FIGURES

LIST OF TABLES

List of Abbreviations

ADDI anomaly detection, discrimination, and identification

DMS distribution management system

DSE dynamic state estimation

DSO distribution system operator

DSSE distribution system state estimation

EKF extended Kalman filter

FASE forecasting-aided state estimation

GPS Global Positioning System

LNI largest normalized innovations

LNR largest normalized residuals

PMU phasor measurement unit

RTDS Real Time Digital Simulator

RTU remote terminal unit

SCADA supervisory control and data acquisition system

SE state estimation

SIR skewness to the largest normalized innovation ratio

SSE static state estimation

TVE total vector error

WLS weighted least square

1

INTRODUCTION

1.1. BACKGROUND AND MOTIVATION

Electric power system deals with the generation, transmission, and distribution of electricity. Security control, along with efficient and optimum economic dispatch, has always been the main strategy in power system operation [1]. In order to achieve this, it is essential to know the states of the system under steady-state conditions by state monitoring. In the control center, there are two ways to know the data of the state: (i) by using the raw power system data from a real-time data acquisition, (ii) by applying state estimation to obtain a better and more comprehensive set of information than using the raw data set [2].

State estimation (SE) is a crucial tool for power system state monitoring since the control center requires a process to deal with a large number of imprecise measurements [3]. As a result, SE can provide the best estimate of the states for many downstream applications, such as power flow, contingency analysis, optimal power flow, dynamic stabilities, etc [4]. The state variables can be the nodal voltage magnitudes and angles in the network. SE provides the solution for the optimization problem that processes the measurements together with the network model to determine the optimal estimate of the states. The importance of utilizing the output from SE for the real-time load flow program is highlighted on a security analysis basis. Having the load flow values under steady-state as a base case makes it possible to detect and analyze any contingency event in the system. If SE is not used, there is not much to be done with the raw data except checking for an abnormality [2]. Also, when using the raw data set of measurements directly, the loss of one measurement made the load flow calculation impossible, and the presence of measurement errors affected the estimation result dramatically. To overcome these issues, SE can recognize any inconsistent data (or missing data) by evaluating the level of consistency between the measurement set and the network topology model. This means that SE has a systematic way to detect the presence of bad data (so-called outliers) and identify which measurement data has the error so that it can be corrected/eliminated.

1

Traditionally, SE algorithms made use of the measurements of active and reactive power of line flow, possibly including magnitudes of bus voltages and branch currents, to estimate bus voltage magnitudes and angles. The complex bus voltages represent the state variables of the network since they can determine all the power flows and injections, given the accurate network model is known [3]. Since these conventional measurements have a low scanning rate of a few seconds provided by the remote terminal units (RTUs) at substations, this caused traditional SE algorithms to perform at a relatively lower refresh rate of a few minutes due to computational limitations [5]. Nowadays, time-synchronized devices like phasor measurement units (PMU) can directly measure and acquire accurate and time-aligned phasors, known as synchrophasors, with typical refresh rates up to 20-60 times per second [1]. Thanks to these high-speed scanning rates, if SE algorithms can perform as fast as the PMU data rate, it will become feasible to capture dynamic behaviors in response to transient events in the power system [4]. As a result, SE procedures can exploit the availability of synchrophasor measurements to achieve a more accurate and more sophisticated estimate of the states.

Several SE methods have been applied and developed for the electric power system in the transmission level in the past several decades. Also, PMUs are usually deployed and studied at the transmission system. Meanwhile, SE for the distribution level remained in the background for a long time since the distribution networks were mainly radial with uni-directional power flows, making classical monitoring and control functions sufficient. Nowadays, the distribution grids are undergoing a fundamental upgrade to more dynamic and complex structures due to the distributed generation (DG) sources, distributed energy storage, etc. The topology of the grid will also change from a mainly radial into a more meshed topology, resulting in bi-directional power flows. In this context, the nature of the distribution grid that was traditionally passive is being transformed into active distribution grids [6]. The addition of distributed generation, and the integration of intermittent and volatile renewable generation, requires more sophisticated monitoring and control of the distribution network via a distribution management system (DMS). Since one of the key functions of DMS for real-time operation is the SE procedure, this calls for the following: (i) development of SE techniques for the distribution level, so-called distribution system state estimation (DSSE); (ii) more deployment of PMU devices in distribution grids; to ensure optimal integration and maximize the grid hosting capacity. At the same time, the advanced DSSE approaches are also needed to be validated through a real-time simulation platform for online data acquisition, visualization, and feature extraction.

Since 1970 when the first SE technique was proposed by Fred Schweppe, most of the studies on the topic were focused on static state estimation (SSE) methods based on weighted least square (WLS). SSE is a data processing algorithm based on only the data of the current time sample. The algorithm is computed by the central computer to perform a “best fit” of the total measurements and estimate the static state vector. Another type of state estimator is the recursive method, such as the well-known Kalman filter-based [7]. The Kalman filter is highly potent in several ways: it supports estimation in past, present, and future states; it can estimate states well even if the accurate model of the system is not known thanks to the ability to incorporate noise characteristics into the computations [1], [8]. The most widely adopted non-linear Kalman filters for SE are

the extended Kalman filter (EKF) and the unscented Kalman filter (UKF) [8]. The former solves SE by calculating the Jacobian matrix to linearize the measurement functions as an approximation, while the latter solves SE by using a statistical distribution of the states [9]. Although the Kalman filter-based SE can obtain better estimation accuracy than the WLS, it requires a higher complexity algorithm resulting in a higher computation effort. The high computational time was one of the main reasons the Kalman filter-based SE was not widely implemented in real-time SE back then [10]. Nowadays, the effectiveness of SE based on the Kalman filter has been recently reconsidered thanks to the PMU measurements that allow SE to perform at a high refresh rate.

Bad data processing is one of the primary functions of any SE algorithm, where bad data refers to errors in the measurements. The erroneous data can arise from problems in the measuring device or the communication system used to transmit the data [3]. Bad data is common in power systems since there are usually a number of measurements collected for SE and several sources of bad data. The estimator can be considerably biased (i.e., immense errors) if a huge magnitude of bad data goes through the estimation process [3]. This means that any estimator should be able to identify and reject bad measurements. However, the SSE can be prone to bad data or loss of data if the measurement redundancy is low, which is a general case for the distribution level since there are not many measurement devices in the distribution grid [8]. The reason for the prone is that rejecting erroneous measurements can impact the observability of the system, and SSE concentrates on only the present measurements. This issue can be overcome by the so-called forecasting-aided state estimation (FASE) since it can maintain data redundancy [11] despite bad data elimination. This is because FASE uses not only the measurements but also the predictions. The FASE is an estimator that considers the time-evolution of the states for the forecasting under the assumption of quasi-steady-state operating conditions. The state variables are bus voltage magnitudes and angles of the system. The Kalman filter is also used to solve the FASE formulation for solutions. It can be considered that the FASE is particularly suitable for distribution systems where the measurement redundancy is usually low. Apart from bad data as the anomaly, sudden changes of states caused by load change or network topology change may occur in the power system [8]. In that case, the FASE will obtain a poor estimation accuracy since the state transition coefficient must take some time instants to adapt to the new operating point. Hence, FASEs need to treat sudden change as one type of anomalies in order to distinguish it from bad data for proper actions to reduce the adverse effects. All in all, the need for the function of anomaly processing for the Kalman filter-based SE is established.

1.2. LITERATURE REVIEW

1.2.1. LITERATURE STUDY ABOUT STATIC AND DYNAMIC STATE ESTIMATION AND ANOMALY PROCESSING FUNCTION

Since 1970, the first method of power system SE was proposed by Fred Schweppe [12]–[14]. The problem was first formulated in terms of SSE and has been studied and applied widely in the power industry. A solid review of state of the art in electric power system SSE can be found in [5], [15], [16]. This SSE method was computed using a single scan of the whole measurement set as a snapshot per time instant, providing that the system

is overdetermined (having redundant telemetry measurements in the network). The bus voltage magnitudes and angles are usually given as the state variables. The power system operating point is assumed to be quasi-steady-state, of which the load and generation change smoothly and slow enough so that dynamic behaviors of the states can be neglected. It is noted by [5] that the utilized SSE was not actually real-time but is only a quasi-static representation of the network since the conventional measurements received from RTUs can be delayed up to a few seconds.

The famous work of R. Kalman was firstly proposed in 1960 [17]. Theoretically, the Kalman filter can provide better estimation accuracy compared to the WLS-based SSE. However, the application of the Kalman filter was not widely used (as the WLS) on power system SE because of the more complex algorithm. Some limitations of the implementation noted by [10] are: (i) the need for the process model that has to be carefully tuned to include the time-evolution of the power system state dynamics; (ii) advanced challenges for the practical aspects, such as the need for anomaly processors that not only deal with bad data but also sudden change since it violates the process model; (iii) the higher computational time, which causes difficulties to real-time application.

In the early 1970s, the approach of dynamic SE (DSE) on power systems was proposed by Debs and Larsonn [18] by applying a linear Kalman filter on a linear process model to describe the system state dynamics. However, the estimation is delayed and has poor accuracy when a sudden state change occurs. Also, the process model was oversimplified, so the forecasting is not optimal.

In the late 1970s, Nishiya et al. [19]–[21] proposed the first method to discriminate/classify anomalies of the DSE formulation into three types: (i) occurrence of bad data, (ii) changes in network configuration, and (iii) sudden state changes. The nonlinear Kalman filter, the so-called extended Kalman filter (EKF), is used for the process model. The method introduced the innovation process to be analyzed on a statistical basis. Specifically, after detecting an anomaly, the skewness of the distribution of the innovations is used to distinguish bad data from the other anomalies. After that, if the normalized innovations associated with the power flow measurements exceed a certain threshold, the sudden topology change is suspected and re-estimated. Otherwise, the sudden state change is recognized. Although the process model is also simplified as [18], the innovation analysis proposed in this study has paved the way for the anomaly processing development for the Kalman filter-based SE.

Da Silva et al. [22] proposed the DSE based on EKF with the process model that can track the operating points of the power system under quasi-steady-state. The state transition coefficients of the process model are assessed using the Holt's linear exponential smoothing method, proposed in the same study. Also, the paper showed that the predictions are pretty unreliable under a sudden change in the system, and that the process model needs some snapshots of time to adjust its coefficient and then provide reliable predictions again. One way was suggested to help the adjustment faster was to reduce the time period in each snapshot of the SE algorithm so that more measurements could be processed. The anomaly was processed using logical check routines; if the maximum number of bad data per region is exceeded, the sudden change is characterized. All in all, this study proves that the Holt's forecasting method has a very good forecasting capability for the EKF-based SE under normal operations. However, the logical check routines

for processing anomaly is not so reliable because it highly depends on each system.

The author of [23] then proposed a new method to discriminate bad data and sudden change by using both innovations and residuals. This approach combines the pre-estimation procedure (i.e., innovation analysis) and the post-estimation procedure (i.e., residuals analysis) to obtain more reliable detection and discrimination of anomalies. The EKF-based DSE and the forecasting method as [22] were used for normal operations. Once an anomaly is detected by checking the high value of normalized innovations (known as a-test), the SSE is performed instead in order to guarantee reliable residuals. Then, the values of normalized residuals are checked against a particular threshold (known as b-test). If one exceeds the threshold value, the anomaly is characterized as bad data. Then, the suspected bad measurements are identified based on the innovation analysis and are eliminated by substituting them with the forecasted data. Otherwise, the sudden change is characterized. The technique of this paper contributes significantly to the development of anomaly processing because: (i) it can distinguish small magnitude of bad data from sudden change while the pre-estimation method may not; (ii) the WLS filter of SSE can provide a good estimation under sudden change. However, the technique is conducted after the estimation, resulting in higher computational effort and time. Therefore, careful attention has to be considered for real-time applications.

Coutto Filho et al. [24] proposed a debugging procedure for anomaly detection and discrimination. The anomaly can be discriminated into (i) gross measurement errors, (ii) topological errors, or (iii) forecasting errors due to sudden changes in the system operating point. This paper used the Holt's linear exponential smoothing method for the process model and used only the WLS for the state filtering. The concept of using innovations and residuals for anomaly processing is similar to [23] for bad data and sudden change. The anomaly will be classified as topology errors under the condition that the number of suspicious bad data is more than the expected maximum number of bad data in the system.

The same author then proposed state-of-the-art for a particular estimator of the DSE concept, the so-called FASE [11], [25]. This estimator considers the quasi-stationary regime to track the static-state of the system and its time evolution as static-state dynamics while disregarding transients. The state variables specifically refer to the bus voltage magnitudes and angles.

1.2.2. LITERATURE STUDY ABOUT PMU-BASED STATE ESTIMATION AND DISTRIBUTION SYSTEM STATE ESTIMATION

Phasor measurement units (PMUs) are measurement devices that can take the direct magnitude and phase angle of voltage and current measurements and have these data time-stamped with high precision. The typical reporting rate can be up to 20-60 times per second. The PMU measurements are usually synchronized with the Global Positioning Systems (GPS) receivers; thus, they can be from several areas, even across widely dispersed locations [26].

Since the development of PMUs, many researchers in the SE area have conducted to see how to use the devices to obtain better observability of the system. Reference [27] discussed that the voltage phasors from PMUs can significantly improve the phase angle estimation accuracy with the proper PMU placement. This is because the phase angle

cannot be monitored for the traditional technology and thus has to be calculated by the SE process. Another benefit of PMUs is that the high reporting rate of PMUs can lead to a high time step resolution in the power system monitoring. If the SE algorithm is computationally efficient enough, the proper tracking of dynamic behavior, e.g., fault event, will become possible [28].

It is possible to include the voltage and current phasors from PMUs into the SE process that is already based on SCADA measurements to increase the performance. This type of state estimator is known as a hybrid state estimator [29]–[34]. However, there are still improvement limitations in case if the SCADA measurements are needed for the network observability or to ensure the measurement redundancy. Also, some works [35] discussed that the data from PMU and SCADA should be collected and utilized separately because the PMU data is far superior to the SCADA data. Suppose a number of PMUs can cover some portions of the grid and provide enough observability and redundancy. In that case, the estimation performance of the states in those portions can be improved considerably [36], [37].

Regarding the PMUs and distribution system, Reference [38] proposed a computationally efficient method to conduct distribution system states estimation (DSSE) with PMU measurements and pseudo-measurements in a weakly meshed topology. The important technique is to select the branch current as the state variables, use the rectangular coordinate, and convert power injection measurements into current injection measurements to obtain a constant Jacobian measurement matrix.

In terms of real-time simulation, one of the prominent works to the best of our knowledge is the dissertation [10], which deployed a PMU on every bus to obtain linear state estimation and have full observability. The distribution feeder has a radial topology with distributed generation. The rectangular coordinate is selected. The DSSE algorithm is conducted in real-time and has a computational time from only a few ms up to 10 ms, depending on a wide range of real-time application. The algorithm is adequately fast to locate the fault and possibly contribute to the backup protection scheme. However, it is pretty rare and costly for a distribution grid to have PMU at every bus in real-life. Another real-time DSSE approach is presented in [39] using Real Time Digital Simulator (RTDS). The study used PMU measurements and pseudo-measurements. The processing time of this algorithm is about 500 ms to find the faulty node.

In summary, the knowledge of the static state estimation (SSE) and the forecasting-aided state estimation (FASE), also known as dynamic state estimation (DSE), for transmission systems have been studied and implemented for a long time. Meanwhile, anomaly processing functions have also been limited to the transmission system due to the high measurement redundancy. Regarding the distribution system state estimation (DSSE) with PMU measurements, several methods have been proposed and studied on the radial topology with a combination of pseudo-measurements and real measurements. However, only a few studies had implemented the algorithm in real-time to validate the theoretical methodologies. Therefore, the research topics about implementing PMU-based DSSE algorithms with the anomaly processing function into the ring distribution grid in real-time still have a gap to be discovered.

In this thesis, we present how to implement DSSE algorithms on the real-life active ring distribution network composed of PMU devices. It is expected in the near future that the deployment of synchrophasor measurements will be increased in distribution grids since the modern grid topology is gradually becoming more meshed with the integration of distributed generation. Two types of estimators are focused on in this study. First, the WLS-based SSE is selected since it is the most successful and widely-used algorithm in the power industry and academia, thanks to its simplicity and low computational time. Second, the EKF-based FASE is selected because the Kalman filter has the promising capability to track the dynamic behaviors of the power system states, and the EKF version of the Kalman filter utilizes the same Jacobian matrix as for the non-linear measurement model of the SSE. With the high reporting rate of PMU measurements, the power system can be considered under quasi-steady-state operations since it can be assumed that there is no significant variation in the states between the time samples. The quasi-steady-state makes the FASE a good candidate to solve for the bus voltage magnitudes and angles in distribution grids, which usually have low measurement redundancy. This thesis's significance and contribution is the experimental validation of the theoretical SE algorithm by fully integrating the SE into our real-time simulation platform to utilize real-time data from software PMUs simulated by Real Time Digital Simulator (RTDS) and streamed over the internet.

Special attention will be given to anomaly processing, the so-called anomaly detection discrimination and identification (ADDI), for the validation against possible disturbances in power systems and some telecommunication failures for real-life network adaptability. Due to the recent availability of PMU devices, the ADDI has been challenged in terms of real-time practicability. The reason is that any state estimator coupled with the ADDI should consume lower computational time than the fast refresh rate of PMUs so that the SE will not lose any measurements. This challenge was not raised before because there was sufficient time to perform the ADDI due to the slow update of the conventional measurement at several seconds or more. In this study, three different methods of anomaly detection and discrimination from the literature are selected to be compared and tested with several levels and locations of anomalies in the distribution grid. The criteria for discrimination are based on the statistical analysis of innovations and/or residuals, depending on the method. In addition, the most traditional way to perform anomaly identification and countermeasures are adopted to prevent the estimation from being biased. Finally, we assess the performance of the proposed state estimator coupled with the ADDI algorithm under normal and abnormal operating conditions and also compare the results with the other estimators in this study that are not coupled with the ADDI module.

1

1.3. RESEARCH OBJECTIVES

This thesis aims to implement distribution system state estimation (DSSE) algorithms coupled with the auxiliary function, the so-called anomaly detection discrimination and identification (ADDI), into an existing 50 kV ring distribution network, namely Enduris MV grid, equipped with PMU measurements using our real-time simulation platform. The summaries of objectives are as the following:

1. To create the mathematical model of the topology of the Enduris MV grid in MATLAB.
2. To set up the real-time simulation platform (our experimental setup) to stream the simulated PMU signals from RTDS facilities via the internet connection into a computer to run SE on MATLAB.
3. To implement DSSE algorithms, i.e., the WLS-based SSE and the EKF-based FASE, using our real-time simulation platform.
4. To create the ADDI algorithm and couple it with the EKF-based FASE to process anomaly in the measurements as follows: (i) anomaly detection and discrimination, (ii) anomaly identification and countermeasures.
5. To accurately estimate voltage magnitudes and angles at the 150 kV and 50 kV substations of the Enduris MV grid in real-time under normal and abnormal operating conditions.

1.4. RESEARCH CONTRIBUTIONS

The contributions of this study are listed below:

1. Included in Chapter 2 - The mathematical model of the Engurid MV grid topology as the network admittance matrix is created in MATLAB. The model consists of three-phase series components of generic transmission lines and transformers using two-port parameters. Objective 1 is fulfilled by this contribution.
2. Included in Chapter 4 – The real-time experimental setup to send online PMU streams from RTDS via the internet into the data acquisition and the SE algorithm in MATLAB is established. Objective 2 is fulfilled by this contribution.
3. Included in Chapter 2, 5 – The formulations of the WLS-based SSE and EKF-based FASE are created in MATLAB in Chapter 2. Both DSSE algorithms are successfully implemented on the real-time experimental setup, and the estimation results are compared under normal operating conditions in Chapter 5. Objective 3 is fulfilled by this contribution.
4. Included in Chapter 3, 5 – The ADDI module is created and coupled with the EKF-based FASE in MATLAB. The module consists of algorithms of (i) anomaly detection and discrimination and (ii) anomaly identification and countermeasures. Several levels and locations of anomalies are tested against the ADDI module in Chapter 5. Objective 4 is fulfilled by this contribution.

5. Included in Chapter 5 – The performance indices for the measurement noise filtering capability and the estimation accuracy are displayed and analyzed under normal and abnormal operating conditions. The results aim to compare the cases when there is (or is not any) ADDI module coupled with the DSSE algorithms in order to prove the necessity of the ADDI module. Objective 5 is fulfilled by this contribution.

1.5. RESEARCH QUESTIONS

Besides the research objectives that are already defined, some important questions are also helpful to guide the thesis direction. The questions are answered in detail with brief results as follows.

1.5.1. WHICH SE TECHNIQUE IS SUITABLE IN TERMS OF ACCURACY TO ESTIMATE THE STATES OF THE DISTRIBUTION GRID UNDER NORMAL OPERATIONS AND WHY?

Generally, two sources of uncertainties that can considerably influence the estimation accuracy are the available measurement infrastructure in the network and the accuracy of that measurement type [28]. But since the question is regarding which technique of SE, the factor contributing to the estimation accuracy is the procedure of SE itself in this context.

The traditional weighted least square (WLS) algorithm for the static state estimation (SSE), or the WLS-SSE, usually solves the solution from the flat start initialization, i.e., all the bus voltages are set at 1 p.u. and in phase with each other [15]. As a result, the performance index to evaluate the estimation accuracy, the mean absolute error (MAE) compared to true values, showed that the MAE of voltage magnitudes and angles using the WLS-SSE is approximately 8×10^{-6} in p.u. and rad under normal operations, which has a very low error.

However, apart from the SE measurement model that the WLS-SSE considers, the accuracy could be improved if the process model is included in the SE model. The main algorithm is known as the forecasting-aided state estimation (FASE) and is solved using the extended Kalman filter (EKF) technique. In short, it will be referred to as the EKF-FASE. Since forecasting is possible and can be done as the extra step, the initial guess will be the forecasted values, which are closer to true values than the flat start initialization. The MAE of voltage magnitudes and angles using the EKF-FASE is approximately 4×10^{-6} in p.u. and rad under normal operations.

In summary, the obtained MAE values from both algorithms have insignificant differences since they are in the same order of 10^{-6}. By multiplying the 10^{-6} p.u. with the base value of 50 kV, the voltage magnitude will be only 0.05 V line-to-line, which is negligible in real life for 50 kV substations. Therefore, both algorithms are suitable to give an adequately accurate estimation for the distribution grid under normal operations. But in order to decide which algorithm for practical implementation in real-time, more aspects should be compared and investigated, such as the computational time and the robustness against erroneous measurements.

1.5.2. IS IT FEASIBLE TO RUN THE REAL-TIME SE ALGORITHM AND ITS AUXILIARY FUNCTION IN A COMPUTATIONALLY EFFICIENT WAY TO BE COMPATIBLE WITH THE HIGH REPORTING RATE OF THE SYNCHRONIZED PHASOR MEASUREMENTS IN THE DISTRIBUTION GRID?

Since the PMU devices are capable of providing high-speed refresh rate phasor measurements, the SE algorithm that takes the measurements as input should be designed in a way that it can fastly process every measurement data and avoid losing data as much as possible. In order to begin answering this question, we first mention some main challenges that we have to overcome since they can cause a significant computational burden to the SE algorithm in several aspects.

First, the state estimation (SE) is formulated as non-linear equations in this study because of the choice of the state variables and the measurements we made. The selected options are (i) polar node-voltage as the states and (ii) polar node-voltage and polar branch-current for the phasor measurements from PMUs. We chose them so that the SE algorithm can directly estimate voltage magnitudes and angles, and the current magnitudes and angles can be handled easily. In turn, the SE model has non-linear measurement functions, possibly resulting in a more computational burden.

Second, the estimator is developed using the three-phase model since a distribution network usually has an unbalanced load and other electrical quantities. This three-phase model development, together with a possibly high number of nodes for the distribution system, can result in a large system and then lead to a very high computational burden.

Third, the high R/X ratio of distribution lines makes the SE algorithm impossible to apply the fast decoupled load flow technique that is commonly used for the transmission system for simplification. For instance, for a given low R/X ratio of transmission lines, the resistance can be neglected with reasonable approximation, leading to a more simplified (decoupled) Jacobian measurement matrix. However, since the technique cannot be applied to the distribution system, the SE measurement model has to consist of a full Jacobian measurement matrix, which may lead to a higher computational burden.

As a result of the challenges above, the traditional weighted least square (WLS) algorithm for the static state estimation (SSE), or the WLS-SSE, we developed can converge within 4-5 iterations under normal operations, which has the overall execution time of 25.3 ms. It is apparent that this execution time exceeds the refresh rate of PMUs at 20 ms per measurement. In order to overcome this limitation, we developed another approach that can converge in only one iteration, using the extended Kalman filter (EKF) technique, with a proper initialization based on predictions. The main algorithm is known as the forecasting-aided state estimation (FASE). The execution time of the EKF-FASE algorithm is only 10.7 ms. After integrating/coupling the auxiliary function of the anomaly detection discrimination and identification (ADDI) into the EKF-FASE, the execution time becomes slightly higher at 13.7 ms. This should be highlighted as a significant contribution that the coupled EKF-FASE estimator will not miss any measurement under normal operations as the PMU streaming rate is 20 ms per sample. Therefore, it can be concluded that it is feasible to run the real-time SE algorithm with its auxiliary function computationally efficiently to be compatible with the high reporting rate of PMUs in the distribution grid.

1.6. THESIS OUTLINE

This thesis is organized into six chapters. The overview of Chapters 2-6 is explained as follows.

In Chapter 2, we introduce theories about PMU-based SE. First, we describe the formulation of SE problems, the concept of distribution state estimation (DSSE), and the impact of PMUs in SE. Second, the general requirements of SE in this study are explained. Third, the network admittance matrix for the Enduris MV gird is created by using the three-phase series components of generic lines and transformers. We describe the particular characteristics of the non-linear measurement model that link the state variables and the available measurements, consisting of online phasor measurements and pseudo-measurements. This followed by describing the process model representing the time evolution of the power system states to conduct forecasting. Finally, the equations of the WLS-based SSE and EKF-based FASE are formulated and presented as flowcharts.

In Chapter 3, the whole process of the ADDI module is explained in detail. We describe the classification of anomalies. Three different methods of anomaly detection and discrimination in this study are introduced and depicted. Following this, the process for anomaly identification and countermeasures for each method is fully described.

Chapter 4 is related to the preparation for the implementation of the SE algorithms in real-time. First, we elaborate on how to set up the real-time simulation platform using the facilities in our RTDS laboratory of TU Delft. Second, the schematic of the Enduris MV grid and the measurement configurations are depicted. Third, the assessment of measurement noise and process noise covariance matrices are explained with some assumptions. This step aims to tune the uncertainties from the sources of measurements and process noise to match with the simulated power system in real-time. Lastly, the performance indices used to assess the filtering capability and estimation accuracy of SE are introduced.

Chapter 5 shows the experimental results of the real-time simulation. First, the performance indices by the WLS-SSE and EKF-FASE are compared under normal operation scenarios. This is followed by testing several levels and locations of anomalies against three methods of the ADDI module. Their computational efforts are compared, and then the best method is selected. Lastly, the results of the proposed EKF-FASE coupled with the ADDI module and the DSSE algorithms without the ADDI module are compared under both normal and abnormal operating conditions.

Chapter 6 summarizes the results of this study and suggests future work.

2

THEORY ABOUT PMU-BASED STATE ESTIMATION

We introduce theories about PMU-based SE. First, we describe the formulation of SE problems, the concept of distribution state estimation (DSSE), and the impact of PMUs in SE. Second, the general requirements of SE in this study are explained. Third, the network admittance matrix for the Enduris MV gird is created by using the three-phase series components of generic lines and transformers. We describe the particular characteristics of the non-linear measurement model that link the state variables and the available measurements, consisting of online phasor measurements and pseudo-measurements. This followed by describing the process model representing the time evolution of the power system states to conduct forecasting. Finally, the equations of the WLS-based SSE and EKF-based FASE are formulated and presented as flowcharts.

2.1. INTRODUCTION OF DISTRIBUTION SYSTEM STATE ESTIMATION AND PMU MEASUREMENTS

This section aims to introduce concepts of SE with PMU devices and general facts about the distribution system compared to the transmission system. They are organized into three subsections. First, the formulation of the SE problem is explained. Second, the distribution system state estimation (DSSE) is introduced. Third, the role and impact of PMUs in SE are described.

2.1.1. FORMULATION OF THE STATE ESTIMATION PROBLEM

The problem formulation of the SE in power systems is to determine the state variables of the network based on the SE mathematical models and the real-time measurements received from the meters at the field. The aim is to solve for the states that can lead to a better approximation of the true measurements [28]. The SE mathematical models generally consist of the network topology model and the measurement model for the static

state estimation (SSE). However, for the dynamic state estimation (DSE), the SE mathematical models also have to include the process model, representing dynamic characteristics of the states, since the approach also relies on tracking the time evolution of the states historically with respect to the previous time samples in order to predict the states one step ahead.

2.1.2. DISTRIBUTION SYSTEM STATE ESTIMATION

The electric power system consists of generation, transmission, and distribution systems. Typically, a distribution network consists of High-to-Medium Voltage (HV/MV) transformation centers, the MV grid, Medium-to-Low Voltage (MV/LV) transformation centers, and the LV grid. The LV grid is mainly connected by residential and commercial users., while the MV grid is connected by industrial users. Recently, due to the liberalization of the energy market, growing penetration of distributed generation, mainly renewable energy sources, and distributed energy resources such as electric vehicles, the distribution system has been gradually changing from passive into active grids. This requires more sophisticated monitoring and control of the network, which is relevant to the smart grid (SG) scenario. In the SG scenario, the smarter energy management system solution by the distribution system operator (DSO) aims to fulfill customers' demands without harming the service quality and infrastructure. The precise and reliable operation of the management and control functions by DSO are based on the information of the operating condition of the grid [40].

One way to achieve the real-time network conditions is to use the distribution system state estimation (DSSE) algorithm to provide the states of the distribution system as a snapshot by using the measurements from the field and the other network information if available. Figure 2.1 illustrates the relevant applications of the DSSE results for a new distribution management system (DMS) by the distribution system control center [40].

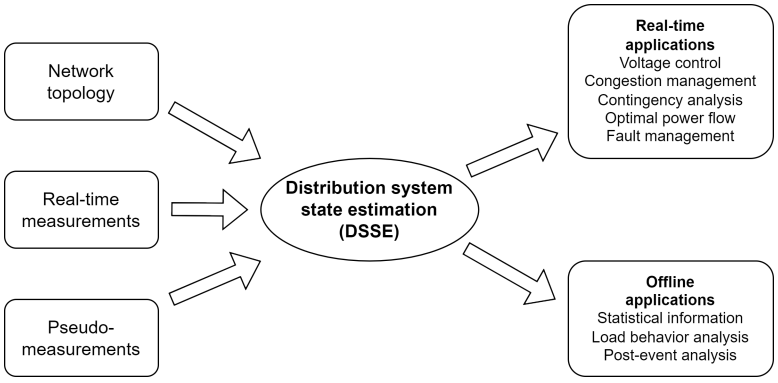

Figure 2.1: The relevant applications of the DSSE results for DMS [40].

In order to conduct DSSE, the measurement infrastructure available in the network is the most critical factor that determines how fast and accurate the states can be solved. For the transmission level, there are usually a number of measurement devices deployed in the grid. However, in general, the measurement and monitoring devices are in short

supply for distribution networks, basically limited to only HV/MV substations. For MV grids, the currents and voltages of MV lines to the main feeder are usually monitored for the local protection system, and their average values are sent to system operators in the utility control center via a SCADA system. The updating rate of these conventional measurements can be a few seconds up to minutes [40]. Due to the lack of measurement redundancy, the distribution networks are never observable in practice [41]. This calls for the use of historical data or forecast measurements regarding power consumption and generation for the location that lacks a measurement device to obtain minimal observability (100%). These data are so-called pseudo-measurements, which usually have large uncertainties to reflect the low confidence of the data.

Traditionally, the SE algorithm has been developed and exploited for decades in transmission grids, i.e., the so-called transmission system state estimation (TSSE). The technique is generally formulated as a weighted least square (WLS) problem and then solved based on the iterative Newton method. In principle, the same framework of TSSE could be applied to the distribution grid. Still, the approach has to be conceptually different because of the characteristics of a typical distribution grid, as shown in Table 2.1. Some of the main points are explained below [28], [40].

First, the number of measurement devices in distribution systems is poor. Because of this, pseudo-measurements that are derived from statistical or historical data are needed to obtain network observability, as mentioned before. This causes a high uncertainty in the DSSE results, and the estimator's robustness is limited when there is a loss of measurement or data degradation because of the low redundancy. Second, the topology of distribution systems is mainly radial or weakly meshed, which is suitable for using the back/forward sweep-based method to solve for the states in the DSSE. Note that the Newton-based method that is commonly used in the TSSE can also be applied to the DSSE, but a higher execution time can be expected, and some cautions should be noted to avoid possible numerical difficulties due to a particular transformer configuration [41]–[43]. Third, the DSSE estimator should be modeled as the full three-phase since the electrical quantities, such as loads, are non-symmetrical, and there are also two-phase and single-phase laterals in the network. With the penetration of distributed generation, the characteristic of the unbalanced electrical system is increased. By contrast, the electrical quantities for transmission systems can be considered balanced. Thus, the TSSE algorithm is usually modeled as a single-phase model as the positive sequence of the electrical quantities. Fourth, the characteristic of the distribution lines is the high R/X ratio, possibly equal to one. This high R/X ratio disables the possibility of the fast decoupled load flow technique, which is commonly applied for transmission lines with a low R/X ratio to neglect the resistances for simplicity.

In general, the low availability of measurements is the critical problem that affects the estimator's robustness and can lead to a poor estimation accuracy of the DSSE. However, these problems will be alleviated thanks to the availability of PMU devices that have very high accuracy in the Enduris MV distribution grid we considered in this study. Our DSSE algorithms were designed using a three-phase model with a full Jacobian matrix (not using the fast decoupled load flow technique). The iterative Newton method is used to solve the WLS problem for the static state estimation (SSE).

Table 2.1: Main differences between transmission system and distribution systems [28].

	Transmission System	Distribution System
Monitoring	Many measurement devices	Few measurement devices
Main measurement types	Real measurements	Pseudo-measurements
Topology	Meshed	Radial/weakly meshed
Three-phase system	Balanced	Unbalanced
Injections	Concentrated loads	Distributed loads
Nodes number	Low/medium	High
Line impedance	Low R/X ratio	High R/X ratio

2.1.3. ROLE AND IMPACT OF PMUS IN STATE ESTIMATION

The characteristics of the PMUs impact the SE functionalities and performance significantly in several aspects. Some important characteristics are summarized as the following [28]:

1. Availability of phasor measurements
2. Synchronization with respect to the UTC
3. High reporting rate
4. High accuracy and compliance with the measurement of dynamic signals

First, the availability of PMU measurements is capable of providing phasors consisting of magnitudes and angles of voltages and currents. Concerning the conventional measurement, which can give only magnitudes, the additional information of angles from PMUs raises the measurement redundancy for the input of the SE algorithm. This leads to enhanced robustness of the SE process and expanded observability of the monitored network. Therefore, the SE algorithm tends to have a higher ability to deal with some erroneous or loss of measurements due to problems in the telecommunication system, e.g., bad data or topology errors, since the problems largely depend on the level of measurement redundancy in the network. In addition, another advantage of the PMU measurements is related to the convergence properties of the SE algorithm. It is acknowledged that the current measurements can cause SE convergence difficulties by the lack of the current angles measurements. To be more specific, the possible bi-directional power flow of a modern grid can cause the convergence problem since more caution should be considered to define the power flow direction. Hence, these problems will be alleviated thanks to the availability of phasor measurements.

Second, one of the most important features of the PMUs is that the measurements are synchronized with the universal time reference (UTC). One benefit is that each measurement has its own time-stamped so that all the data from PMUs can be referred to precisely. If there is no time-stamped, the SE results will not be able to refer to the exact instant of time. This is usually not a big concern for the transmission grid since the steady-state conditions are realistic shortly. However, this point becomes more consequential for the distribution grid in case there are intermittent renewable sources and distributed generation since the system operating conditions vary rapidly. Therefore,

the synchronized measurements from PMUs can guarantee consistent measurements for the SE algorithm and then provide more reliable estimation results for the system operator in the control center.

Third, the capability of PMUs to provide synchrophasor measurements at high-speed rates is exceptional. Suppose the SE algorithm and the telecommunication system are designed efficiently in terms of computational time. In that case, it is possible to exploit the high reporting rate of PMUs, resulting in the high time sample resolution for monitoring the system operating conditions. Traditionally, conventional measurements with low refresh rates are utilized; the SE algorithm can perform at the rate for up to a few minutes in transmission systems. It is widely known that this rate is too slow to observe the dynamic behavior of the modern gird. This calls for a faster SE computational time and a more frequent reporting rate of measurement devices. Therefore, it can be essential to have the high report rates of PMU measurements to monitor the power system's dynamics using a fast SE execution to support an energy management system.

Fourth, PMU devices are designed to provide highly accurate measurements in digital. It is apparent that the more accurate the measurement for the input of SE is, the more precise the estimation result can be. In order to monitor dynamic behaviors, given a reliable SE algorithm, it is crucial to ensure that the measurement instruments can deal with the dynamic signals properly and provide sufficiently accurate measurements in such conditions. Typically, the accuracy of the conventional meters is defined in steady-state conditions, but the accuracy degradation is unknown while under dynamic conditions. For the PMU devices, those who meet the synchrophasor standard IEEE C37.118.1 [44] will be guaranteed a minimum accuracy level for a specific situation, i.e., 1% of total vector error (TVE) for steady-state and of 3% for dynamic conditions. Here, 1% of TVE corresponds to a maximum deviation of 1% in amplitude estimation or a maximum deviation of 1 crad (0.01 rad) for phase angle. However, the occurrence of a fast transient such as step changes can significantly degrade the measurement accuracy, depending on how suitably the reported data is marked.

2.2. REQUIREMENTS OF STATE ESTIMATION

In general, the following three essential requirements are used to evaluate a suitable SE algorithm for an application: estimation accuracy, time frame, and robustness [28].

2.2.1. ACCURACY OF THE ESTIMATION

Since the state variables in power systems are required for many applications, such as system security control and constraints on economic dispatch [45], it is fundamental to assess the efficiency of the estimation in terms of accuracy because the applications depend on it.

In reality, since it is impossible to know the true states of the network, the estimation accuracy is used to represent the maximum expected deviation of the estimate from the true value. However, the actual values are known in this thesis since we can read the values directly from the real-time simulation infrastructure. Here, the estimation accuracy expresses how close the estimated states are to their actual values, reflecting the level of uncertainty of the estimated quantities.

Generally, two sources of uncertainties that can considerably influence the estimation accuracy are the available measurement infrastructure in the network and the accuracy of that measurement type [28]. They act as the bottlenecks affecting the precision between the estimated values and actual values from the power system. The two sources of uncertainties are explained as the following.

First, the availability of the measurement infrastructure is the most critical factor for estimation accuracy. As noted earlier, poor estimation accuracy can be expected when a certain number of pseudo-measurements is used due to an insufficient number of real measurements in the general distribution grid. In this thesis, many PMUs are equipped in the Enduris MV distribution grid, covering MV substations and cables. This makes the network highly observable and needs only a few pseudo-measurements. Therefore, a high estimation accuracy can be expected, mainly depending on the accuracy of phasor measurements.

Second, the measurement accuracy depends on the specification of the reading meter of each type. For phasor measurements, the information from the datasheet of PMU devices in the field has to be carefully used to determine the uncertainty for the SE measurement model. In this work, however, since the PMUs are simulated as software in the RTDS, the measurement accuracy of the devices can be considered ideal. In turn, additional measurement noises have to be manually added to the ideal/actual measurements using MATLAB so that the uncertainty level in the SE measurement model can be determined appropriately.

2.2.2. TIME FRAME

The time frame is the time window that the estimated states are considered valid. For online SE implementation, the SE algorithm must run with the power system monitoring in real-time. In the 2000s, the scanning rate was every 2 s for SCADA measurements. Still, the practical estimators ran every few minutes due to computational limitations [5]. A reasonable shorter time window will be required with more advanced measurement devices and methodologies in the near future for the smart grid [28].

For a given high reporting rate at every 20 ms of the PMU devices, the execution time of the whole SE algorithm, including auxiliary functions, e.g., bad data detection, topology error identification, and other anomaly processors, should be at or below 20 ms. This way, the countermeasure by the auxiliary function can be applied against any abnormal conditions in the system before the time the new set of measurements arrives. This can lead to a more reliable SE result for the power system monitoring in the control center.

2.2.3. ROBUSTNESS

The robustness indicates the SE capacity to provide the system state with a given quality; when the input data is degraded [28]. The causes of the degradation due to gross errors (or outliers) can be either the unreliable dynamical model or several data quality issues of PMU measurements. The data quality issues can result from carrying bad data, non-Gaussian measurement noise, missing data, cyberattacks, etc [46]. This thesis considers only bad data due to the observation outliers that affect the metered values. In reality, these outliers may result from significant biases in phasor measurements due

to infrequent calibration of PMUs, device failures, and impulsive communication noise [47].

For the robust static state estimation (SSE), one crucial method is to reduce the weight given to erroneous measurements to minimize the influence of the bad data. Also, when an estimator has the principle of automatically eliminating bad data, it also has a robust property [6].

For a particular type of SE that considers the time evolution of the state, such as the forecasting-aided state estimation (FASE), the presence of observation outliers can significantly degrade the estimation performance if some proper actions are not taken. To alleviate this degradation, the pre-estimation techniques based on the innovation analysis are usually conducted to detect, identify, and eliminate the gross errors to obtain unbiased state estimates [46]. Apart from bad data, potentially inaccurate estimation results are obtained with the presence of a sudden state change due to load changes, distributed energy resource fluctuations, system topology changes, etc. This is because the predictions will become unreliable under an unexpected change of states. Hence, further actions are needed to avoid losing the system states' trajectory. One of the widely used actions is applying an adaptive filtering scheme. It aims to automatically adjust the weight of the predicted states through its error covariance matrix [48]–[51]. However, this method is usually complex and may not be attractive from the computational point of view [23], [24]. In order to have a less complex algorithm and more attractive execution time, this thesis proposed an anomaly processor, the so-called anomaly detection discrimination and identification (ADDI) algorithm, as an auxiliary function of the FASE to perform systematic procedures against anomalies.

2.3. MATHEMATICAL MODELS FOR STATE ESTIMATION

This study utilized the three-phase component and topology models to perform the distribution system state estimation (DSSE) since the three phases of the distribution system are generally not balanced in real life, unlike the transmission system.

This section introduces the mathematical models of the network topology and the required models for the SE process in this work. Subsection 2.3.1 shows the modeling of the three-phase components: three-phase transmission line and transformer. Subsection 2.3.2 shows how to create the compound bus admittance matrix of the network. Subsections 2.3.3 and 2.3.4 show main equations with assumptions of the measurement model and the process model of SE, respectively.

2.3.1. MODELING OF THREE-PHASE COMPONENTS

The model of a component, such as a transmission line and transformer, is a subsystem and can be used to build the entire network. Here, each three-phase element is connected in series to each edge of the bus n and bus m. Each component is modeled as follows [42]:

$$\mathbf{i}_{nm} = \mathbf{y}_{nm}^{(n)}\mathbf{v}_n - \mathbf{y}_{nm}^{(m)}\mathbf{v}_m \tag{2.1}$$

$$\mathbf{i}_{mn} = \mathbf{y}_{mn}^{(m)}\mathbf{v}_m - \mathbf{y}_{mn}^{(n)}\mathbf{v}_n \tag{2.2}$$

where $\mathbf{i}_{nm}(\mathbf{i}_{mn})$ is a 3×1 dimensional vector of current phasor flowing from bus n to bus m (bus m to bus n, respectively); $\mathbf{v}_n(\mathbf{v}_m)$ is a vector (3×1) of voltage phasor of bus n (bus m, respectively); $\mathbf{y}_{nm}^{(n)}, \mathbf{y}_{mn}^{(m)}$ are matrices (3×3) of self-admittance of the component between bus n and bus m, measured from the edge of bus n (bus m, respectively); $\mathbf{y}_{nm}^{(m)}, \mathbf{y}_{mn}^{(n)}$ are matrices (3×3) of mutual admittance of the component between bus n and bus m, measured from the edge of bus n (bus m, respectively). The transmission line and transformer are derived in the current-voltage models as in the subsections below.

2.3.1.1 TRANSMISSION LINE

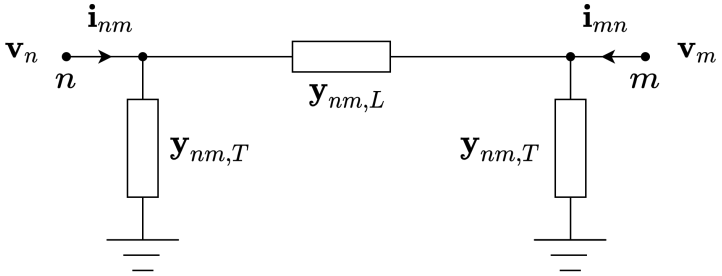

Figure 2.2: Three-phase two-port π-model of a generic network branch.

The line was modeled as the four-wire grounded wye line segment. It is assumed that the line has a multi-grounded neutral. By applying the Kron reduction technique, the phase admittance matrices are dimensional 3×3 [52]. The general three-phase line model is shown in Figure 2.2 and has the current-voltage equations as the following [7], [53]:

$$\begin{bmatrix} \mathbf{i}_{nm} \\ \mathbf{i}_{mn} \end{bmatrix} = \begin{bmatrix} \mathbf{y}_{nm,L} + \mathbf{y}_{nm,T} & -\mathbf{y}_{nm,L} \\ -\mathbf{y}_{mn,L} & \mathbf{y}_{mn,L} + \mathbf{y}_{mn,T} \end{bmatrix} \begin{bmatrix} \mathbf{v}_n \\ \mathbf{v}_m \end{bmatrix} \tag{2.3}$$

Comparing (2.3) with (2.1)-(2.2) to express in terms of the two-port parameters yield:

$$\mathbf{y}_{nm}^{(n)} = \mathbf{y}_{mn}^{(m)} = \mathbf{y}_{nm,L} + \mathbf{y}_{nm,T} \tag{2.4}$$

$$\mathbf{y}_{nm}^{(m)} = \mathbf{y}_{mn}^{(n)} = \mathbf{y}_{nm,L} \tag{2.5}$$

where

$$\mathbf{y}_{nm,L} = \mathbf{g}_{nm,L} + j\mathbf{b}_{nm,L} \tag{2.6}$$

$$\mathbf{y}_{nm,T} = \mathbf{g}_{nm,T} + j\mathbf{b}_{nm,T} \tag{2.7}$$

$$\mathbf{y}_{mn,T} = \mathbf{g}_{mn,T} + j\mathbf{b}_{mn,T} \tag{2.8}$$

are the series admittance $\mathbf{y}_{nm,L}$, and the two shunt admittances $\mathbf{y}_{nm,T}$ and $\mathbf{y}_{mn,T}$, respectively; j is the imaginary unit; $\mathbf{g}_{nm,L}$ and $\mathbf{b}_{nm,L}$ are the series conductance and susceptance, respectively; $\mathbf{g}_{nm,T}$ and $\mathbf{b}_{nm,T}$($\mathbf{g}_{mn,T}$ and $\mathbf{b}_{mn,T}$) are the shunt conductance and susceptance, measured from the side of bus n (bus m, respectively). The series admittance $\mathbf{y}_{nm,L}$ is dimensional (3×3) matrix and given by [7]:

$$\mathbf{y}_{nm,L} = \begin{bmatrix} g^{aa}_{nm,L} + jb^{aa}_{nm,L} & g^{ab}_{nm,L} + jb^{ab}_{nm,L} & g^{ac}_{nm,L} + jb^{ac}_{nm,L} \\ g^{ba}_{nm,L} + jb^{ba}_{nm,L} & g^{bb}_{nm,L} + jb^{bb}_{nm,L} & g^{bc}_{nm,L} + jb^{bc}_{nm,L} \\ g^{ca}_{nm,L} + jb^{ca}_{nm,L} & g^{cb}_{nm,L} + jb^{cb}_{nm,L} & g^{cc}_{nm,L} + jb^{cc}_{nm,L} \end{bmatrix} \tag{2.9}$$

Note that these parameters can be expressed in terms of the series impedance $\mathbf{z}_{line}$, and the shunt admittance $\mathbf{y}_{line}$of the three-phase transmission line:

$$\mathbf{y}_{nm,L} = \mathbf{z}^{-1}_{line} \tag{2.10}$$

$$\mathbf{y}_{nm,T} = \mathbf{y}_{mn,T} = \mathbf{y}_{line,T}/2 \tag{2.11}$$

2.3.1.2 THREE-PHASE TRANSFORMER

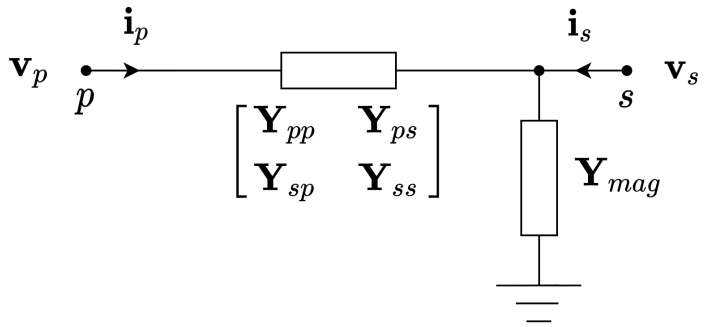

Figure 2.3: General three-phase two-port transformer model.

At the distribution level, two blocks can appropriately model a three-phase transformer. A series block represents the per unit leakage admittance, and a shunt block represents the core losses of the transformer. The general three-phase transformer model is shown in Figure 2.3, and the current-voltage equations are as follows [53].

$$\begin{bmatrix} \mathbf{i}_p \\ \mathbf{i}_s \end{bmatrix} = \begin{bmatrix} \mathbf{Y}_{pp} & \mathbf{Y}_{ps} + \mathbf{Y}_{mag} \\ \mathbf{Y}_{sp} & \mathbf{Y}_{ss} + \mathbf{Y}_{mag} \end{bmatrix} \begin{bmatrix} \mathbf{v}_p \\ \mathbf{v}_s \end{bmatrix} \tag{2.12}$$

where $\mathbf{Y}_{pp}, \mathbf{Y}_{ps}, \mathbf{Y}_{sp}, \mathbf{Y}_{ss}$ are the submatrices (3×3), and $\mathbf{Y}_{mag}$is the magnetizing admittance matrix (3×3) calculated in. Comparing (2.12) with (2.1)-(2.2) to express in terms of the two-port parameters yield:

$$\begin{aligned}\mathbf{y}_{nm}^{(n)} &= \mathbf{Y}_{pp}\\ \mathbf{y}_{nm}^{(m)} &= -\mathbf{Y}_{ps} - \mathbf{Y}_{mag}\\ \mathbf{y}_{mn}^{(n)} &= -\mathbf{Y}_{sp}\\ \mathbf{y}_{mn}^{(m)} &= \mathbf{Y}_{ss} + \mathbf{Y}_{mag}\end{aligned} \tag{2.13}$$

The transformer submatrices $\mathbf{Y}_{pp}, \mathbf{Y}_{ps}, \mathbf{Y}_{sp}, \mathbf{Y}_{ss}$ for (2.12)-(2.13) for the common step-down transformer are shown in Table 2.2 [53], where the neutral transformer tap changer position is assumed for simplification. The submatrices are defined depending on the type of transformer winding.

Table 2.2: Transformer submatrices for common three-phase step-down transformer connections.

Connection	$\mathbf{Y}_{pp}$	$\mathbf{Y}_{ps}$	$\mathbf{Y}_{sp}$	$\mathbf{Y}_{ss}$
YNyn	$\mathbf{Y}_{I}$	-$\mathbf{Y}_{I}$	-$\mathbf{Y}_{I}$	$\mathbf{Y}_{I}$
YNy, Yyn, Yy, Dd	$\mathbf{Y}_{II}$	-$\mathbf{Y}_{II}$	-$\mathbf{Y}_{II}$	$\mathbf{Y}_{II}$
YNd	$\mathbf{Y}_{I}$	$\mathbf{Y}_{III}^{T}$	$\mathbf{Y}_{III}$	$\mathbf{Y}_{II}$
Yd, Dy	$\mathbf{Y}_{II}$	$\mathbf{Y}_{III}^{T}$	$\mathbf{Y}_{III}$	$\mathbf{Y}_{II}$
Dyn	$\mathbf{Y}_{II}$	$\mathbf{Y}_{III}^{T}$	$\mathbf{Y}_{III}$	$\mathbf{Y}_{I}$

The particular submatrices in Table 2.2 are defined as:

$$\begin{aligned}\mathbf{Y}_{I} &= \begin{bmatrix}1&0&0\\0&1&0\\0&0&1\end{bmatrix}\begin{bmatrix}\underline{Y}_{sc}\\ \underline{Y}_{sc}\\ \underline{Y}_{sc+n}\end{bmatrix};\\ \mathbf{Y}_{II} &= \tfrac{1}{3}\begin{bmatrix}2&-1&-1\\-1&2&-1\\-1&-1&2\end{bmatrix}\underline{Y}_{sc};\\ \mathbf{Y}_{III} &= \tfrac{1}{\sqrt{3}}\begin{bmatrix}-1&1&0\\0&-1&1\\1&0&-1\end{bmatrix}\underline{Y}_{sc},\end{aligned} \tag{2.14}$$

where $\underline{Y}_{sc} = 1/\underline{Z}_{sc}$; $\underline{Y}_{sc+n} = 1/(\underline{Z}_{sc} + \underline{Z}_{n})$; $\underline{Z}_{sc}$ is the short circuit impedance; and $\underline{Z}_{n}$ is the impedance between neutral and ground.

The transformer magnetizing admittance $\mathbf{Y}_{mag}$ for (2.12)-(2.13) is defined as:

$$\mathbf{Y}_{mag} = \mathbf{A}\mathbf{Y}_{mag}^{012}\mathbf{A}^{-1} = \frac{1}{3}\begin{bmatrix}2\underline{Y}_{mag}^{1} + \underline{Y}_{mag}^{0} & -\underline{Y}_{mag}^{1} + \underline{Y}_{mag}^{0} & -\underline{Y}_{mag}^{1} + \underline{Y}_{mag}^{0}\\ -\underline{Y}_{mag}^{1} + \underline{Y}_{mag}^{0} & 2\underline{Y}_{mag}^{1} + \underline{Y}_{mag}^{0} & -\underline{Y}_{mag}^{1} + \underline{Y}_{mag}^{0}\\ -\underline{Y}_{mag}^{1} + \underline{Y}_{mag}^{0} & -\underline{Y}_{mag}^{1} + \underline{Y}_{mag}^{0} & 2\underline{Y}_{mag}^{1} + \underline{Y}_{mag}^{0}\end{bmatrix} \tag{2.15}$$

where A is the Fortescue transformation matrix; $\mathbf{Y}_{mag}^{012} = diag\left\{\underline{Y}_{mag}^{0}, \underline{Y}_{mag}^{1}, \underline{Y}_{mag}^{2}\right\}$; $\underline{Y}_{mag}^{1} = \underline{Y}_{mag}^{2}$ is the positive (equal to negative) sequence of the transformer magnetizing admittance, and $\underline{Y}_{mag}^{0}$ is the zero sequence of the transformer magnetizing admittance [53].

2.3.2. Y-BUS CONSTRUCTION FOR NETWORK TOPOLOGY MODEL

The bus admittance matrix of the network can be constructed using the component models from the previous section 2.3.1. The following matrix equation is derived from Kirchhoff's current law (KCL) at each bus and then formed as a set of nodal equations of the entire network [15].

$$\mathbf{I}_{BUS} = \begin{bmatrix} \mathbf{i}_{inj,1} \\ \mathbf{i}_{inj,2} \\ \vdots \\ \mathbf{i}_{inj,N} \end{bmatrix} = \begin{bmatrix} \mathbf{Y}_{11} & \mathbf{Y}_{12} & \cdots & \mathbf{Y}_{1N} \\ \mathbf{Y}_{21} & \mathbf{Y}_{22} & \cdots & \mathbf{Y}_{2N} \\ \vdots & \vdots & \ddots & \vdots \\ \mathbf{Y}_{N1} & \mathbf{Y}_{N2} & \cdots & \mathbf{Y}_{NN} \end{bmatrix} \begin{bmatrix} \mathbf{v}_1 \\ \mathbf{v}_2 \\ \vdots \\ \mathbf{v}_N \end{bmatrix} = \mathbf{Y}_{BUS} \times \mathbf{V}_{BUS} \tag{2.16}$$

where $\mathbf{I}_{BUS}$,$\mathbf{V}_{BUS}$ are vectors (3N×1) of bus external current injection phasors and bus voltage phasors, respectively; N is the total number of buses in the network; $\mathbf{Y}_{BUS}$ is the bus admittance matrix (3N×3N); $\mathbf{i}_{inj,n}$,$\mathbf{v}_n$ are vectors (3×1) of three-phase net current injection and voltage phasor at bus n, respectively; $\mathbf{Y}_{nm}$ is the (n,m)-th element of $\mathbf{Y}_{BUS}$. By using the same notation from (2.1)-(2.2), the diagonal and non-diagonal parts of $\mathbf{Y}_{BUS}$ can be calculated as [42]:

$$\mathbf{Y}_{nn} = \sum_{m \in \aleph_n} \mathbf{y}_{nm}^{(n)}, \mathrm{n} \in \aleph \tag{2.17}$$

$$\mathbf{Y}_{nm} = -\mathbf{y}_{nm}^{(m)}, \mathrm{m} \in \aleph_n \tag{2.18}$$

where $\aleph$ is the set of buses in the network; $\aleph_n$ is the set of neighboring buses to bus n. Here, the shunt components of the transmission line and transformer models are already added to their corresponding diagonal elements.

The expression of the generic element $\mathbf{Y}_{nm}$of the bus admittance matrix $\mathbf{Y}_{BUS}$ is:

$$\mathbf{Y}_{nm} = \begin{bmatrix} G_{nm}^{aa} + jB_{nm}^{aa} & G_{nm}^{ab} + jB_{nm}^{ab} & G_{nm}^{ac} + jB_{nm}^{ac} \\ G_{nm}^{ba} + jB_{nm}^{ba} & G_{nm}^{bb} + jB_{nm}^{bb} & G_{nm}^{bc} + jB_{nm}^{bc} \\ G_{nm}^{ca} + jB_{nm}^{ca} & G_{nm}^{cb} + jB_{nm}^{cb} & G_{nm}^{cc} + jB_{nm}^{cc} \end{bmatrix} \tag{2.19}$$

Note that the relationship between the flow current $\mathbf{i}_{nm}$ in (2.1) and the injection current $\mathbf{i}_{inj,n}$ in (2.16) is abided by KCL at each bus $n \in \aleph$ as follows [42]:

$$\mathbf{i}_{inj,n} = \sum_{m \in \aleph_n} \mathbf{i}_{nm}, \mathrm{n} \in \aleph \tag{2.20}$$

The network topology model will be used for the next section to determine the measurements-state variables model, so-called the measurement model.

2.3.3. MEASUREMENT MODEL

In this study, the primary measurements in the MV distribution grid are the synchronized voltage and current phasors measured by PMU devices. Theoretically, a linear measurement model can be achieved if the state variables and the observed measurements are expressed in a suitable coordinate, either polar or rectangular; there must not

be conventional power measurements, i.e., active and reactive power injections or power flows. However, in this thesis, not every bus is equipped with a PMU device. Therefore, those buses in the HV area are assigned pseudo-measurements as (i) constant voltage phasor at the slack bus, (ii) active and reactive power injections for simplicity and to ensure full observability. The mixed set of the phasor and the conventional measurements cause the measurement model to become non-linear because of the non-linear relationship between the non-phasor measurements and the system states [7]. In this thesis, the state variables in the network with N buses are expressed in polar coordinates.

$$\mathbf{x} = \left[\mathbf{V}_1^{a,b,c}, ..., \mathbf{V}_i^{a,b,c}, ..., \mathbf{V}_N^{a,b,c}, \boldsymbol{\delta}_1^{a,b,c}, ..., \boldsymbol{\delta}_i^{a,b,c}, ..., \boldsymbol{\delta}_N^{a,b,c}\right]^T, \mathrm{i} \in \aleph \tag{2.21}$$

where

$$\mathbf{V}_i^{a,b,c} = [V_i^a, V_i^b, V_i^c] \tag{2.22}$$

$$\boldsymbol{\delta}_i^{a,b,c} = [\delta_i^a, \delta_i^b, \delta_i^c] \tag{2.23}$$

are the magnitude and phase, respectively, of the voltage phasor at bus i in the three-phase a, b, and c; $\aleph$ is the set of buses in the network. Given that the state vector has n state variables and dimension (n×1), the number n is equal to 3·(2N) magnitude and phase of the voltage phasors.

The measurements in the network consist of the bus power injections as the pseudo-measurement, the bus voltage phasors, the branch current phasors. Given there are m measurements in the system, which are expressed as the measurement vector with dimension (m×1):

$$\mathbf{z} = \left[\mathbf{z}_{PQinj}, \mathbf{z}_V, \mathbf{z}_{Iflow}\right]^T \tag{2.24}$$

where

$$\mathbf{z}_{PQinj} = \left[\mathbf{P}_{inj,1}^{a,b,c}, ..., \mathbf{P}_{inj,m_1}^{a,b,c}, \mathbf{Q}_{inj,1}^{a,b,c}, ..., \mathbf{Q}_{inj,m_1}^{a,b,c}\right]^T \tag{2.25}$$

$$\mathbf{z}_V = \left[\mathbf{V}_1^{a,b,c}, ..., \mathbf{V}_{m_2}^{a,b,c}, \boldsymbol{\delta}_1^{a,b,c}, ..., \boldsymbol{\delta}_{m_2}^{a,b,c}\right]^T \tag{2.26}$$

$$\mathbf{z}_{Iflow} = \left[\mathbf{I}_1^{a,b,c}, ..., \mathbf{I}_{m_3}^{a,b,c}, \boldsymbol{\theta}_1^{a,b,c}, ..., \boldsymbol{\theta}_{m_3}^{a,b,c}\right]^T \tag{2.27}$$

are, respectively, the measurement vectors composed of (i) 3·($2m_1$) active and reactive power injections; (ii) 3·($2m_2$) magnitudes and angles of the bus voltage; (iii) 3·($2m_3$) magnitudes and angles of the branch. Note that the number of m is equal to 3·($2m_1$)+ 3·($2m_2$)+ 3·($2m_3$).

With the state vector and measurement vector mentioned before, the measurement model of the state estimation represents the link between the measurements and the states and has the equation as the following:

$$\mathbf{z} = \mathbf{h}(\mathbf{x}) + \mathbf{e} \tag{2.28}$$

where $h(\mathbf{x})$ is the non-linear measurement function; $\mathbf{e}$ is the measurement noise vector, which is assumed to be white and Gaussian with zero mean and its covariance matrix $\mathbf{R}$.

$$p(\mathbf{e}) \sim \mathrm{N}(0, \mathbf{R}) \tag{2.29}$$

and can also be written as:

$$E\{\mathbf{e}\} = 0, E\left\{\mathbf{e}\mathbf{e}^T\right\} = \mathbf{R} \tag{2.30}$$

Here, $\mathbf{R}$ is the measurement noise covariance matrix. Each diagonal element of $\mathbf{R}$ is the variance of each measurement, which indicates the uncertainty of the measurement, e.g., sensors from actual PMUs. The off-diagonal elements represent the correlation between the measurements, which is assumed to be negligible in this study.

$$\mathbf{R} = \begin{bmatrix} \sigma_1^2 & & & \\ & \sigma_2^2 & & \\ & & \ddots & \\ & & & \sigma_m^2 \end{bmatrix} \tag{2.31}$$

where σ_i is the standard deviation of each corresponding measurement; m is the number of measurements.

2.3.3.1 MEASUREMENT FUNCTION

The expressions of each type of measurement in terms of the states, i.e., the measurement function $h(\mathbf{x})$, are given below. All measurement functions have to be in terms of the voltage magnitudes and angles (states). The subscripts n and m denote the bus index; the subscripts p and l denote the phase, i.e., phase a, b, or c.

The active and reactive power injection at bus n are expressed as [7]:

$$P_{inj,n}^p = V_n^p \sum_{m=1}^{N} \sum_{l \in \{a,b,c\}} V_m^l (G_{nm}^{pl} \cos\delta_{nm}^{pl} + B_{nm}^{pl} \sin\delta_{nm}^{pl}) \tag{2.32}$$

$$Q_{inj,n}^p = V_n^p \sum_{m=1}^{N} \sum_{l \in \{a,b,c\}} V_m^l (G_{nm}^{pl} \sin\delta_{nm}^{pl} - B_{nm}^{pl} \cos\delta_{nm}^{pl}) \tag{2.33}$$

where $\delta_{nm}^{pl} = \delta_n^p - \delta_m^l$;

The magnitudes and angles of the three-phase branch current phasors flowing on the transmission line between bus n and bus m are expressed as:

$$I_{nm}^p = \left|\underline{I}_{nm}^p\right| = \sqrt{\mathrm{Re}^2\left\{\underline{I}_{nm}^p\right\} + \mathrm{Im}^2\left\{\underline{I}_{nm}^p\right\}} \tag{2.34}$$

$$\theta_{nm}^p = \arctan\frac{\mathrm{Im}\left\{\underline{I}_{nm}^p\right\}}{\mathrm{Re}\left\{\underline{I}_{nm}^p\right\}} \tag{2.35}$$

where $\mathrm{Re}\left\{\underline{I}^{p}_{nm}\right\}$ and $\mathrm{Im}\left\{\underline{I}^{p}_{nm}\right\}$ denote the real and imaginary part of the current phasor $\underline{I}^{p}_{nm}$ between bus n and bus m at phase p. Note that $\underline{I}^{p}_{nm}$ means the current phasor is measured from the side of bus n, while $\underline{I}^{p}_{mn}$ means it is measured from the side of bus m.

Here, since this study utilizes the polar coordinates, $\mathrm{Re}\left\{\underline{I}^{p}_{nm}\right\}$ and $\mathrm{Im}\left\{\underline{I}^{p}_{nm}\right\}$ can be expressed in terms of the voltage magnitudes and angles as [7]:

$$\begin{aligned}\mathrm{Re}\left\{\underline{I}^{p}_{nm}\right\} = &\sum_{l\in\{a,b,c\}}\left[g^{pl}_{nm,L}(V^{l}_{n}\cos\delta^{l}_{n} - V^{l}_{m}\cos\delta^{l}_{m}) - b^{pl}_{nm,L}(V^{l}_{n}\sin\delta^{l}_{n} - V^{l}_{m}\sin\delta^{l}_{m})\right]\\ &+\sum_{l\in\{a,b,c\}}\left[g^{pl}_{nm,T}(V^{l}_{n}\cos\delta^{l}_{n}) - b^{pl}_{nm,T}(V^{l}_{n}\sin\delta^{l}_{n})\right]\end{aligned} \tag{2.36}$$

$$\begin{aligned}\mathrm{Im}\left\{\underline{I}^{p}_{nm}\right\} = &\sum_{l\in\{a,b,c\}}\left[g^{pl}_{nm,L}(V^{l}_{n}\sin\delta^{l}_{n} - V^{l}_{m}\sin\delta^{l}_{m}) + b^{pl}_{nm,L}(V^{l}_{n}\cos\delta^{l}_{n} - V^{l}_{m}\cos\delta^{l}_{m})\right]\\ &+\sum_{l\in\{a,b,c\}}\left[g^{pl}_{nm,T}(V^{l}_{n}\sin\delta^{l}_{n}) + b^{pl}_{nm,T}(V^{l}_{n}\cos\delta^{l}_{n})\right]\end{aligned} \tag{2.37}$$

In order to utilize the measurement function $h(\mathbf{x})$, the function is linearized around a system operating point by executing Taylor series expansion and eliminating high-order terms [54]. Once the non-linear terms are neglected, the Jacobian matrix $\mathbf{H}$ is obtained for the state estimation process.

$$\mathbf{H}(\mathbf{x}) = \frac{\partial h(\mathbf{x})}{\partial \mathbf{x}} \tag{2.38}$$

Considering the available measurements in this study, the Jacobian matrix will be in the form of submatrices:

$$\mathbf{H} = \begin{bmatrix}\mathbf{H}_{PQinj}\\ \mathbf{H}_{V}\\ \mathbf{H}_{Iflow}\end{bmatrix} \tag{2.39}$$

where $\mathbf{H}_{PQinj}$is the submatrix consists of the partial derivatives of the bus active and reactive power injections with respect to the states; $\mathbf{H}_{V}$is the submatrix consists of the partial derivatives of the bus voltage magnitude and angle with respect to the states; $\mathbf{H}_{Iflow}$is the submatrix consists of the partial derivatives of the branch current magnitude and angle with respect to the states.

The first submatrix $\mathbf{H}_{PQinj}$is given by:

$$\mathbf{H}_{PQinj} = \begin{bmatrix}\frac{\partial P_{inj,n}}{\partial V} & \frac{\partial P_{inj,n}}{\partial \delta}\\ \frac{\partial Q_{inj,n}}{\partial V} & \frac{\partial Q_{inj,n}}{\partial \delta}\end{bmatrix} \tag{2.40}$$

The partial derivatives relevant to the active power injections are [7]:

$$\frac{\partial P^{p}_{inj,n}}{\partial V^{l}_{n}} = V^{l}_{n} G^{pl}_{nn} + \sum_{m=1}^{N} V^{l}_{m} \left(G^{pl}_{nm} \cos\delta^{pl}_{nm} + B^{pl}_{nm} \sin\delta^{pl}_{nm} \right) \tag{2.41}$$

$$\frac{\partial P^{p}_{inj,n}}{\partial V^{l}_{m}} = V^{p}_{n} \left(G^{pl}_{nm} \cos\delta^{pl}_{nm} + B^{pl}_{nm} \sin\delta^{pl}_{nm} \right) \tag{2.42}$$

$$\frac{\partial P^{p}_{inj,n}}{\partial \delta^{l}_{n}} = -(V^{l}_{n})^{2} B^{pl}_{nn} + V^{p}_{n} \sum_{m=1}^{N} V^{l}_{m} \left(-G^{pl}_{nm} \sin\delta^{pl}_{nm} + B^{pl}_{nm} \cos\delta^{pl}_{nm} \right) \tag{2.43}$$

$$\frac{\partial P^{p}_{inj,n}}{\partial \delta^{l}_{m}} = V^{p}_{n} V^{l}_{m} \left(G^{pl}_{nm} \sin\delta^{pl}_{nm} - B^{pl}_{nm} \cos\delta^{pl}_{nm} \right) \tag{2.44}$$

The partial derivatives relevant to the reactive power injections are [7]:

$$\frac{\partial Q^{p}_{inj,n}}{\partial V^{l}_{n}} = -V^{l}_{n} B^{pl}_{nn} + \sum_{m=1}^{N} V^{l}_{m} \left(G^{pl}_{nm} \sin\delta^{pl}_{nm} - B^{pl}_{nm} \cos\delta^{pl}_{nm} \right) \tag{2.45}$$

$$\frac{\partial Q^{p}_{inj,n}}{\partial V^{l}_{m}} = V^{p}_{n} \left(G^{pl}_{nm} \sin\delta^{pl}_{nm} - B^{pl}_{nm} \cos\delta^{pl}_{nm} \right) \tag{2.46}$$

$$\frac{\partial Q^{p}_{inj,n}}{\partial \delta^{l}_{n}} = -(V^{l}_{n})^{2} G^{pl}_{nn} + V^{p}_{n} \sum_{m=1}^{N} V^{l}_{m} \left(G^{pl}_{nm} \cos\delta^{pl}_{nm} + B^{pl}_{nm} \sin\delta^{pl}_{nm} \right) \tag{2.47}$$

$$\frac{\partial Q^{p}_{inj,n}}{\partial \delta^{l}_{m}} = V^{p}_{n} V^{l}_{m} \left(-G^{pl}_{nm} \cos\delta^{pl}_{nm} - B^{pl}_{nm} \sin\delta^{pl}_{nm} \right) \tag{2.48}$$

The second submatrix $\mathbf{H}_V$ is given by [7]:

$$\mathbf{H}_V = \begin{bmatrix} \Psi & \Gamma \\ \Lambda & \Phi \end{bmatrix} \tag{2.49}$$

where

$$\Psi^{np,V}_{ml,V} = \begin{cases} 1, \text{ if } n = m \text{ and } p = l \\ 0, \text{ if } n \neq m \text{ or } p \neq l \end{cases} \tag{2.50}$$

$$\Gamma^{np,V}_{ml,\delta} = 0 \tag{2.51}$$

$$\Lambda^{np,V}_{ml,\delta} = 0 \tag{2.52}$$

$$\Phi^{np,\delta}_{ml,\delta} = \begin{cases} 1, \text{ if } n = m \text{ and } p = l \\ 0, \text{ if } n \neq m \text{ or } p \neq l \end{cases} \tag{2.53}$$

In (2.50)-(2.53), the superscripts refer to bus n, phase p, and voltage magnitude V, or voltage angle δ of the PMU measurements. The subscripts refer to bus m, phase l, and voltage magnitude V, or voltage angle δ of the state variables. For example, $\Psi^{np,V}_{ml,V}$is the connection between measurement V_{np} and state V_{ml}.

The third submatrix $\mathbf{H}_{Iflow}$is given by:

$$\mathbf{H}_{Iflow} = \begin{bmatrix} \frac{\partial I_{nm}}{\partial V} & \frac{\partial I_{nm}}{\partial \delta} \\ \frac{\partial \theta_{nm}}{\partial V} & \frac{\partial \theta_{nm}}{\partial \delta} \end{bmatrix} \tag{2.54}$$

The partial derivatives relevant to the current magnitudes are:

$$\begin{aligned} \frac{\partial I^p_{nm}}{\partial V^l_n} &= \frac{\mathrm{Re}\left\{\underline{I}^p_{nm}\right\}}{\left|\underline{I}^p_{nm}\right|}\left[(g^{pl}_{nm,L}+g^{pl}_{nm,T})\cos\delta^l_n-(b^{pl}_{nm,L}+b^{pl}_{nm,T})\sin\delta^l_n\right] \\ &+\frac{\mathrm{Im}\left\{\underline{I}^p_{nm}\right\}}{\left|\underline{I}^p_{nm}\right|}\left[(g^{pl}_{nm,L}+g^{pl}_{nm,T})\sin\delta^l_n+(b^{pl}_{nm,L}+b^{pl}_{nm,T})\cos\delta^l_n\right] \end{aligned} \tag{2.55}$$

$$\begin{aligned} \frac{\partial I^p_{nm}}{\partial V^l_m} &= \frac{\mathrm{Re}\left\{\underline{I}^p_{nm}\right\}}{\left|\underline{I}^p_{nm}\right|}\left[-g^{pl}_{nm,L}\cos\delta^l_m+b^{pl}_{nm,L}\sin\delta^l_m\right] \\ &+\frac{\mathrm{Im}\left\{\underline{I}^p_{nm}\right\}}{\left|\underline{I}^p_{nm}\right|}\left[-g^{pl}_{nm,L}\sin\delta^l_m-b^{pl}_{nm,L}\cos\delta^l_m\right] \end{aligned} \tag{2.56}$$

$$\begin{aligned} \frac{\partial I^p_{nm}}{\partial \delta^l_n} &= \frac{\mathrm{Re}\left\{\underline{I}^p_{nm}\right\}}{\left|\underline{I}^p_{nm}\right|}V^l_n\left[-(g^{pl}_{nm,L}+g^{pl}_{nm,T})\sin\delta^l_n-(b^{pl}_{nm,L}+b^{pl}_{nm,T})\cos\delta^l_n\right] \\ &+\frac{\mathrm{Im}\left\{\underline{I}^p_{nm}\right\}}{\left|\underline{I}^p_{nm}\right|}V^l_n\left[(g^{pl}_{nm,L}+g^{pl}_{nm,T})\cos\delta^l_n-(b^{pl}_{nm,L}+b^{pl}_{nm,T})\sin\delta^l_n\right] \end{aligned} \tag{2.57}$$

$$\begin{aligned} \frac{\partial I^p_{nm}}{\partial \delta^l_m} &= \frac{\mathrm{Re}\left\{\underline{I}^p_{nm}\right\}}{\left|\underline{I}^p_{nm}\right|}V^l_m\left[g^{pl}_{nm,L}\sin\delta^l_m+b^{pl}_{nm,L}\cos\delta^l_m\right] \\ &+\frac{\mathrm{Im}\left\{\underline{I}^p_{nm}\right\}}{\left|\underline{I}^p_{nm}\right|}V^l_m\left[-g^{pl}_{nm,L}\cos\delta^l_m+b^{pl}_{nm,L}\sin\delta^l_m\right] \end{aligned} \tag{2.58}$$

The partial derivatives relevant to the current angles are:

$$\frac{\partial\theta^p_{nm}}{\partial V^l_n} = \frac{\mathrm{Re}\left\{\underline{I}^p_{nm}\right\}}{\left|\underline{I}^p_{nm}\right|^2}\left[(g^{pl}_{nm,L}+g^{pl}_{nm,T})\sin\delta^l_n + (b^{pl}_{nm,L}+b^{pl}_{nm,T})\cos\delta^l_n\right] - \frac{\mathrm{Im}\left\{\underline{I}^p_{nm}\right\}}{\left|\underline{I}^p_{nm}\right|^2}\left[(g^{pl}_{nm,L}+g^{pl}_{nm,T})\cos\delta^l_n - (b^{pl}_{nm,L}+b^{pl}_{nm,T})\sin\delta^l_n\right] \tag{2.59}$$

$$\frac{\partial\theta^p_{nm}}{\partial V^l_m} = \frac{\mathrm{Re}\left\{\underline{I}^p_{nm}\right\}}{\left|\underline{I}^p_{nm}\right|^2}\left[-g^{pl}_{nm,L}\sin\delta^l_m - b^{pl}_{nm,L}\cos\delta^l_m\right] - \frac{\mathrm{Im}\left\{\underline{I}^p_{nm}\right\}}{\left|\underline{I}^p_{nm}\right|^2}\left[-g^{pl}_{nm,L}\cos\delta^l_m + b^{pl}_{nm,L}\sin\delta^l_m\right] \tag{2.60}$$

$$\frac{\partial\theta^p_{nm}}{\partial\delta^l_n} = \frac{\mathrm{Re}\left\{\underline{I}^p_{nm}\right\}}{\left|\underline{I}^p_{nm}\right|^2}V^l_n\left[(g^{pl}_{nm,L}+g^{pl}_{nm,T})\cos\delta^l_n - (b^{pl}_{nm,L}+b^{pl}_{nm,T})\sin\delta^l_n\right] - \frac{\mathrm{Im}\left\{\underline{I}^p_{nm}\right\}}{\left|\underline{I}^p_{nm}\right|^2}V^l_n\left[-(g^{pl}_{nm,L}+g^{pl}_{nm,T})\sin\delta^l_n - (b^{pl}_{nm,L}+b^{pl}_{nm,T})\cos\delta^l_n\right] \tag{2.61}$$

$$\frac{\partial\theta^p_{nm}}{\partial\delta^l_m} = \frac{\mathrm{Re}\left\{\underline{I}^p_{nm}\right\}}{\left|\underline{I}^p_{nm}\right|^2}V^l_m\left[-g^{pl}_{nm,L}\cos\delta^l_m + b^{pl}_{nm,L}\sin\delta^l_m\right] - \frac{\mathrm{Im}\left\{\underline{I}^p_{nm}\right\}}{\left|\underline{I}^p_{nm}\right|^2}V^l_m\left[g^{pl}_{nm,L}\sin\delta^l_m + b^{pl}_{nm,L}\cos\delta^l_m\right] \tag{2.62}$$

2.3.4. PROCESS MODEL

The process model is used to represent the time evolution of the system states as a function of the previous states, the process noise, and the controllable input (if any). The process model, also was called the dynamic model [22], [24], can be utilized only by the particular type of state estimators that can predict the states by modeling their time evolution, such as the Kalman filter (KF) based SE [7]. On the other hand, the static SE (SSE) utilizes only the measurement model for the present measurement set; therefore, it can estimate only the present states due to the lack of forecasting capability. For the particular case of this study, the process model can be formulated as the state space representation for discrete time-variant systems as follows [7], [11], [25], [46]:

$$\mathbf{x}_k = \mathbf{F}_{k-1}\mathbf{x}_{k-1} + \mathbf{g}_{k-1} + \mathbf{w}_{k-1} \tag{2.63}$$

where

- k is the time sample.
- $\mathbf{x}_k$ is the (n×1) state vector as noted in (2.21) at the time instance k.
- $\mathbf{F}_{k-1}$ is the (n×n) state transition matrix, which indicates how fast the system states change from the time sample $k-1$ into k.
- $\mathbf{g}_{k-1}$ is the (n×1) state transition vector, which is related to the historic trend behavior that links to the system states at the time k.
- $\mathbf{w}_{k-1}$ is the (n×1) process noise, which represents the model uncertainties.

Two parameters of the matrices $\mathbf{F}_{k-1}$ and $\mathbf{g}_{k-1}$ can be assessed online and offline according to Holt's linear exponential smoothing technique of forecasting [22]. The technique conducts short-term forecasting based on the reducing weights of the previous dataset. The assumption is that the system states are independent and uncorrelated. The process noise $\mathbf{w}_{k-1}$ is assumed to be white and Gaussian with zero mean and covariance matrix $\mathbf{Q}_{k-1}$.

$$p(\mathbf{w}_{k-1}) \sim \mathrm{N}(0, \mathbf{Q}_{k-1}) \tag{2.64}$$

and also can be written as

$$E\{\mathbf{w}_{k-1}\} = 0, E\left\{\mathbf{w}_{k-1}\mathbf{w}_{k-1}^T\right\} = \mathbf{Q}_{k-1} \tag{2.65}$$

Here, $\mathbf{Q}$ is the process noise covariance matrix, and the elements of $\mathbf{Q}$ represent the process model's uncertainties corresponding with each state. Here, $\mathbf{Q}$ is assumed to be diagonal for simplicity in this study.

$$\mathbf{Q} = \begin{bmatrix} \sigma_1^2 & & & \\ & \sigma_2^2 & & \\ & & \ddots & \\ & & & \sigma_n^2 \end{bmatrix} \tag{2.66}$$

where σ_i is the standard deviation of each corresponding process uncertainty; n is the number of states. The matrix $\mathbf{Q}$ can be assessed based on normal operation scenarios. The detailed assessment will be explained in Chapter 4.

2.4. WEIGHTED LEAST SQUARE-BASED STATIC STATE ESTIMATION

This section describes the concept of the weighted least square (WLS), static state estimation (SSE) with PMU measurements, and the process of the WLS-SSE in detail. They are organized into three subsections as follows.

2.4.1. WEIGHTED LEAST SQUARE TECHNIQUE

The weighted least square (WLS) term are used to find a solution for an overdetermined system, i.e., there are more equations than unknowns. In this case, it means that the number of measurements m is more than the number of state variables n in the power system. Suppose an ideal linear measurement model is given as:

$$\mathbf{z} = \mathbf{A}\mathbf{x} \tag{2.67}$$

where $\mathbf{z}$ is the measurement vector (m×1); $\mathbf{A}$ is the linear measurement matrix (m×n); $\mathbf{x}$ is the state vector (n×1). Then it can be seen that this equation cannot be solved for the state vector $\mathbf{x}$ due to the overdetermined equations ($m > n$). In practice, the measurement is not ideal (imperfect), and the measurement model is non-linear in this study. The equation (2.67) should be written as:

$$\mathbf{z} = h(\mathbf{x}) + \mathbf{e} \tag{2.68}$$

where $\mathbf{h}$ is the non-linear measurement function; $\mathbf{e}$ is the noise/error vector of the measurement with dimension (m×1), which has the properties as stated in (2.29) rewritten here as

$$p(\mathbf{e}) \sim \mathrm{N}(0, \mathbf{R}) \tag{2.69}$$

where $\mathbf{R}$ is the measurement noise covariance matrix. The WLS problem is solved based on the assumption that the measurement errors are random, independent, and normally distributed with mean zero and variances in the form of the covariance matrix $\mathbf{R}$. Suppose $\mathbf{R}$ is assumed diagonal for simplicity,

$$\mathbf{R} = \begin{bmatrix} \sigma_1^2 & & & \\ & \sigma_2^2 & & \\ & & \ddots & \\ & & & \sigma_m^2 \end{bmatrix} \tag{2.70}$$

where σ_i is the standard deviation of each corresponding measurement; m is the number of measurements. The objective function $J(\mathbf{x}^+)$ of the power system state estimation is to find the estimated state vector $\mathbf{x}^+$ that minimizes [3]

$$J(\mathbf{x}^+) = \left[\mathbf{z} - h(\mathbf{x}^+)\right]^T \mathbf{R}^{-1} \left[\mathbf{z} - h(\mathbf{x}^+)\right] = \sum_{i=1}^{m} \frac{\left[z_i - h_i\left(\mathbf{x}^+\right)\right]^2}{R_{ii}} \tag{2.71}$$

where $\mathbf{z}$ is the observed measurement vector; $\mathbf{x}^+$ is the estimated state; subscript i is the i_{th} index of the measurements. Note that the difference between the observed measurement $\mathbf{z}$ and the estimated measurement $h\left(\mathbf{x}^+\right)$ is defined as the measurement residual (so-called residual). It can be understood that the aim is to minimize the sum of the squares of the weighted residuals.

Note that if the uncertainty of the measurement is large, a larger corresponding residual is accepted (compared to the residual with smaller uncertainty). Meanwhile, the smaller measurement uncertainty needs the corresponding residual to be small to minimize the objective function.

Since the measurement function h is non-linear, the objective (2.71) has to be minimized recursively by linearizing $h(\mathbf{x})$ at the operating point $\mathbf{x}^j$, where superscript j is the j_{th} number of iteration [3].

$$h(\mathbf{x}) = h\left(\mathbf{x}^j\right) + \mathbf{H}\left(\mathbf{x} - \mathbf{x}^j\right) \tag{2.72}$$

Here, x is the actual state vector; $\mathbf{x}^j$ is the estimated state vector at the j_{th} iteration;$\mathbf{H}$ is the measurement Jacobian matrix, which consists of the first partial derivatives of the h with respect to the state x at the operating point $\mathbf{x}^j$. The iterative solution of (2.71) can be written as [3]:

$$\mathbf{G}\Delta\mathbf{x} = \mathbf{H}^T\mathbf{R}^{-1}\Delta\mathbf{z} \tag{2.73}$$

$$\Delta\mathbf{x} = \mathbf{G}^{-1}\mathbf{H}^T\mathbf{R}^{-1}\Delta\mathbf{z} \tag{2.74}$$

where

$$\Delta\mathbf{x} = \mathbf{x} - \mathbf{x}^j, \Delta\mathbf{z} = \mathbf{z} - h\left(\mathbf{x}^j\right) \tag{2.75}$$

$$\mathbf{G} = \mathbf{H}^T\mathbf{R}^{-1}\mathbf{H} \tag{2.76}$$

Here, $\mathbf{G}$ is known as the gain matrix. The matrix is large, sparse, symmetric, and non-negative definite. The full-network observability can be ensured if the matrix $\mathbf{G}$ is positive definite or the matrix $\mathbf{H}$ has full rank [10]. The inverse of $\mathbf{G}$ represents the covariance of the estimated states. The set of equations given by (2.73)-(2.74) are referred to as the Normal Equations. The solution of $\Delta\mathbf{x}$ can be solved using Gaussian elimination. Note that the equation (2.74) performs one iteration of the conventional WLS filtering. The idea is to set a threshold of $\Delta\mathbf{x}$ so that the WLS filtering can be performed iteratively until the estimate converges and obtain the estimated (filtered) state $\mathbf{x}_k^+$.

2.4.2. STATIC STATE ESTIMATION WITH PHASOR MEASUREMENTS

Traditionally, the available measurements in real-time for SE processing were from a supervisory control and data acquisition (SCADA) system composed of remote terminal units (RTUs) in the substations. The conventional measurements were analog, such as bus voltage magnitude, active and reactive power flow/injection, and branch current magnitude flow. The scanning rate was every two seconds, which took long enough that the system slightly changed into a different state when the scan finished, compared with the old state since start scanning [3]. This is so-called time-skewed. The practical estimators even ran every few minutes due to the limitation of the computational hardware at that time. The concept of "static" is the assumption that the system does not change during the scan. This also depends on how long the scan is and how fast the variation of load and generation during the scan. Static SE (SSE) processes the real-time measurements as snapshots of measurements together with static network data. The static network data indicates that the network has constant parameters (does not change through time) and has basic substation configurations [5].

Nowadays, with the use of synchronized phasor measurements, angle measurements of voltage and current can be included in the SE process as direct measurements. Also,

the scanning rate is significantly faster than the conventional one, which is only tens of milliseconds. This is one step closer to the dynamic and real-time SE thanks to a more sophisticated telemetered system and the time-tagged measurements by Global Positioning System (GPS) [5]. One important issue is that each sampling instant of SE requires the determination of the reference for PMU data since the PMU measurements have the universal time as a reference, unlike the conventional SE that can use a specific bus like the slack bus as a reference. If including the angle measurement without taking the issue of the different references into account, the SE is likely not able to converge. One solution is to install a PMU device at the slack bus to use its angle as the reference for the conventional SE with PMUs [3]. In this work, all the voltage and current angle measurements are subtracted by the reference angle of the slack bus in the real-time simulation before sending them into the SE process. Note that this study utilizes the PMU measurements and the state variables in polar coordinates, not in rectangular, in order to deal with magnitudes and angles of the currents easily. Also, there are some conventional measurements, i.e., pseudo-measurements as power injections at some unobservable buses at HV buses. Therefore, the branch currents and power injections (measurements) are expressed in non-linear functions of the voltage magnitudes and angles (state variables).

2.4.3. WLS-SSE PROCESS

This subsection describes how the algorithm of the WLS-based static SE (WLS-SSE) works using the Normal Equations approach. At each time instance k, the state vector $\mathbf{x}_k$ needs to be initialized to start performing the iterative process for the solution. The initial point to begin usually is the flat voltage profile (also known as the flat start), i.e., all the bus voltages are set at 1 p.u. and in phase with each other [15]. The whole flowchart of the plain WLS-SSE algorithm is shown in Figure 2.4. Each step is explained below.

- **Step 1:** Set the iteration $j = 0$ at the time sample k.
- **Step 2:** Read the latest measurement dataset $\mathbf{z}_k$ from the real-time simulation platform that is streaming the PMU measurements at the refresh rate of 50 Hz.
- **Step 3:** Initialize the state vector $\mathbf{x}_k^j$ as a flat start since the iteration $j = 0$ to prepare to perform the first iteration of the WLS filtering using the Normal Equation.
- **Step 4:** Calculate the measure-state variables $h\left(\mathbf{x}_k^j\right)$. In simple words, calculate the measurements from the state vector $\mathbf{x}_k^j$ and the non-linear function based on Ohm's and Kirchhoff's laws, using the equations (2.32)-(2.35). The measurements are so-called estimated measurements.
- **Step 5:** Calculate the increment of the measurements $\Delta\mathbf{z}_k^j$, which is the difference between the observed measurement set $\mathbf{z}_k$ at **Step 2** and the estimated measurements $h\left(\mathbf{x}_k^j\right)$ at **Step 4**. The more iterations the states have been filtered (estimated), the more convergence of $h\left(\mathbf{x}_k^j\right)$ into $\mathbf{z}_k$.

- **Step 6:** Calculate the measurement Jacobian matrix $\mathbf{H}\left(\mathbf{x}_k^j\right)$ at the operating point of $\mathbf{x}_k^j$. This matrix is not the exact link between the measurements and the states anymore, only an approximation. Also, calculate the measurement noise covariance matrix $\mathbf{R}_k$ based on the received measurements at **Step 2**. $\mathbf{R}_k$ will have to be recalculated when there is a new measurement set.
- **Step 7:** Calculate the gain matrix $\mathbf{G}\left(\mathbf{x}_k^j\right)$. Note that since $\mathbf{H}$ is very sparse, the product will also be sparse. Nonzero elements in $\mathbf{G}$ can be calculated using sparse technique to increase the computational efficiency.
- **Step 8:** Solve the Normal Equation for $\Delta\mathbf{x}_k^j$.
- **Step 9:** Update the state vector $\mathbf{x}_k^{j+1}$ and calculate the absolute value of $\Delta\mathbf{x}_k^j$ to check for the convergence threshold.
- **Step 10:** If the absolute value of $\Delta\mathbf{x}_k^j$ is below the threshold 10^{-5}, the solution is converged. Otherwise, the next iteration is required, so the algorithm repeats from **Step 4** for the new iterative solution.
- **Step 11:** Display the SE results at the time instance k and store them in the database.
- **Step 12:** Move on to the next time sample $k+1$ for a new measurement set and repeat the SE process from **Step 1** again.

Further comments

The WLS-SSE utilized in this thesis is the plain algorithm, which mainly focuses on the matrix formulation to solve the state estimation as an unconstrained optimization problem using PMU data. Apart from the main function, there are more applications of traditional SE. For example, the network topology processor is a SE function used to receive the circuit breaker status from telemetered communication to recognize the present topology of the network. This can be done by constructing the bus-branch model based on the information of the breaker/switch statuses. Another function recommended for SE is bad data detection and identification. Post-estimation processing is used to filter the bad PMU data to prevent it from contaminating the solution. The well-known methods are the Chi-squares test and the largest normalized residual test [4].

It is fundamental to note that the main drawback of the WLS-SSE is the computational burden due to the iterative method. Suppose the gain matrix $\mathbf{G}$ can be calculated as an approximate constant per time sample k. In that case, the step of calculating $\mathbf{G}$ can be done only once (outside the iterative loop in Figure 2.4). This tends to reduce the computational time, but in turn, leads to less accuracy as a trade-off. Another possible solution is to initialize the state vector $\mathbf{x}_k$ as the previous operating point instead of the flat start. This can be considered as the simple tracking SE. Utilizing the latest states will significantly increase the computational speed since fewer iterations are required to converge compared to the flat start. However, suppose there is a sudden change in the power system. In that case, the tracking SE tends to require more iterations or even could not converge in case the present states are dramatically different from the previous states.

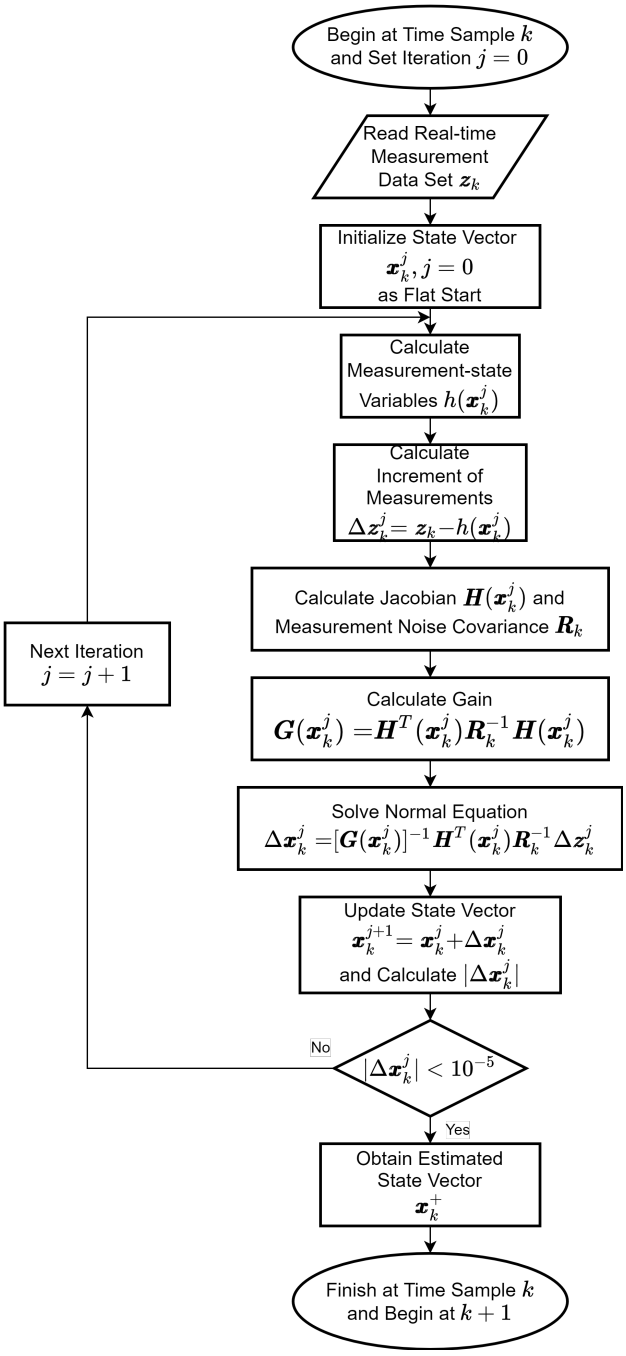

Figure 2.4: Traditional weighted least square (WLS)-based static state estimation (SSE) algorithm.

2.5. EXTENDED KALMAN FILTER-BASED FORECASTING AIDED STATE ESTIMATION

Due to a limitation of the WLS-SSE, dynamic state estimators (DSE) using the Kalman filter (KF) can provide better estimation accuracy. In turn, while the SSE needs only the measurement model, the DSE also needs the process model to represent the time evolution of the power system states. The other limitation of the WLS-SSE is the computational burden issue from the iterative procedure. By using good predictions from the process model to initialize the state vector, the solution from the KF-based SE can be obtained with only one iteration, the so-called "one iteration principle [23]," to assess as fast as possible. This principle can significantly enhance computational performance and thus facilitate real-time applications. As mentioned, it can be seen that the forecasting capability is one of the critical roles that can overcome the limitations from the SE that concentrates only on the present measurements and states.

The Extended Kalman filter (EKF) is a particular type of Kalman filter which deals with non-linear equations, i.e., measurement functions, in terms of the linearized Jacobian matrix, which is the same Jacobian matrix used in the WLS-SSE. The filter has two types of states: the forecasted states and the filtered states. While the SSE conducts only the filtering stage, the EKF-based SE requires two steps to process state estimation: (i) state forecasting, which is a prediction step for the next time sample (ii) state filtering (known as corrector step), where the most recent measurement set is taken into account.

The forecasting-aided state estimation (FASE) is a particular application of the DSE for the quasi-steady state operating conditions in the power system. Here, the changes of the operating point are driven by smooth stochastic variation in the power injections from load and generation while assuming that the dynamics of states are negligible (disregarding transients) [46]. Note that the magnitudes and angles of bus voltage are selected as the state variables from the independent variables related by power flow equations, such as bus load and generation, magnitudes and angles of line flow, and magnitudes and angles of bus voltage. Here, the bus voltages are referred to as the static state of the system and its time evolution as static-state dynamics, which indicates a sequence of stable steady-state operations while neglecting transients [25].

Therefore, the so-called EKF-based FASE is the state estimators that use the EKF technique to solve the non-linear measurement equations for the algebraic state variables that specifically refer to the bus voltage magnitudes and angles. The EKF-FASE formulation consists of the process model and the measurement model, as noted with the notation in (2.63) and (2.28), respectively. The equations are rewritten here.

$$\begin{aligned} \mathbf{x}_k &= \mathbf{F}_{k-1}\mathbf{x}_{k-1} + \mathbf{g}_{k-1} + \mathbf{w}_{k-1} \\ \mathbf{z}_k &= h(\mathbf{x}_k) + \mathbf{e}_k \end{aligned} \tag{2.77}$$

The state $\mathbf{x}_k$ at the time instant k is forecasted from the process model based on the state of previous time $\mathbf{x}_{k-1}$, the transition matrix $\mathbf{F}_{k-1}$, the trend vector $\mathbf{g}_{k-1}$. Then, once the new measurement set $\mathbf{z}_k$ at time k is received, the state $\mathbf{x}_k$ can be solved using the EKF filtering process in the measurement model to obtain the final estimate.

Traditionally, the conventional measurements at each point of time are received from the remote terminal unit (RTUs), which still have some intrinsic limitations such as no

time stamps and low sampling rates from the dynamic point of view. To overcome this, the synchronized measurements from PMU devices are utilized in this study to take one step closer to the dynamic and real-time SE. This following subsection discusses the two stages of state forecasting and filtering, mathematical formulation, and procedures of the FASE.

2.5.1. STATE FORECASTING

By performing conditional expectation on the process model equation (2.63), the relations of the forecasted state vector $\mathbf{x}_k^-$ and its covariance matrix $\mathbf{P}_k^-$ at time sample k are given by [22]

$$\mathbf{x}_k^- = \mathbf{F}_{k-1}\mathbf{x}_{k-1}^+ + \mathbf{g}_{k-1} \tag{2.78}$$

$$\mathbf{P}_k^- = \mathbf{F}_{k-1}\mathbf{P}_{k-1}^+\mathbf{F}_{k-1}^T + \mathbf{Q}_{k-1} \tag{2.79}$$

where $\mathbf{x}_{k-1}^+$ and $\mathbf{P}_{k-1}^+$ are the estimated state vector and its covariance matrix, respectively at time $k-1$. In simple words, this stage predicts the present states from the weighted average of the previous states using Holt's exponential smoothing method. The weight for each set of historical states is exponentially decreased with time. In addition to the prediction of the states, the forecasting error covariance matrix is also calculated.

2.5.1.1 HOLT'S LINEAR EXPONENTIAL SMOOTHING METHOD

Holt's linear exponential smoothing method is a relatively simple technique to do short-term forecasting. Once a reasonable number of datasets is reached, they will be forecasted at the same time. The series of the datasets are smoothed with their trend through two different parameters, α and β, whose values lie between 0 and 1 [22].

Consider $x_{i,k-1}$ is the i_{th} element of the true state vector $\mathbf{x}_{k-1}$ at time sample $k-1$. If $x_{i,k}^-$ and $x_{i,k-1}^-$ are predictions of the state vector at time sample k and $k-1$, respectively, Holt's method expressions are [22]

$$x_{i,k}^- = a_{i,k-1} + b_{i,k-1} \tag{2.80}$$

where $a_{i,k-1}$ and $b_{i,k-1}$reflect the trend of the i_{th} dataset element at time sample $k-1$ towards the forecasted state $x_{i,k}^-$ at time sample k. The parameters are defined as

$$a_{i,k-1} = \alpha_i x_{i,k-1} + (1-\alpha_i)\, x_{i,k-1}^- \tag{2.81}$$

$$b_{i,k-1} = \beta_i \left(a_{i,k-1} - a_{i,k-2}\right) + \left(1-\beta_i\right) b_{i,k-2} \tag{2.82}$$

The equation (2.80) can be rewritten as follows:

$$x_{i,k}^- = F_{i,k-1}\, x_{i,k-1} + g_{i,k-1} \tag{2.83}$$

where

$$F_{i,k-1} = \alpha_i \left(1+\beta_i\right) \tag{2.84}$$

$$g_{i,k-1} = \left[\left(1+\beta_i\right)\left(1-\alpha_i\right)\right] x^-_{i,k-1} - \beta_i a_{i,k-2} + \left(1-\beta_i\right) b_{i,k-2} \tag{2.85}$$

The equation (2.83) can be written in the matrix form and include the process noise $\mathbf{w}_{k-1}$, resulting in the process model in (2.63), which is rewritten here again as:

$$\mathbf{x}_k = \mathbf{F}_{k-1}\mathbf{x}_{k-1} + \mathbf{g}_{k-1} + \mathbf{w}_{k-1} \tag{2.86}$$

where

- $\mathbf{F}_{k-1}$is a (n×n) diagonal matrix with elements of $F_{i,k-1}$defined in (2.84).
- $\mathbf{g}_{k-1}$is a (n×1) vector with elements of $g_{i,k-1}$defined in (2.85).
- $\mathbf{w}_{k-1}$ is white Gaussian sequence with zero mean and covariance $\mathbf{Q}_{k-1}$.

Overall, Holt's technique makes short-term predictions based on the trend of previous states, and it is acknowledged that this technique is very accurate if the power system states change slowly in a stable trend [55].

2.5.2. STATE FILTERING

The objective function $J\left(\mathbf{x}^+\right)$ for the filtering stage is to find the estimated state vector $\mathbf{x}^+$ that minimizes [22]

$$J\left(\mathbf{x}^+\right) = \left[\mathbf{z} - h(\mathbf{x}^+)\right]^T [\mathbf{R}]^{-1} \left[\mathbf{z} - h(\mathbf{x}^+)\right] + \left[\mathbf{x}^+ - \mathbf{x}^-\right]^T [\mathbf{P}^-]^{-1} \left[\mathbf{x}^+ - \mathbf{x}^-\right] \tag{2.87}$$

where the time notation is omitted for simplicity. This means to obtain the estimated state $\mathbf{x}^+_k$, which considers the measurement $\mathbf{z}_k$ and the forecasted state $\mathbf{x}^-_k$ with their covariance matrices $\mathbf{R}_k$ and $\mathbf{P}^-_k$, respectively. The solutions of the objective function for obtaining the estimated state are shown below.

The state forecasting step results in the prediction of system states using the past information when new measurements at time k are not observed yet. After obtaining the new measurements $\mathbf{z}_k$, the states are filtered using the previous forecasted states vector $\mathbf{x}^-_k$ to perform a single iteration filtering based on the EKF technique to obtain the estimated states $\mathbf{x}^+_k$ and its covariance matrix $\mathbf{P}^+_k$ (so-called estimation error covariance matrix) as follows [22]:

$$\mathbf{x}^+_k = \mathbf{x}^-_k + \mathbf{K}_k \boldsymbol{\nu}_k \tag{2.88}$$

$$\mathbf{P}^+_k = [\mathbf{I} - \mathbf{K}_k \mathbf{H}_k]\, \mathbf{P}^-_k \tag{2.89}$$

where $\mathbf{K}_k$ is Kalman gain; $\boldsymbol{\nu}_k$ is the measurement innovation vector (usually called innovations), which is defined as the difference between the forecasted and the observed measurements. It is known that the $\boldsymbol{\nu}_k$ is distributed approximately in Gaussian with zero mean and covariance matrix $\mathbf{S}_k$ [25]. These variables are defined below:

$$\mathbf{K}_k = \mathbf{P}^-_k \mathbf{H}^T_k [\mathbf{S}_k]^{-1} \tag{2.90}$$

$$\boldsymbol{\nu}_k = \mathbf{z}_k - h\left(\mathbf{x}_k^-\right) \tag{2.91}$$

$$\mathbf{S}_k = \mathbf{H}_k \mathbf{P}_k^- \mathbf{H}_k^T + \mathbf{R}_k \tag{2.92}$$

2.5.3. EKF-FASE PROCESS ALGORITHM

This subsection describes how the algorithm of the EKF-based FASE (EKF-FASE) works with the proposed anomaly detection discrimination and identification (ADDI) module. At each time instance k, the estimated state vector and its covariance matrix are needed to be initialized with their previous data at the previous time sample $\mathbf{x}_{k-1}^+$ and $\mathbf{P}_{k-1}^+$. If there is not any previous data, they can be taken from the historical data of the WLS-SSE, i.e., the estimated state and the inverse of the gain matrix, respectively. The whole flowchart of the EKF-FASE algorithm is shown in Figure 2.5. Each step is explained below.

- **Step 1:** Begin at time sample k.
- **Step 2:** Initialize the state vector and its covariance matrix from the previous time sample $\mathbf{x}_{k-1}^+$, $\mathbf{P}_{k-1}^+$.
- **Step 3:** Perform the state forecasting stage by using Holt's exponential smoothing method and the previous state vector $\mathbf{x}_{k-1}^+$. The transition matrix $\mathbf{F}_{k-1}$ and $\mathbf{g}_{k-1}$ provide the trend of the time evolution of the state vector. The weight of the trend decreases exponentially. The more historical time of the data is, the more it will be forgotten; thus, the most recent data will affect $\mathbf{F}_{k-1}$ and $\mathbf{g}_{k-1}$ the most.
- **Step 4:** Read the latest measurement dataset $\mathbf{z}_k$ from the real-time simulation platform that is streaming the PMU measurements at the refresh rate of 50 Hz.
- **Step 5:** Calculate the measurement innovation vector $\boldsymbol{\nu}_k$ and the covariance matrix $\mathbf{S}_k$. The innovation vector is the essential variable for the proposed ADDI module to help recognize (i) whether the system is under abnormal operating conditions, (ii) the type of anomaly in the system.
- **Step 6:** If there is the ADDI module, perform the procedures of state filtering, recognizing and countering the anomaly as presented in Figure 3.1-Figure 3.5 in the next chapter, depending on the selected method of the ADDI algorithm. If there is no ADDI module, perform the EKF filtering (with only one iteration) to obtain the estimated state vector $\mathbf{x}_k^+$ and covariance $\mathbf{P}_k^+$ and move on to the next step.
- **Step 7:** Collect the estimated state vector $\mathbf{x}_k^+$ and covariance $\mathbf{P}_k^+$ to be used at the next time sample $k+1$.
- **Step 8:** Move on to the next time sample $k+1$ for a new measurement set and repeat the process from **Step 1** again.

Further comments

Suppose the power system is operating under normal operations, i.e., steady-state or quasi-steady-state. In that case, the estimation results of the EKF-FASE usually have good accuracy (better than the WLS-SSE) since the input or the trend vector varies slowly. However, if there is a sudden change of states due to sudden load or sudden topology change, the EKF-FASE without the ADDI module will result in poor estimation accuracy. This is because the state transition coefficients cannot adapt immediately but take some time to adjust to a new situation [46]. Therefore, this study proposes the ADDI module for the EKF-FASE to overcome the issue. When the system is under abnormal operating conditions, the ADDI module can deal with different types of anomaly by applying countermeasures to prevent the estimation result from becoming inaccurate. The detailed procedures of the ADDI algorithm are introduced in Chapter 3.

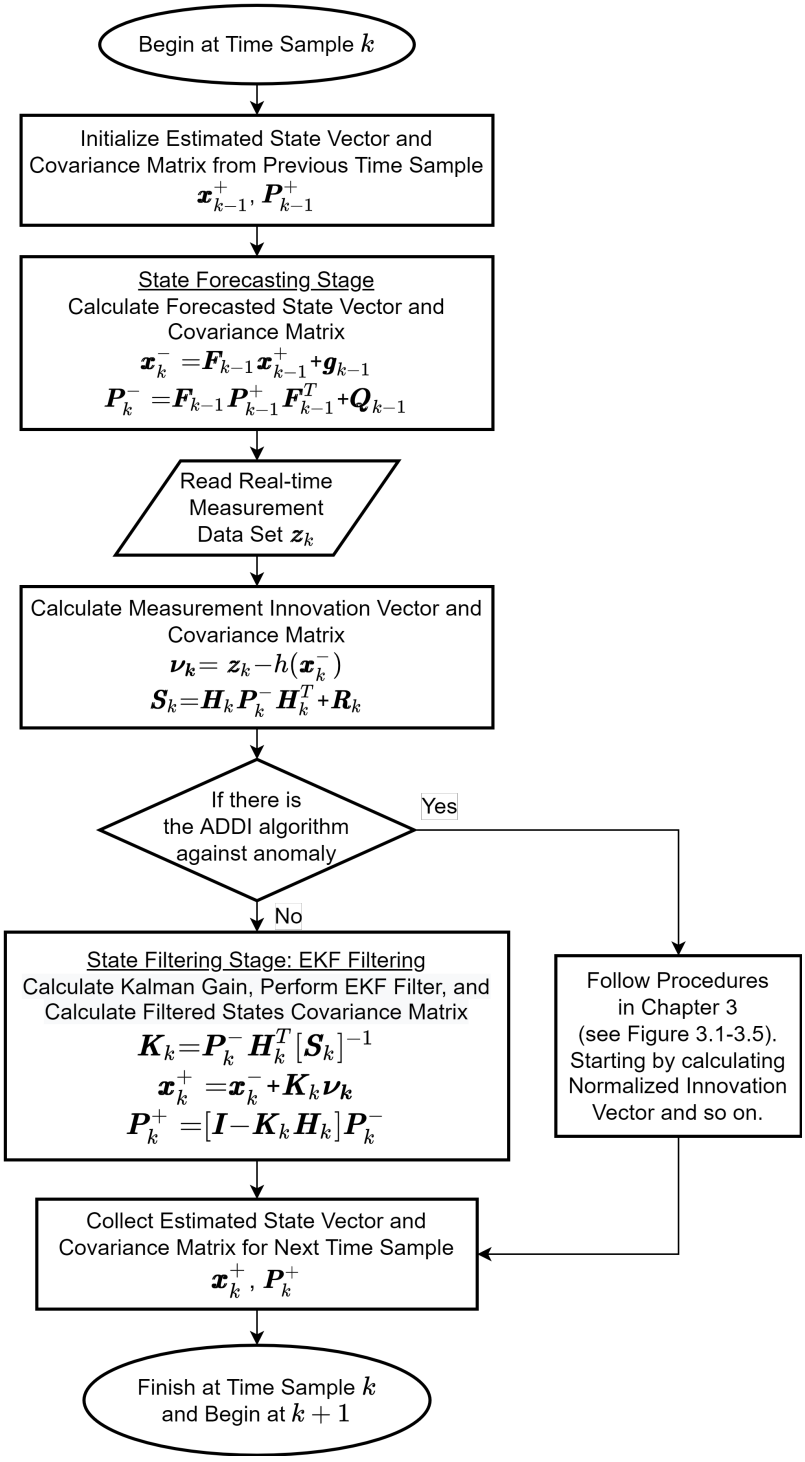

Figure 2.5: Extended Kalman filter (EKF)-based forecasting-aided state estimation (FASE) algorithm with and without the anomaly detection discrimination identification (ADDI) module.

3

Anomaly Detection, Discrimination, and Identification

This chapter elaborates on the adopted procedures for anomaly detection, discrimination, and identification (ADDI). For clarification, detection means recognizing the presence of an anomaly in the measurement set; discrimination means classifying the detected anomaly according to its type; identification means determining which measurements carry the anomaly. Note that the ADDI module was designed to be used with the EKF-FASE and cannot be used directly for the WLS-SSE. By utilizing the prediction results from the state estimator, it can start the algorithm. In the end, the ADDI module will take proper actions, so-called countermeasures, against the anomaly to reduce negative impacts so that the state estimation can remain unbiased.

Section 3.1 introduces the classification of the anomaly in this study. Section 3.2 explains the concept of detection and discrimination in three different methods. Section 3.3 considers the identification and countermeasures according to the selected method.

3.1. Classification of Anomaly

This section introduces the normal and abnormal operating conditions of the power system, the different types of anomalies in the SE process, and why the anomaly has to be classified in this study.

Typically, as far as the SE is concerned, the power system is assumed to operate under normal operating conditions, known as the quasi-stationary regime. The system operating point changes due to smooth, slow load variations and generation adjustments. But when the power system is under abnormal operating conditions, it means that an unexpected thing happens in the system, such as faults in the network, load curtailments, outages of generators or wind turbines. These events will cause a sudden change of the

system states so that the stable equilibrium operating point of the system moves into another stable point.

For SSE, the estimator can always track the system trajectory since it considers only the filtering step and concentrates only on the present measurements. Hence, the sudden change tends not to affect the estimation accuracy of the SSE. In contrast, for FASE, the sudden change can have negative impacts on the estimation performance, resulting in delayed or inaccurate estimation [19]. The reason is that the estimator also considers the predictions based on the historical data before filtering; and that there are significant differences between the predicted values and the present measurement set during the sudden change. Therefore, to overcome this issue, the sudden change (of states) has to be treated as one type of the anomalies.

Apart from the sudden change, bad data is the other well-known anomaly that can significantly deteriorate the SE performance (for both SSE and FASE). Bad data is defined as erroneous measurements consisting of gross errors that deviate the measured values significantly from their expected values. It can be due to information system malfunctions or incorrect telemetered meter readings [19]. In general, bad data is common in power systems; therefore, detecting and identifying bad data is suggested to be one of the main functions of a state estimator [7]. Hence, this study considered bad data as the other type of anomalies so that it can be discriminated from the sudden change. Then a proper action is taken to eliminate bad data using the proposed ADDI module.

Note that it is suggested that any practical estimator should have an anomaly processor (at least for bad data) rather than having a very high filtering capability estimator, but the estimation result still can be seriously distorted due to having no processor against an anomaly [56].

In this thesis, the anomalies can be classified into two types: sudden change of state variables and bad data, as explained above. The sudden change in the power system is simulated by implementing: (i) an unexpected load change such as disconnection of a large load, or (ii) an abnormal state of operation such as the outage of a wind turbine. The bad data is injected into the system by simulating the gross error in the received measurements to mimic the telemetry noise. In order to reduce the negative impacts from these anomalies, the proposed ADDI algorithm needs to recognize (so-called discriminate) the type of detected anomaly to take action properly. The proposed ADDI procedures are explained in the following two sections: (i) anomaly detection and discrimination in Section 3.2, (ii) anomaly identification and countermeasure in Section 3.3.

Note that it is assumed to neglect the possibility of having bad data at the same time with the sudden change. Also, sudden topology change, incorrect topology information, or errors contained in network parameters are more complicated to deal with [15] and consequently are not under the scope of the thesis.

3.2. ANOMALY DETECTION AND DISCRIMINATION

Since the concept of anomaly detection and discrimination is the essential function of the ADDI algorithm, different methods should be studied and validated by the implementation to see which one has the most efficiency. This section introduces three different methods to detect and classify the anomaly into sudden change or bad data. Two

methods are classified as pre-estimation schemes. The other method is the combination of pre- and post-estimation schemes. The word "pre-estimation" basically means before the estimation. The pre-estimation scheme indicates that it can be performed before the filtering stage of the state estimator. In contrast, the post-estimation scheme indicates that it can be performed after the filtering stage [7]. All three methods utilized in this study will be addressed in Subsection 3.2.1-3.2.2.

3.2.1. PRE-ESTIMATION APPROACH

The pre-estimation schemes of anomaly detection and discrimination consist of statistical procedures by analyzing the innovation vector [7], [56]. The innovation vector can be calculated (analyzed) once the state forecasting of the EKF-FASE is performed. The statistical procedures begin with detecting the presence of an anomaly using the largest normalized innovation test (Subsubsection 3.2.1.1). After that, depending on the method adopted, the skewness of normalized innovations distribution (Subsubsection 3.2.1.2) and/or the skewness to the largest normalized innovation ratio (Subsubsection subsubsection 3.2.1.3) are used to discriminate bad data from the sudden change. The two pre-estimation methods of the ADDI module (Subsubsection 3.2.1.4- 3.2.1.5) display how these statistical bases are utilized for anomaly processing.

3.2.1.1 LARGEST NORMALIZED INNOVATION TEST

It is possible to detect the presence of anomalies by conducting an innovation analysis [11]. The principle is based on statistical characteristics of the normalized innovation vector $\boldsymbol{\tau}$ which the i_{th} element is defined as the following:

$$\boldsymbol{\tau}_k(i) = \frac{\boldsymbol{\nu}_k(i)}{\sqrt{\mathbf{S}_k(\mathrm{i,i})}} \tag{3.1}$$

where $\boldsymbol{\nu}_k$ and $\mathbf{S}_k$ are the innovation vector and its covariance matrix, respectively, which are defined in (2.91)-(2.92). Once the normalized innovation vector is calculated, the largest normalized innovation (LNI) can be determined as:

$$LNI_k = \max_i |\boldsymbol{\tau}_k(i)| \tag{3.2}$$

This will be compared with the threshold γ_a. If $\mathrm{LNI}_k > \gamma_a$, the presence of anomaly is detected.

3.2.1.2 SKEWNESS OF DISTRIBUTION OF NORMALIZED INNOVATIONS

Skewness is a measure of asymmetry level in the distributions. When skewness is closer to the zero value, the distribution is more symmetrical, and vice versa. This property of skewness for normalized innovations distribution can be used to discriminate bad data from sudden change since the presence of bad data can shift the distribution of the normalized innovations far away from symmetry. In contrast, under sudden change, the distribution will remain symmetrical. The skewness is defined as follows [9], [19], [55]:

$$\psi_k = \frac{M_{3,k}}{\rho_k^3} \tag{3.3}$$

where M_3 is the third central moment; ρ is the standard deviation of the distribution. They can be obtained as follows:

$$M_{3,k} = E\left\{(\boldsymbol{\tau}_k)^{\cdot *3}\right\} - 3\mu_k E\left\{(\boldsymbol{\tau}_k)^{\cdot *2}\right\} + 2\mu_k^3 \tag{3.4}$$

$$\rho_k^2 = E\left\{(\boldsymbol{\tau}_k)^{\cdot *2}\right\} - \mu_k^2 \tag{3.5}$$

$$\mu_k = E\{\boldsymbol{\tau}_k\} \tag{3.6}$$

where the operator $.*b$ is an element-wise exponentiation for a vector base with the power b. The calculated skewness is tested against threshold ζ. If $\psi_k > \zeta$, the anomaly is recognized as bad data; otherwise, the system is affected by the sudden change. In this thesis, to improve conciseness, the skewness of the distribution of normalized innovation is usually referred to as the skewness.

3.2.1.3 SKEWNESS TO THE LARGEST NORMALIZED INNOVATION RATIO

Apart from the skewness of normalized innovations distribution, it is claimed in [55] that the skewness to the largest normalized innovation ratio (SIR), given as:

$$SIR_k = \frac{\psi_k}{LNI_k} \tag{3.7}$$

has a clear threshold to separate bad data and sudden load change. The threshold is defined as $SIR_{th} = min(1/3, 3\sigma_{max})$, where σ_{max} is the maximum of the standard deviations from the measurement uncertainty. If $SIR_k > SIR_{th}$, the anomaly is recognized as bad data; otherwise, it is classified as a sudden change.

3.2.1.4 THE CONVENTIONAL INNOVATION ANALYSIS METHOD (METHOD 1)

The conventional innovation analysis method, referred to as Method 1 in this study, has been used in [9], [19]–[21], [55]. This method utilizes the LNI test and the skewness of the distribution of normalized innovations. The flowchart of Method 1 is presented in Figure 3.1. The aim is to detect and recognize the type of anomaly for further identification and countermeasure. Four steps of the flowchart are described below.

- **Step 1:** From Figure 2.5, once the state forecasting stage is performed and the innovation vector and its covariance matrix are calculated, the normalized innovation vector $\boldsymbol{\tau}_k$ at time k is calculated using the equation (3.1).
- **Step 2:** Run the LNI test by comparing the maximum of the absolute value of the normalized innovations with the threshold γ_a. If the value exceeds the threshold, the presence of anomaly is detected, and move on to the next step. Otherwise, the system is under normal operations and move on to the number 1 in Figure 3.4.
- **Step 3:** Calculate the skewness value using the equation (3.3).

- **Step 4:** Run the skewness test by comparing the skewness value with the threshold ζ. If the skewness exceeds the threshold, the anomaly is classified as bad data since the skewness of the distribution is distorted with respect to the symmetrical distribution. Then, move on to the number 2 in Figure 3.4. Otherwise, the sudden load change is recognized since the skewness is small. This indicates that the distribution of the normalized innovations is still symmetrical with different mean and variance. Then, move on to the number 3 in Figure 3.4 for further identification and countermeasure.

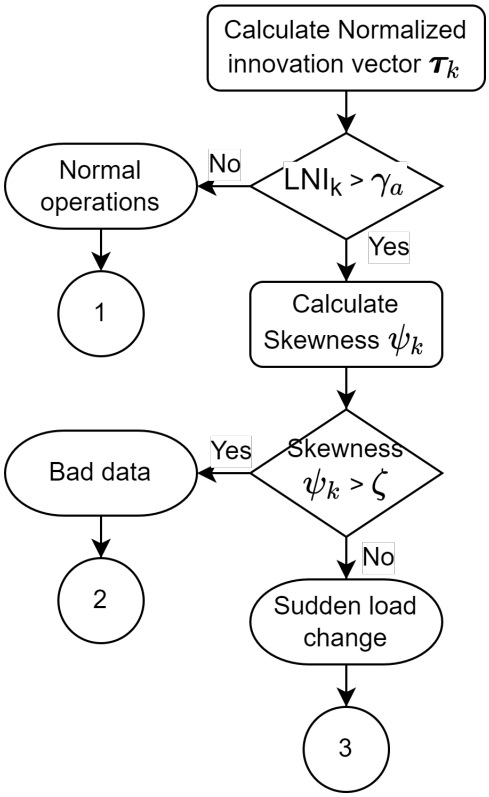

Figure 3.1: The flowchart of anomaly detection and discrimination using the conventional innovation analysis method (Method 1).

3.2.1.5 THE IMPROVED INNOVATION ANALYSIS METHOD (METHOD 2)

The second method is the improved innovation analysis method, referred to as Method 2 in this study. This technique has been proposed by [55] to classify the anomaly into bad data, sudden load change, and sudden topology change by using the LNI test, the skewness, and the SIR. Since the sudden topology change is not under this thesis's scope, the detection and discrimination algorithm from [55] is simplified, resulting in the flowchart shown in Figure 3.2. The flowchart of Method 2 aims to detect and recognize the type of anomaly for further identification and countermeasure. Six steps are described below.

- **Step 1:** From Figure 2.5, once the state forecasting stage is performed and the innovation vector and its covariance matrix are calculated, the normalized innovation vector $\boldsymbol{\tau}_k$ at time k is calculated using the equation (3.1).
- **Step 2:** Run the LNI test by comparing the maximum of the absolute value of the normalized innovations with the threshold γ_a. If the value exceeds the threshold, the presence of anomaly is detected, and move on to the next step. Otherwise, the system is under normal operations and move on to the number 1 in Figure 3.4.
- **Step 3:** If there is only one index of the normalized innovations (i.e., one element of the normalized innovation vector $\boldsymbol{\tau}_k$) that exceeds the threshold γ_a, this indicates the presence of a single bad data. Otherwise, move on to the next step. This is because a sudden change and multiple bad data will cause multiple indexes of the normalized innovations to be higher than the threshold.
- **Step 4:** Calculate the skewness value and the SIR using the equation (3.3) and (3.7), respectively.
- **Step 5:** Run the skewness test by comparing the skewness value with the threshold ζ. Similar to Method 1, if the skewness exceeds the threshold, the anomaly is distinguished as bad data. Otherwise, move on to the next step.
- **Step 6:** Run the SIR test by comparing the SIR value against the threshold SIR_{th}. It will be seen from the simulation results that the presence of bad data usually causes the SIR value to be higher than SIR_{th}. Otherwise, the sudden load change is recognized since it is generally characterized by small skewness, resulting in an extremely small SIR value.

After bad data is recognized from **Step 3, 5, or 6,** move on to the number 2 in Figure 3.4. After sudden load change is recognized from **Step 6**, move on to the number 3 in Figure 3.4.

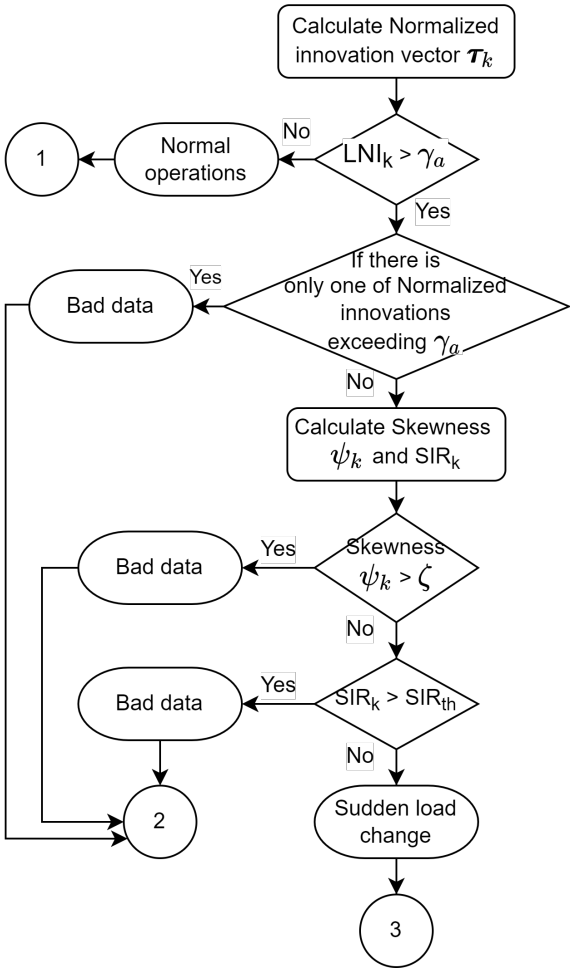

Figure 3.2: The flowchart of anomaly detection and discrimination using the improved innovation analysis method (Method 2).

3.2.2. COMBINATION OF PRE- AND POST-ESTIMATION APPROACH

By including post- into the pre-estimation approaches, the performance of anomaly processing can be improved. Here, this scheme will be referred to shortly as the combined method. It consists of the procedure for using innovation and residual vectors. Since the residuals indicate how well the measurement set fits the network topology model, the analysis based on both innovations and residuals can enhance the reliability and preciseness of anomaly detection and discrimination [7]. However, this advantage can cause an excessive computational burden since the iterative filtering of WLS is always needed.

The first subsubsection introduces the analysis of residuals to confirm the presence of bad data or sudden change. The second subsubsection shows how the combined

method utilizes the innovations and residuals for anomaly processing.

3.2.2.1 LARGEST RESIDUAL TEST

It is possible to validate the presence of an anomaly after the WLS filtering stage using the residual analysis. The residuals indicate the consistency between the observed measurements and the network topology model. By analyzing the residuals, the level of consistency can be determined. Therefore, this can help distinguish the anomalies since bad data causes the measurements to become inconsistent with the network model [7], while the measurements under sudden change can be considered to have full consistency [24]. In order to start conducting the residual analysis, the residual vector, defined as the difference between the observed measurements and the estimated measurement, is calculated as:

$$\mathbf{r}_k = \mathbf{z}_k - h\left(\mathbf{x}_k^+\right) \tag{3.8}$$

where $\mathbf{z}_k$ is the observed measurement vector; $h\left(\mathbf{x}_k^+\right)$ is the estimated measurement vector, calculated by substituting the estimated state into the measurement function h. It is known that $\mathbf{r}_k$ is distributed approximately in white Gaussian with zero mean and covariance matrix $\mathbf{\Omega}_k$ [25]. The $\mathbf{\Omega}_k$ is given by:

$$\mathbf{\Omega}_k = \mathbf{R}_k - \mathbf{H}_k \mathbf{P}_k^+ \mathbf{H}_k^T \tag{3.9}$$

Using (3.8)-(3.9), the normalized residual vector can be calculated according to:

$$\boldsymbol{v}_k(i) = \frac{\mathbf{r}_k(i)}{\sqrt{\mathbf{\Omega}_k(\mathrm{i},\mathrm{i})}} \tag{3.10}$$

Once the normalized residual vector is calculated, the largest normalized residual (LNR) can be determined as:

$$LNR_k = \max_i |\boldsymbol{v}_k(i)| \tag{3.11}$$

This will be compared with the threshold γ_b. If $LNR_k > \gamma_b$, the presence of erroneous data is confirmed and the anomaly is classified as bad data. Otherwise, the sudden change is recognized.

Remark

By substituting the covariance of the estimated states $\mathbf{P}_k^+$ by $[\mathbf{G}_k]^{-1}$, the WLS-SSE can also use the equations (3.8)-(3.11) to run the residual analysis and the LNR test to (i) detect the presence of bad data, and (ii) validate the network topology model because the residuals determine the level of consistency of the measurement set with the network topology model. The two points can be conducted by checking the ideal properties of the normalized residuals of having mean zero and unit variance. This will be shown in the following explanation. Firstly, the relationship between the residuals $\mathbf{r}_k$ and the measurement errors $\mathbf{e}_k$ can be expressed as [15]:

$$\mathbf{r}_k = \mathbf{C}_k \mathbf{e}_k \tag{3.12}$$

where $\mathbf{C}_k = \mathbf{I} - \mathbf{H}_k[\mathbf{G}_k]^{-1}\mathbf{H}_k^T[\mathbf{R}_k]^{-1}$ is known as the residual sensitivity matrix, representing the sensitivity of the residual vector $\mathbf{r}_k$ to the measurement error vector $\mathbf{e}_k$. It can be seen that the residuals are expressed in a linear combination of the measurement errors. Since the elements of the measurement error vector $\mathbf{e}_k$ are assumed to be random independent and normally distributed with mean zero and covariance $\mathbf{R_k}$, i.e., $p(\mathbf{e}_k) \sim \mathrm{N}(0, \mathbf{R}_k)$, the corresponding elements of the residual vector $\mathbf{r}_k$ will have a normal distribution with mean zero and covariance $\mathbf{\Omega}_k$, i.e., $p(\mathbf{r}_k) \sim \mathrm{N}(0, \mathbf{\Omega}_k)$. Finally, after normalizing as in the equation (3.10), the normalized residuals ideally have a normal distribution with mean zero and unit variance [16], i.e.,

$$p(\boldsymbol{\nu}_k) \sim \mathrm{N}(0,1) \tag{3.13}$$

3.2.2.2 THE COMBINED METHOD (METHOD 3)

This method has been used for the distinction of anomalies between sudden change and bad data [11], [24], [56]. Here, it is referred to as Method 3 in this study. There are four steps for each time instant k, as shown in Figure 3.3. The flowchart of Method 3 aims to detect and recognize the type of anomaly for further identification and countermeasure. Each step is explained below.

- **Step 1:** From Figure 2.5, once the state forecasting stage is processed and the innovation vector and its covariance matrix are calculated, the normalized innovation vector $\boldsymbol{\tau}_k$ at time k is calculated using the equation (3.1).
- **Step 2:** Run the LNI test with the threshold value γ_a. If the LNI is larger than the threshold, an anomaly is detected then the algorithm moves on to the next step. Otherwise, the system runs in normal operations, and move on to the number 4 in Figure 3.5.
- **Step 3:** Perform the SSE with the WLS filtering to do the anomaly processing after the filtering stage (so-called post-estimation).
- **Step 4:** Calculate the normalized residuals vector $\boldsymbol{\nu}$ by running the residual analysis using the equation (3.10).
- **Step 5:** Run the LNR test against the threshold γ_b to discriminate the anomaly between sudden load change and bad data. If the LNR is larger than the threshold, the presence of bad data is recognized since bad data causes the measurement set to become inconsistent with the network model, which reflects in a high value of LNR. Then, move on to the number 5 in Figure 3.5. Otherwise, the system is under sudden load change and move on to the number 6 in Figure 3.5.

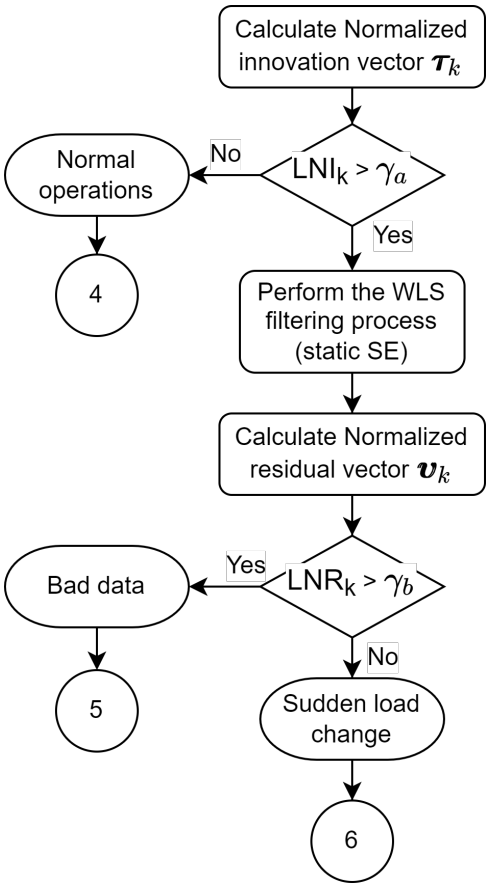

Figure 3.3: The flowchart of anomaly detection and discrimination using the combined methods (Method 3).

3.3. ANOMALY IDENTIFICATION AND COUNTERMEASURES

After the type of the anomaly is determined in Section 3.2, the identification stage is conducted to identify which measurements carry the anomaly in order to counter it appropriately. The methodologies are explained in two parts (depending on the adopted method: Method 1, 2, or 3): using the pre-estimation and combined methods. In each part, there are three scenarios for the adopted state estimator: normal operating conditions, bad data, and sudden load change. The identification methodologies and countermeasures are elaborated as the following.

3.3.1. USING THE PRE-ESTIMATION METHOD (METHOD 1 OR 2)

The system is operating in normal conditions when there is no anomaly detected in the scanned measurements (the number 1 in Figure 3.4). The EKF filtering can be executed directly since all of the measurements are valid.

Suppose the anomaly is recognized as bad data using the pre-estimation method (the number 2 in Figure 3.4). In that case, the PMU measurements corrupted with bad data are identified by finding the measurements associated with the innovations that exceed the threshold γ_a. For example, if the i_{th} element of the innovation vector is higher than γ_a, then the i_{th} innovation (and so the i_{th} measurement) is suspected. To do bad data suppression, all of the identified (suspected) measurements are eliminated simultaneously by substituting them with the corresponding forecasted measurements. Mathematically, the implementation is to set all the suspected innovation values into zero. After removing bad data, the EKF filtering process is executed then the algorithm moves on into the next time instant.

Suppose the anomaly is recognized as sudden load change (the number 3 in Figure 3.4). Only the PMU measurement associated with the LNI is identified to locate the PMU nearest to the bus with the sudden load change event. Then, most importantly, performing the WLS-based SSE instead of the EKF filtering because the predictions of the EKF are unreliable under the sudden change.

3.3.2. USING THE COMBINED METHOD (METHOD 3)

Regarding the case of normal operating conditions (the number 4 in Figure 3.5), the EKF filtering is executed directly. No additional actions are needed.

For the case of bad data recognition (the number 5 in Figure 3.5), the PMU measurements with gross errors are identified by searching for the corresponding measurements that have both the innovations and the residuals under suspicion. If the i_{th} innovation and the i_{th} residual are both higher than γ_a and γ_b, respectively, both the i_{th} innovations and the i_{th} residuals (and so the i_{th} measurement) are suspected. This approach is different from the pre-estimation approaches that identify based on only the suspected innovations. This combined method can be considered a sensitive test because it can overcome the difficulty of detecting and discriminating a small magnitude of bad data (from the other anomalies), which is one of the main problems for an anomaly processing algorithm [23]. Next, the same methodologies of bad data suppression and further countermeasures as the pre-estimation are applied.

Once the anomaly is recognized as sudden load change (the number 6 in Figure 3.5), regarding the countermeasures, there is no need to execute the WLS filtering anymore

because it has been already done during the detection and discrimination stage in Figure 3.3. Therefore, the algorithm only identifies the PMU measurement with the LNI to locate the event, which is the same as in the pre-estimation method, then moves on to the next time sample.

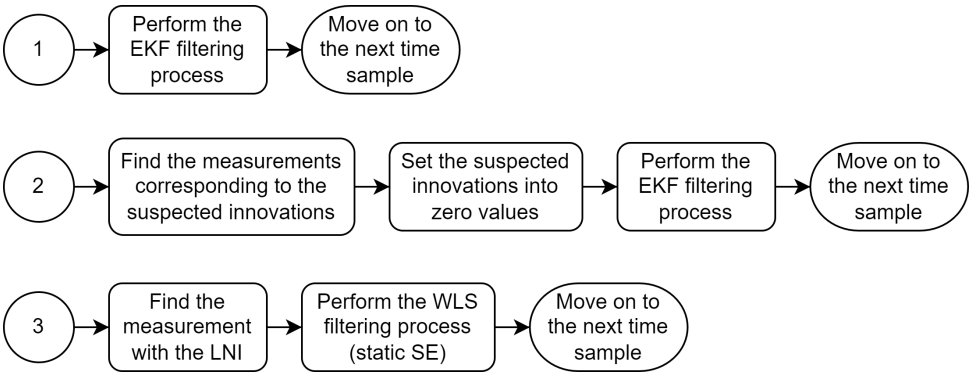

Figure 3.4: The flowchart of anomaly identification and countermeasures for the pre-estimation method (Method 1 or 2).

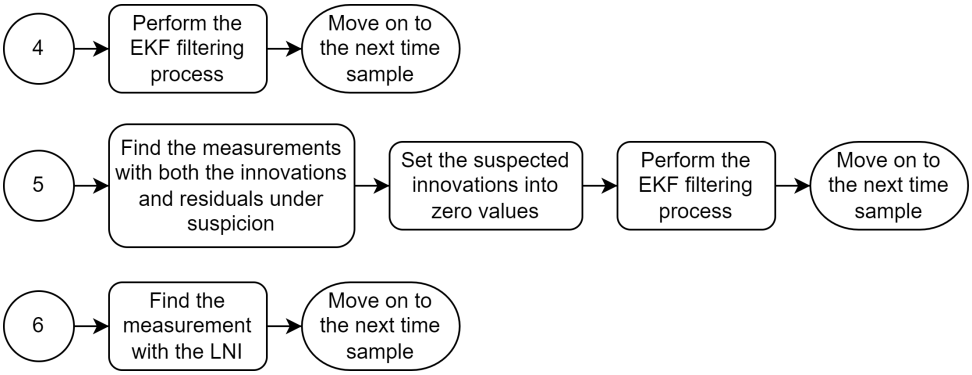

Figure 3.5: The flowchart of anomaly identification and countermeasures for the combined method (Method 3)

4

IMPLEMENTATION ASPECTS

This chapter involves the implementation aspects of how the real-time SE was conducted using our real-time simulation platform, including the schematic of the considered distribution network, the relevant settings of the SE mathematical models for the available measurements, and the performance indices. They are organized into the following sections. Section 4.1 elaborates the test setup and its architecture for real-time SE. Section 4.2 explains the topology of the Enduris MV distribution grid and the measurement configurations utilized in this thesis. Section 4.3 assesses the settings of the measurement and the process noise covariance matrices. Section 4.4 shows the performance indices for evaluating the SE results.

4.1. REAL-TIME EXPERIMENTAL SETUP

Real Time Digital Simulator (RTDS) is capable of simulating very complex and large models in real-time, with a sampling time as low as tens of microseconds. With the integration of distributed generators, the complexity of the power system has grown; therefore, the RTDS is extremely useful to study the dynamics of the system [39]. Figure 4.1 shows the adopted architecture of the real-time experimental setup for SE in the RTDS laboratory at TU Delft, Intelligent Electrical Power Grid (IEPG) group. The setup utilizes two racks from a six-rack RTDS of RTDS Technology Inc. Canada, a phasor data concentrator, a router, and two desktop PCs. In this study, Computer A and Computer B specifications are i7-8750H @ 2.20GHz CPU, 16GB RAM, and i7-9700 @ 3.00GHz CPU, 8GB RAM, respectively.

One desktop PC (Computer A) is used to run RSCAD software to communicate with RTDS via a TCP/IP channel to simulate the real-time power system. Software PMUs (GTNET) by RTDS are utilized to produce the PMU signals obtained from the power system simulation. The software PMUs are synchronized to an accurate time source, e.g., a GPS clock. This is because a GTSYNC card receives the reference clock and ensures the synchronization of the RTDS clock with the GPS reference clock [57]. The precision time protocol (PTP) provided by the GTSYNC card is specified in IEEE Std 1588 v2 [58],

[59]. The refresh rate of the PMUs is set at 50 samples per second or 50 Hz in this study. All of the time-stamped data of PMUs are sent to the phasor data concentrator (PDC) model SEL-5073 via a LAN cable. The received synchronized data is then time-aligned at the PDC before sending it in a single channel to the other desktop PC (Computer B). The synchro-measurement application development framework (SADF) [60] is used in Computer B to receive the online PMU time-series data. The data transfer is according to IEEE Standard C37.118.2-2011 [44]. Meanwhile, the PMU data is processed in real-time by implementing the SE algorithms on MATLAB 2020b. Both algorithms of the SADF and SE are run in parallel by the same computer.

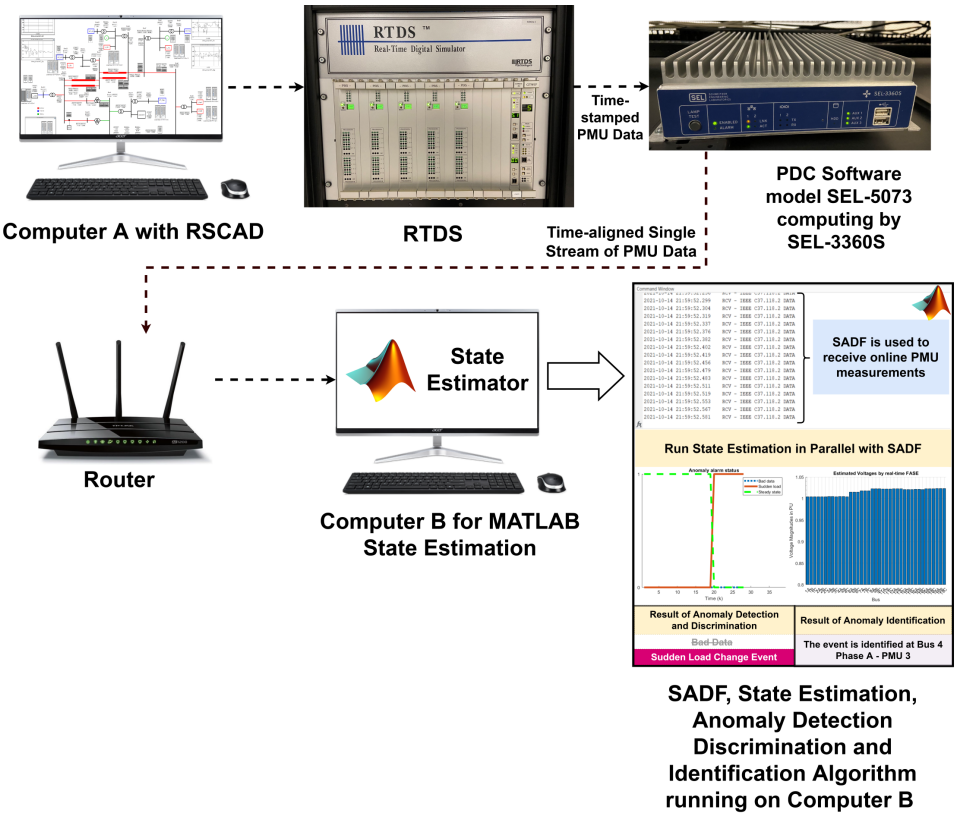

Figure 4.1: Architecture of the real-time experimental setup for state estimation using RTDS.

4.2. REAL-TIME POWER SYSTEM MODEL: ENDURIS MV DISTRIBUTION GRID

In this thesis, the actual 50 kV ring Enduris network located in the southwest of the Netherlands is used as a test benchmark. The Enduris MV grid model is developed in the RSCAD software, which is a graphical user interface software to control the RTDS hardware through Ethernet-based communication. The grid model is divided into two subsystems and simulated in two separate racks of RTDS using 65 us fixed time step. There are ten PB-5 processor cards for each rack. These racks are interconnected using fiber optic cable for inter-rack communication. For simplicity, each wind turbine is modeled with the average model using a permanent magnet synchronous machine (PMSM). Each generator is modeled with a governor and constant excitation system. Each load is modeled with the three-phase balancing.

The measurement configuration of the Enduris network is depicted in Figure 4.2. The 150 kV substation (bus 1) is the slack bus without a PMU device; hence, we assigned bus 1 to have a pseudo-measurement as a constant voltage phasor for the SE measurement model. For the 50 kV area, there are five PMU voltage measurements on every substation at bus 2-6 and six PMU current measurements on the three-phase 50 kV cables. Apart from this, a pseudo measurement of active and reactive power injection at the nominal power and virtual measurements[1] of zero injection[2] are simulated for simplicity and to ensure the full network observability. This thesis will focus on estimating the states at bus 1-6, i.e., all 150 kV and 50 kV substations.

The operation scenario in the schematic is under steady-state on Sunday morning of 17-1-2016 [61]. This scenario will be used as the base operation in this thesis. The three-phase active and reactive power injection values of each bus are depicted. The power injection values (in MW and MVAR) shown in the schematic denote the withdrawn power at a given bus. The positive sign is the consumed power of that bus by the load attached to the bus. In contrast, the negative sign is the generated power into the bus.

4.3. ASSESSMENT OF MEASUREMENT AND PROCESS NOISE COVARIANCE MATRICES

This section involves the settings of the covariance matrices of the measurement noise **R** and the process noise **Q** based on assumptions. The assessment of the **R** and **Q** are essential since they represent the measurement noises and the process noises in the SE models. Therefore, they will directly impact the estimation accuracy since EKF-based FASE optimality depends on a proper assessment of both matrices **R** and **Q** [10]. Meanwhile, only the assessment of **R** affects the WLS-based SSE estimation since it has no process model.

[1] Virtual measurements are measurements with very small uncertainties that are used to approximate the exact information about zero injection buses [10].

[2] Zero injection bus means a bus with no generation and no load attached, so the difference between the net power injected and withdrawn at the bus is zero.

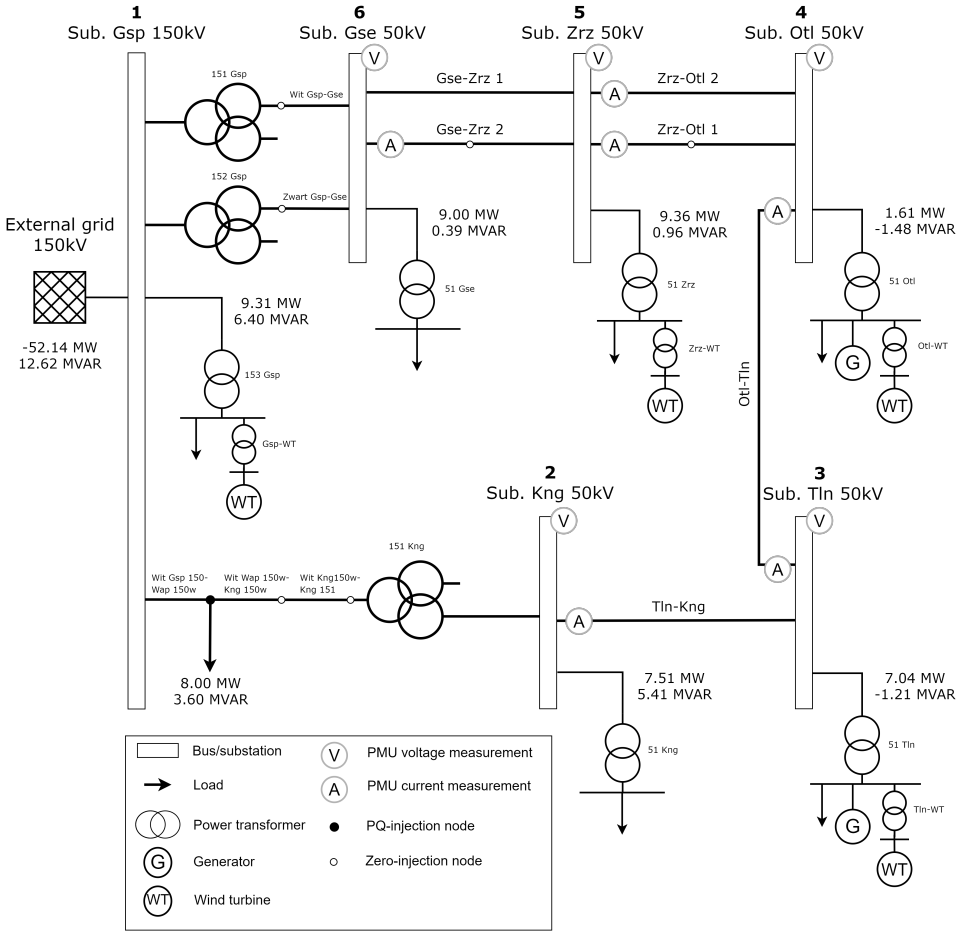

Figure 4.2: The schematic of the Enduris MV distribution grid and the available measurement configurations.

4.3.1. MEASUREMENT NOISE COVARIANCE MATRIX R

As introduced before in Section 2.3.3, **R** represents the uncertainties for each corresponding measurement. They are generally originated from voltage and current sensors and PMU devices installed in a real network. In this thesis, since the PMU data from RTDS is simulated ideally, there is no noise coming from any sensor and PMU device. Since the contribution of the measurement noise to the matrix **R** is not known, the elements of **R** are needed to be tuned experimentally [8]. The noises are simulated as Gaussian distributed random errors with zero mean and have variances associated with the measurement uncertainties, i.e., diagonal elements $\mathbf{R}_{ii}$, from Table 4.1. By adding these random noises to the true measurements (i.e., voltage and current-flow phasors from RTDS), the so-called received/observed measurements are obtained and will be processed in the SE algorithm.

This study uses two common assumptions for the measurement model, as noted in the equations (2.29) and (2.31). Firstly, the measurement errors are Gaussian with zero means [15]. Secondly, the measurements are independent and identically distributed [10]. This implies that there is no correlation between measurements of different PMU devices and the same device; therefore, each measurement has a particular standard deviation. These assumptions make the measurement error covariance matrix $\mathbf{R}_k$ diagonal (subscript k denotes the time sample). The diagonal elements of $\mathbf{R}_k$ represent variances of measurements, i.e., $\boldsymbol{\sigma}_k^2$.

In order to set up the matrix $\mathbf{R}_k$ for the measurement system, we assume that the observed measurement value $\mathbf{z}_k(i)$ represents the mean value of the distribution of the i_{th} measurement. The standard deviation $\boldsymbol{\sigma}_k(i)$ is defined by the error (the so-called uncertainty) of the measurement. Then, the range $\pm 3\boldsymbol{\sigma}_k(i)$ deviation around the mean will cover about 99.7% of the Gaussian distribution. Therefore, for a given maximum measurement error in percentage, i.e., $error_i$ [%], on the mean $\mathbf{z}_k(i)$, the standard deviation for each type of measurement can be calculated. For voltage magnitudes from PMUs, the standard deviation $\boldsymbol{\sigma}_k(i)$ is assessed as [62], [63]:

$$\boldsymbol{\sigma}_k(i) = \frac{error_i\,[\%]}{100} \cdot \frac{\mathbf{z}_k(i)}{3} \tag{4.1}$$

The standard deviation $\boldsymbol{\sigma}_k(i)$ for current magnitudes from PMU and pseudo measurements of power injection can be assessed as [48]:

$$\boldsymbol{\sigma}_k(i) = \frac{error_i\,[\%]}{100} \cdot \frac{\mathbf{z}_k(i)}{3} + k_f \cdot \mathbf{f}(i) \tag{4.2}$$

where k_f is a scaling coefficient; $\mathbf{f}(i)$ is a full-scale meter value. The equation (4.2) is designed in a way to improve estimation accuracy by preventing the standard deviation from being too low if the measurement observes a very light load. This is because a tiny value of the standard deviation can considerably bias the weighting factors of SE, resulting in inaccurate estimation.

Considering a maximum measurement error in rad, i.e., $error_i\,[rad]$, for PMU voltage and current angle measurements, the standard deviation $\boldsymbol{\sigma}_k(i)$ is assessed as:

$$\boldsymbol{\sigma}_k(i) = \frac{error_i\,[rad]}{3} \tag{4.3}$$

Table 4.1 shows the measurement uncertainty for each type of measurement for the equations (4.1)-(4.3). Here, V_{mag} and V_{angle} denote bus voltage magnitude and voltage angle, respectively; I_{mag} and I_{angle} denote branch current magnitude and current angle, respectively. The real-time phasor measurement uncertainties are considered as follows: 3×10^{-3}% for V_{mag}, 3×10^{-5} rad for V_{angle}, 1% for I_{mag}, 2×10^{-1} rad for I_{angle}. It is worth noting that these assigned uncertainties are very small since the synchrophasors standard IEEE Std C37.118-2005 [64] allows a 1% vectorial error in phasor estimation, i.e., a maximum deviation of 1% in amplitude estimation or a maximum deviation of 1 crad (0.01 rad) for phase angle [65]. For pseudo-measurements, the uncertainty for power injection is assigned at typically very high at 20% to substitute a constant value equal to the nominal power. In contrast, the pseudo-measurement of V_{mag} and V_{angle} at bus 1 is assigned the same uncertainty as to the phasor measurements from PMUs since it is the

slack bus; therefore, it is reasonable to consider the voltage phasor of bus 1 as a constant for SE process.

Table 4.1: Measurement uncertainty for each type of measurement.

PMU measurements				Pseudo measurements
V_{mag}	V_{angle}	I_{mag}	I_{angle}	Power Injection
3E-3%	3E-5 rad	1%	2E-1 rad	20%

4.3.2. PROCESS NOISE COVARIANCE MATRIX Q

Q represents the uncertainties of the process model for each state variable. The assessment of **Q** is complicated since the process noise varies when the power system states change over time. For example, a sudden state change will significantly increase the process noise level [48]. If **Q** is fixed and not carefully considered, there can be a considerable error in the EKF-based FASE estimation result. In this thesis, the algorithm of ADDI will be used to cope with this sudden change issue to avoid the complexity of the **Q** assessment and still obtain an accurate estimation. Here, the process noise covariance matrix **Q** is kept constant with diagonal terms equal to 1×10^{-11}. Having only the diagonal elements infers that it is considered no correlation among the process noises of the states. The setting of the diagonal value is selected based on a number of offline simulations to give optimal estimates under the steady-state condition.

It is worth discussing that the adopted uncertainty of the process model at 1×10^{-11} in this work is significantly smaller than other studies at 1×10^{-6} [9], [22], [55]. This is because most of the measurement types of those studies are based on the conventional or SCADA measurements from RTUs, which have significantly higher measurement uncertainties (higher $\mathbf{R}_{ii}$) than the synchronized phasor measurements, e.g., 0.1-0.2% for the conventional voltage magnitude measurement. Hence, if the value of $\mathbf{R}_{ii}$ is low, the $\mathbf{Q}_{ii}$ should also be adopted at a low value for the consistency to reach an optimum point of EKF-based estimation performance under normal operations.

4.4. PERFORMANCE INDICES FOR STATE ESTIMATION

This section presents the indices to assess the proposed state estimation algorithm. By using true, measured, and estimated values, the first performance indicator can be formed as [9], [23], [56]:

$$J_k = \frac{\sum_{i=1}^{m} \left| \mathbf{z}_k^{+}(i) - \mathbf{z}_k^{true}(i) \right|}{\sum_{i=1}^{m} \left| \mathbf{z}_k(i) - \mathbf{z}_k^{true}(i) \right|} \tag{4.4}$$

where m is the number of measurements; $\mathbf{z}_k^{+}(i)$, $\mathbf{z}_k^{true}(i)$, and $\mathbf{z}_k(i)$ represent the estimated, true, and observed values of the i_{th} measurement. The performance index J_k is the overall performance of the filtering process at each time sample k. The numerator

indicates how accurate the estimate can be compared with the true values. The denominator indicates the level of uncertainty on the measurements. A good filtering performance can be confirmed when the index J_k is smaller than one. This infers that the uncertainty level in the observed measurements is reduced after the filtering process. Note that the index J_k is evaluated separately for each measurement type as follows: V_{mag}, V_{angle}, I_{mag}, and I_{angle}. The next performance index, which is calculated by comparing the estimated with actual values, is defined as [9], [66]–[68]:

$$MAE_k = \frac{1}{n}\sum_{i=1}^{n}\left|\mathbf{x}_k^+(i) - \mathbf{x}_k^{true}(i)\right| \tag{4.5}$$

Here, n is the number of state variables; $\mathbf{x}_k^+(i)$ is the estimated (filtered) state vector; $\mathbf{x}_k^{true}(i)$ is the true state vector. The index MAE_k is the mean absolute error at the time sample k, which indicates the estimation error for V_{mag} and V_{angle} states in p.u. and rad, respectively.

5

RESULTS OF REAL-TIME SIMULATIONS

This chapter presents the experimental results from the real-time DSSE implemented into the Enduris MV distribution grid, using our real-time simulation platform. Three different algorithms of DSSE were tested to compare their performance: the traditional WLS-based SSE, the basic EKF-based FASE without the ADDI module, and the proposed EKF-based FASE coupled with the ADDI module. All algorithms conduct SE based on the online synchrophasor measurements from the simulated PMUs in RTDS. The findings are divided into three sections. Section 5.1 considers the SE results under normal operations and validates the network topology model. Section 5.2 displays and analyzes the results of simulating several test cases of anomalies against the ADDI module. Section 5.3 deals with the SE results under abnormal operations considering the ADDI module. For easy understanding of the variables' symbol in this chapter, V_{mag} and V_{angle} denote bus voltage magnitude and voltage angle, respectively; I_{mag} and I_{angle} denote branch current magnitude and current angle, respectively.

5.1. STATE ESTIMATION UNDER NORMAL OPERATIONS

In this work, the normal operation scenarios refer to conditions that there is no anomaly in the power system, such as sudden state change and bad data. In this context, the normal operation is the steady state or the quasi-steady-state operation, whose simulating conditions are explained in Subsection 5.1.1 and 5.1.2, respectively.

5.1.1. STEADY STATE

This subsection is divided into three subsubsections. The first introduces the condition of steady-state operation and how it is simulated. The second shows the validation of the SE network topology model that is reasonably accurate by using the WLS-SSE. Then, it can be confirmed that the model can be used further on the EKF-FASE for more advanced SE algorithms. The third compares the estimation performance under steady-

state between the WLS-SSE and EKF-FASE.

5.1.1.1 OPERATING CONDITIONS UNDER STEADY-STATE

The steady-state operating condition was obtained by simulating the real-time power system (using RSCAD/RTDS) with constant power at every load and generator. As noted earlier in Figure 4.2 from Section 4.2, this scenario came from the actual operating condition of the Enduris MV grid on Sunday morning of 17-1-2016 [61]. The three-phase nominal power injections of each substation and the equipment attached to the substation are shown in Table 5.1 and Table 5.2, respectively. The positive sign of the power is the consumed power, and the negative sign is the generated power into the bus.

Table 5.1: Three-phase Nominal Power Injection at Substations.

Nominal Power Injection of Sub.	Bus 2	Bus 3	Bus 4	Bus 5	Bus 6
Pinj of Sub. (MW)	7.51	7.04	1.61	9.36	9.00
Qinj of Sub. (MVAR)	5.41	-1.21	-1.48	0.96	0.39

Table 5.2: Three-phase Nominal Power of Equipment attached to each Substation.

Nominal Power of Equipment Attached to Each Sub.	Bus 2	Bus 3	Bus 4	Bus 5	Bus 6
P of Load (MW)	7.50	13.00	10.70	20.00	9.00
Q of Load (MVAR)	5.00	1.50	2.50	2.00	0.00
P of Wind Turbine (MW)	-	-3.00	-4.00	-10.80	-
Q of Wind Turbine (MVAR)	-	-0.30	-1.50	-4.00	-
P of Generator (MW)	-	-3.00	-5.00	-	-
Q of Generator (MVAR)	-	-2.00	-2.00	-	-

5.1.1.2 VALIDATION OF NETWORK TOPOLOGY MODEL FOR STATE ESTIMATION

As to the validation of the network topology model, some statistical properties of the normalized residuals from the WLS-SSE have to be investigated and compared to the common theoretical characteristics when the system is under normal operations.

Figure 5.1 and Figure 5.2 show statistics of the distributions of the WLS normalized residuals during the steady-state operation for 1000 time samples. The distributions are shown as box plots[1]. It can be seen that the normalized residuals are mostly within the range 4 and -4 for every measurement type. With this information, the network topology model utilized for SE in this study can be claimed that there are no bad data and topology model errors because the obtained absolute values of normalized residuals are below a common threshold of 3 or 4 [10].

[1]The box plot represents the distribution of the data values. On each box, the horizontal middle bar is the median. The top and bottom edges of the box are the upper and lower quartiles of the data. The ends of the dashed lines are the minimum and maximum [69], [70].

In addition, in order to support the claim, the arithmetic mean and variance were extracted from the data in Figure 5.1 and Figure 5.2, as shown in Figure 5.3 and Figure 5.4, respectively. Ideally, each measurement error is assumed to be independent, having a normal distribution with mean zero and variance $\mathbf{R}_{ii}$. Hence, the distribution of normalized residuals for each measurement should be normal with mean zero and unit variance, as mentioned in the equation (3.13). The findings from Figure 5.3 and Figure 5.4 show that all mean values of the normalized residuals are near zero, except only I_{angle} that has mean values from around -0.25 to -0.35. The possible reason is that the measurement uncertainty settings, i.e., variances $\mathbf{R}_{ii}$, of the corresponding measurement I_{angle} are not perfectly matched with the received current phasor measurement signals. However, the variances of the normalized residuals corresponding to each measurement are approximately one or below. This can be considered that the obtained variances are within the ideal unit variance and that there are no outliers and no topology errors in the system.

It is interesting that the normalized residuals associated with the measurement V_{mag} and V_{angle} at bus 1 have the precise zero mean and zero variance. This is because the voltage phasor measurements at bus 1 (the slack bus) are assumed to be the constant magnitude and angle using the pseudo-measurements since there is no PMU device at the slack bus of the Enduris grid. The zero mean and zero variance confirm that the assigned pseudo-measurements of V_{mag} and V_{angle} at bus 1 are matched and consistent with the actual phasor voltage of the slack bus in the real-time simulation under the steady-state operation scenario.

To summarize, according to the data range, mean values, and variances of the normalized residual distributions under steady-state, it can be claimed that the network topology model utilized in MATLAB for SE is reasonably matched with the actual topology model of the Enduris grid in the RSCAD software.

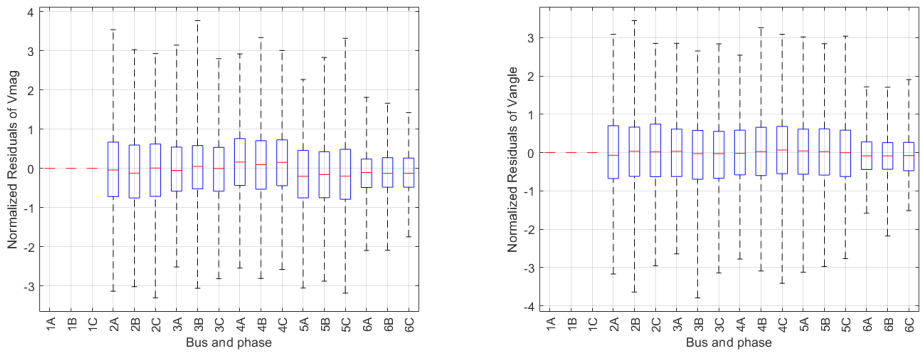

Figure 5.1: Statistics of the distributions of the normalized measurement residuals for V_{mag} (left figure) and V_{angle} (right figure) using the WLS-SSE.

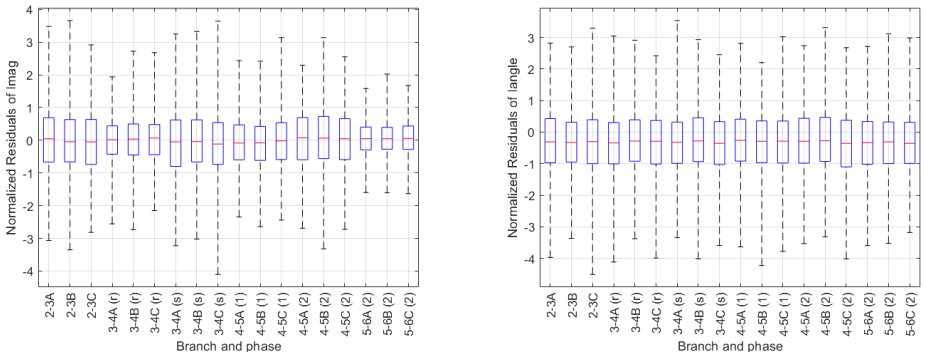

Figure 5.2: Statistics of the distributions of the normalized measurement residuals of I_{mag} (left figure) and I_{angle} (right figure) using the WLS-SSE.

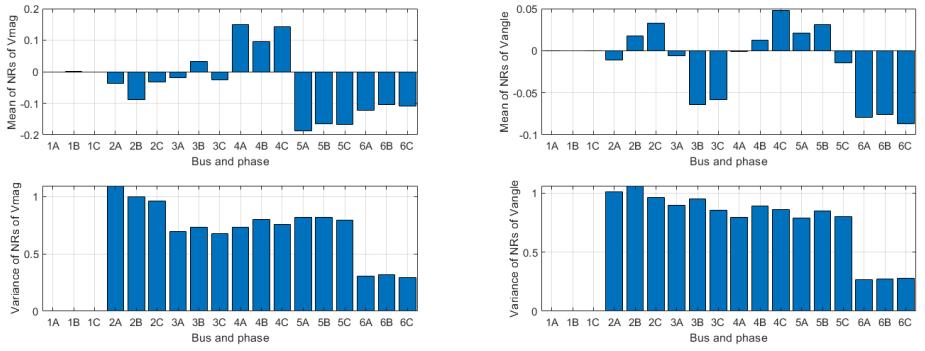

Figure 5.3: Mean and Variance of the distributions of the normalized measurement residuals for V_{mag} (left figure) and V_{angle} (right figure), extracted from Figure 5.1 to make the statistical inference.

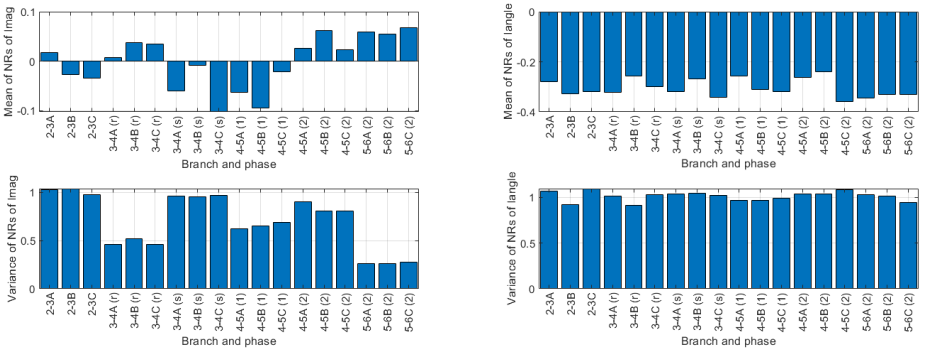

Figure 5.4: Mean and Variance of the distributions of the normalized measurement residuals for I_{mag} (left figure) and I_{angle} (right figure), extracted from Figure 5.2 to make the statistical inference.

5.1.1.3 PERFORMANCE OF STATE ESTIMATION UNDER STEADY-STATE

The comparison of the performance indices J_k and MAE_k between the WLS-SSE and the EKF-FASE algorithm for 7 seconds is displayed in Figure 5.5 and Figure 5.6, respectively. Note that the ADDI module has not been activated yet since the system is under normal operations.

Regarding the index J_k, recalled from Section 4.4 that the J_k indicates the capability of filtering the measurement noise. If J_k is less than one, this means that the SE filtering process is effective, and the noise level in the measurements has been reduced (filtered out). The results in Figure 5.5 show that using the EKF-FASE obtains lower J_k than the WLS-SSE, especially for the state variables V_{mag} and V_{angle}. This infers that the EKF estimator is clearly more efficient than the WLS-SSE in dealing with the random Gaussian noises and estimating the state variables.

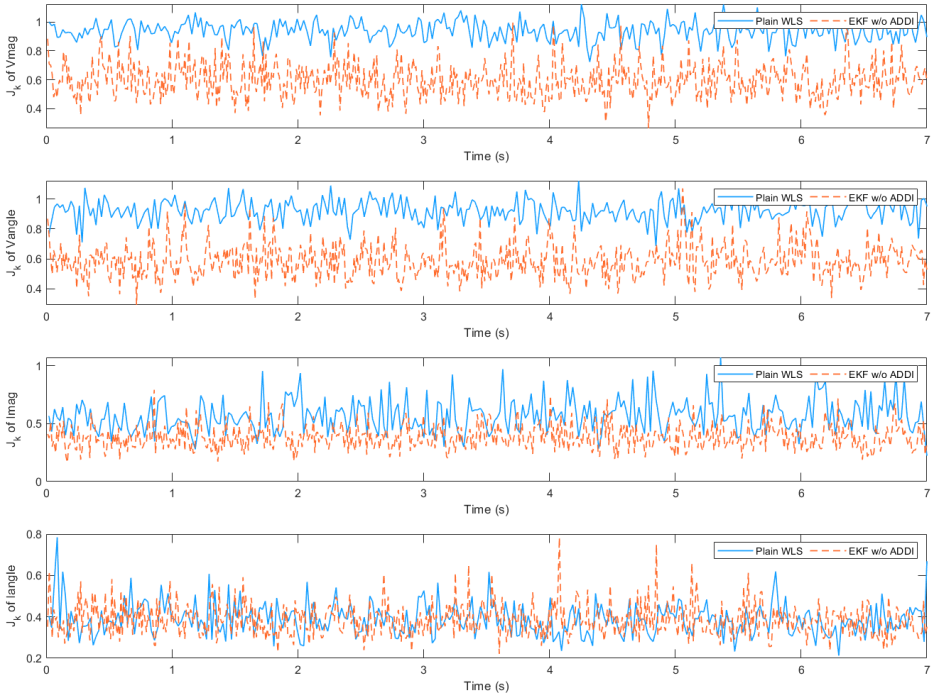

Figure 5.5: Performance indices J_k of V_{mag}, V_{angle}, I_{mag}, and I_{angle} under steady-state.

Regarding the index MAE_k, the MAE_k of V_{mag} and V_{angle} show that the errors are in the order of 1×10^{-6} p.u. and 1×10^{-6} rad (compared with actual values), which are very low. This means that both estimators of the WLS-SSE and EKF-FASE can provide very accurate states of buses 1-6. The lower MAE_k values of V_{mag} and V_{angle} of the EKF than the WLS show that the EKF always reaches higher SE accuracy under the steady-state. The gain is approximately two-fold.

Remark: It is worth mentioning that the EKF can obtain an even higher estimation accuracy if more optimum values of the exponential smoothing parameters, i.e., α and β for the equations (2.84)-(2.85), are selected to produce better predictions from previous measurements. However, no investigation was made to determine the optimal parameters α and β, but the adopted $\alpha = 0.9$ and $\beta = 0.4$ in this study were found to produce adequately good results.

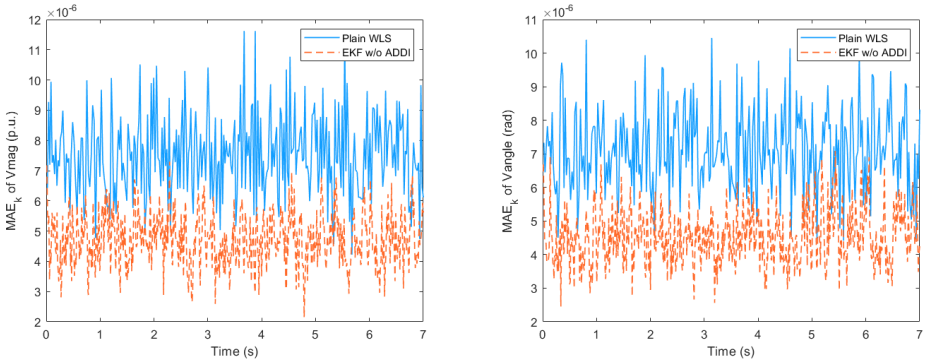

Figure 5.6: Performance indices MAE_k of V_{mag} (left figure) and V_{angle} (right figure) under steady-state.

5.1.2. QUASI-STEADY-STATE

This subsection is divided into three subsubsections. First, the operating condition of the quasi-steady-state is explained. Second, the statistical properties of the normalized innovations are illustrated and analyzed since they are essential properties to determine a threshold for anomaly detection. Third, the performance indices between the WLS-SSE and EKF-FASE are shown and analyzed.

5.1.2.1 OPERATING CONDITIONS UNDER QUASI-STEADY-STATE

The quasi-steady-state condition was simulated by varying the loads attached to substations from the nominal power (shown in Table 5.2 in the previous subsection). The rate of change of load variation is an increasing linear trend in both active and reactive power, including a random fluctuation. The linear slope was given differently for each load group, i.e., 1% for load buses 3-5 and 5% for load buses 2 and 6 over 14 seconds. The added fluctuation is a random number with normal distribution with zero mean and standard deviations: 0.1% of the trend value for load buses 3-5 and 0.15% for load buses 2 and 6. As a result, the power injections at bus 1 and bus 2-6 are shown in Figure 5.7 and Figure 5.8, respectively. Note that each load varied not continuously due to the limited load resolution in RSCAD that has to change the load profile discretely. This is the reason why the gentle slopes for the load variation were selected in this thesis. If a steep slope is set, the ADDI module will see the discrete variation as sudden load changes inevitably, and the quasi-steady-state condition will not be held anymore.

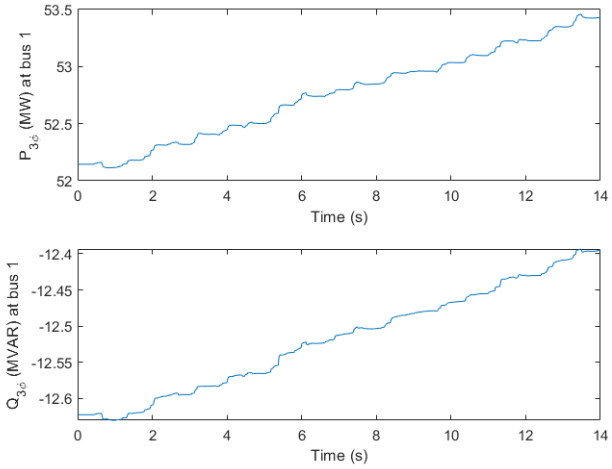

Figure 5.7: Time evolution of the three-phase power injections at bus 1 (the 150 kV substation).

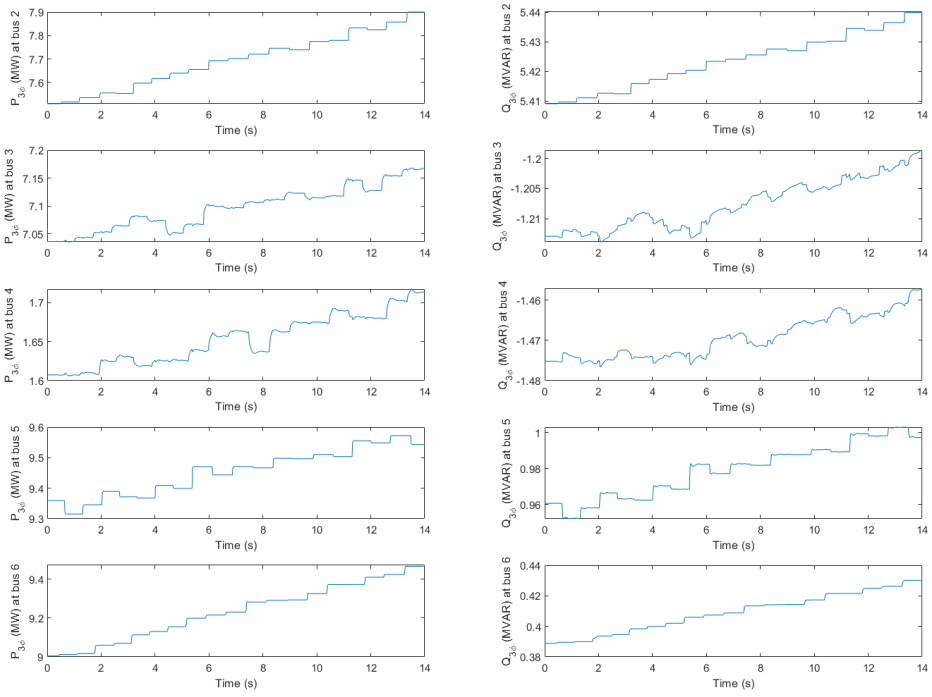

Figure 5.8: Time evolution of the three-phase power injections at bus 2-6 (the 50 kV substations).

5.1.2.2 DISTRIBUTION OF NORMALIZED INNOVATIONS DURING QUASI-STEADY-STATE

This subsubsection shows the statistics of the distributions of the normalized innovations during the quasi-steady-state operation for 1000 time samples. It is crucial to select a proper threshold of normalized innovations to indicate that the system states are under normal operating conditions. The threshold value is fundamental to recognize the presence of an anomaly in the set of received measurements at each time instant (as noted in Section 3.2). Since the results from Figure 5.9 and Figure 5.10 reveal that all of the normalized innovations are between 4.5 and -4.5, the threshold γ_a at 4.5 is selected in this study.

It is important to note that the values of normalized innovations also depend on the value of the adopted $\mathbf{Q}$, which is 1×10^{-11} at diagonals in this study. This is because the normalized innovation vector $\boldsymbol{\tau}$ are calculated from (3.1), which depends on $\mathbf{S}$. The $\mathbf{S}$ is computed by (2.92) depending on $\mathbf{P}^-$, and $\mathbf{P}^-$ depends on $\mathbf{Q}$ from (2.79). Hence, if the value of $\mathbf{Q}$ is reassessed, the range of normalized innovations will change, and a new threshold γ_a has to be reselected based on the new distributions of normalized innovations under normal operations.

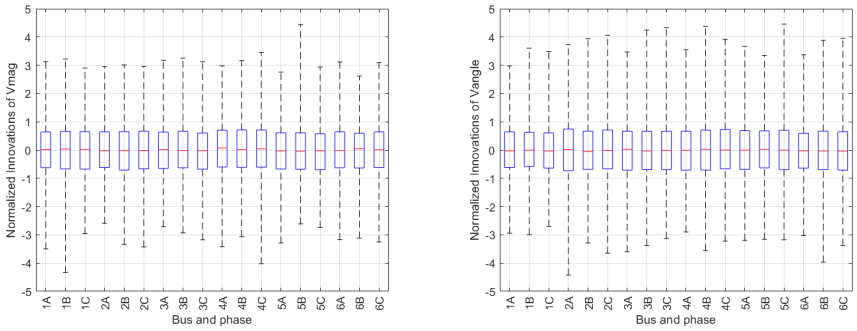

Figure 5.9: Statistics of the distributions of the normalized measurement innovations for V_{mag} and V_{angle} using the EKF-FASE.

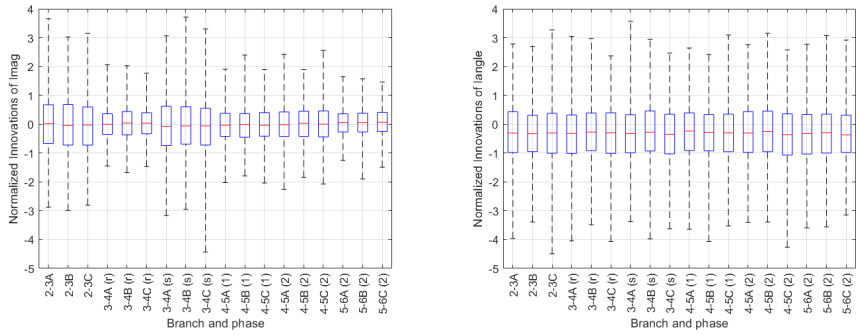

Figure 5.10: Statistics of the distributions of the normalized measurement innovations for V_{mag} and V_{angle} using the EKF-FASE.

5.1.2.3 PERFORMANCE OF STATE ESTIMATION UNDER QUASI-STEADY STATE

Figure 5.11 and Figure 5.12 compare the performance indices J_k and MAE_k between the WLS-SSE and the basic EKF-FASE without ADDI for 14 seconds under quasi-steady-state. Here, the values of J_k are similar to Figure 5.5 under steady-state, except that there are some peaks' values higher than 1 for the EKF estimator (see the orange figures). Since these peaks originated from the inevitable small discrete changes of the load profiles in RSCAD, we can consider neglecting them to avoid misinterpretation of these high-value peaks as sudden load changes.

Regarding MAE_k from buses 1-6 states, it can be seen that the MAE_k of V_{mag} gradually increased, unlike under steady-state. This phenomenon is due to the constant voltage magnitude and angle of the pseudo-measurement at bus 1 (the slack bus). When the power injections gradually varied as the quasi-steady-state conditions, the actual voltage magnitude of the slack bus tended to change slightly; hence, the assumed constant voltage magnitude of the pseudo-measurement leads to a more significant estimation error as long as the power injections varied more through time. By contrast, the MAE_k of V_{angle} is maintained at the same level, similar to the steady-state case. It means that the actual voltage angle at bus 1 has not changed since it is the reference angle for the whole network. All of these arguments are supported by Figure 5.13, showing the actual voltage states compared with their estimate at the slack bus. In addition, Figure 5.14 displays the MAE_k of V_{mag} and V_{angle} calculated by using only buses 2-6 states to infer that the MAE_k of V_{mag} can maintain the same accuracy if not considering the bus 1 states.

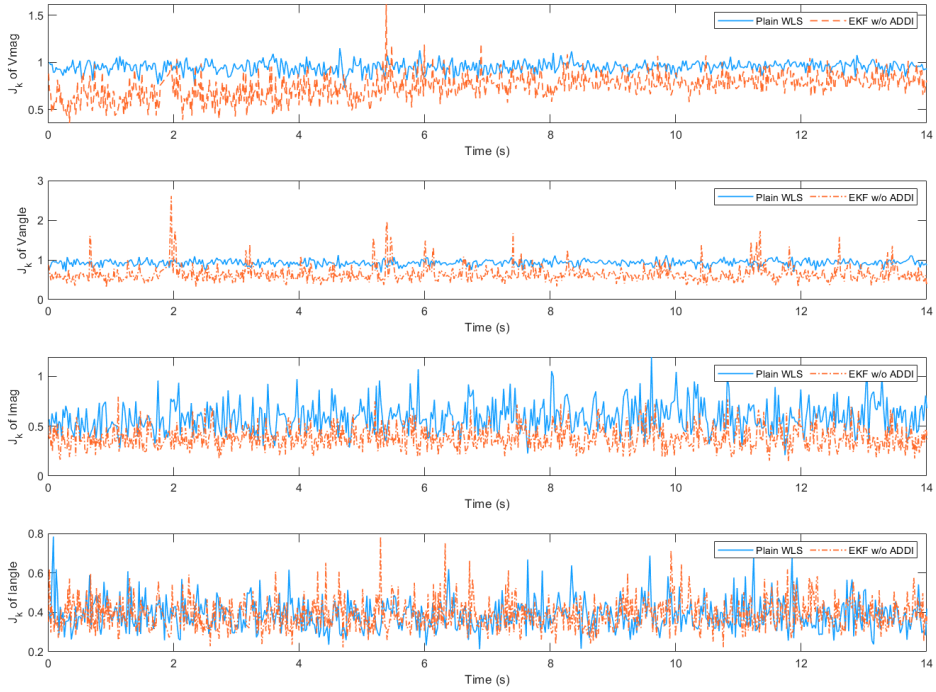

Figure 5.11: Performance indices J_k of V_{mag}, V_{angle}, I_{mag}, and I_{angle} under quasi-steady-state.

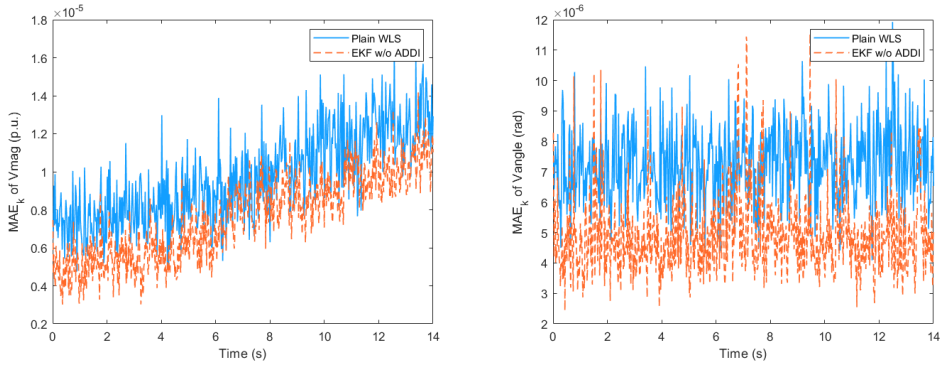

Figure 5.12: Performance indices MAE_k of V_{mag} (left figure) and V_{angle} (right figure) under quasi-steady-state.

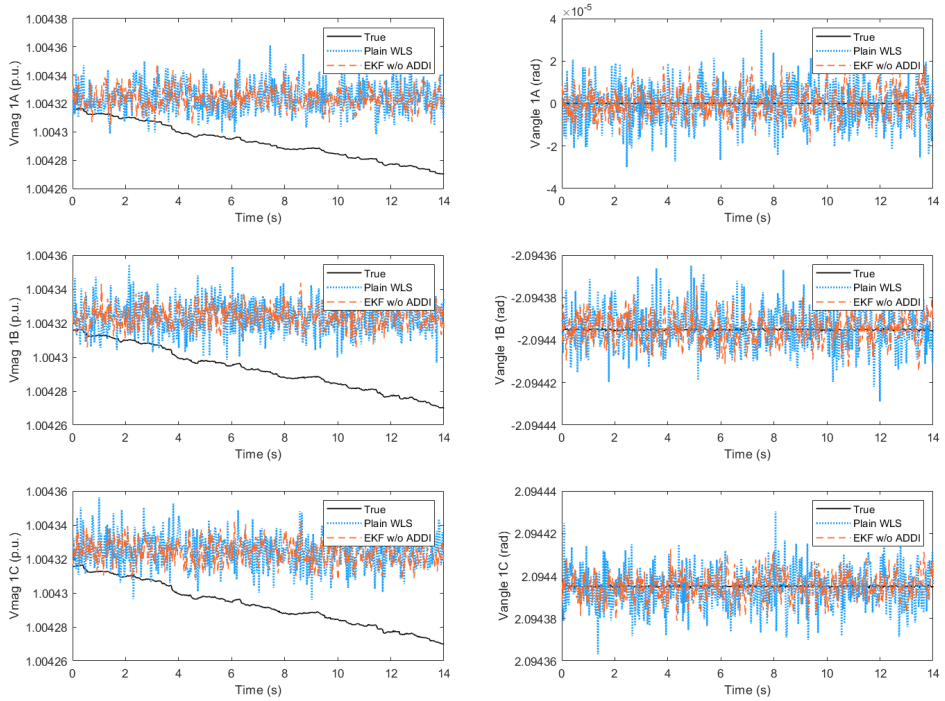

Figure 5.13: True and estimated states of V_{mag} and V_{angle} at bus 1 (the slack bus) phases A, B, and C.

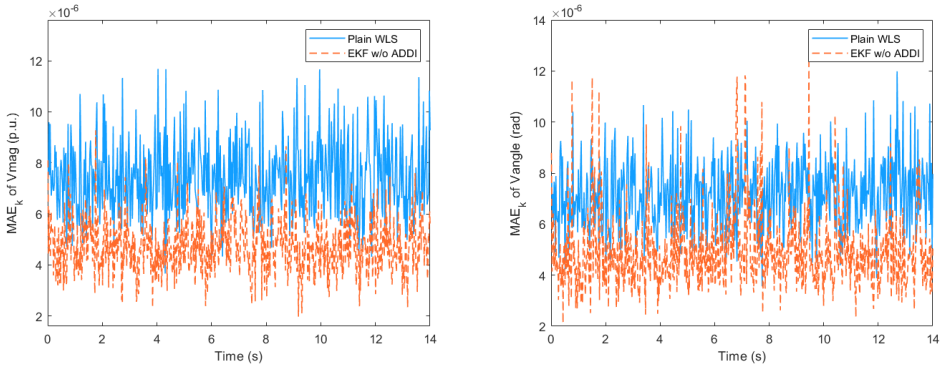

Figure 5.14: Performance indices MAE_k of V_{mag} (left figure) and V_{angle} (right figure) when considering only bus 2-6 states under quasi-steady-state.

5.2. DETECTION, DISCRIMINATION, AND IDENTIFICATION AGAINST AN ANOMALY

This section investigated the results of performing anomaly detection discrimination and identification using three different kinds of methods (i.e., Method 1, 2, and 3) of the ADDI module, as the methodologies presented in Section 3.2. The adopted threshold settings of the criteria are shown and explained in Subsection 5.2.1. The three methods of the ADDI were tested against several levels of anomalies, i.e., sudden load change (Subsection 5.2.2) and single/multiple bad data (Subsection 5.2.3), in order to prove the algorithm's reliability to recognize the anomaly. It will be seen that the proposed ADDI module coupled with the EKF-FASE can classify the anomaly into bad data and a sudden change in the power system. The performances are also compared in terms of computational time for the real-time applicability in Subsection 5.2.4. Note that, in this section, the base scenario is the steady state operating condition for simplicity. All the test cases were simulated by adding the anomaly into the base scenario.

5.2.1. THRESHOLD SETTINGS FOR ANOMALY DETECTION AND DISCRIMINATION

Overall, there are four criteria for anomaly detection and discrimination. Depending on the selected method (i.e., Method 1, 2, or 3), certain criteria are adopted to compare the thresholds with the values resulting from the analysis based on innovations and/or residuals. This subsection explains how the thresholds have been selected in this study, and their values are shown in Table 5.3.

The threshold γ_a for the LNI test is selected to ensure that anomalies will not be detected wrongly in their absence. Regarding the setting, the threshold $\gamma_a = 4.5$ is adopted based on the evaluation of normalized innovations during normal operating conditions (see Figure 5.9-Figure 5.10 from the previous section) [24].

The threshold ζ for the skewness of normalized innovations distribution ψ_k depends on the system [9], particularly the topology and measurement configuration of the network. Its value is also determined based on simulations of a large number of different anomaly scenarios [19]. Based on several test cases of simulations conducted in this study, the value of $\zeta = 3.2$ is selected.

Due to the fact that the σ_{max} in our system is 0.2/3 (current angle measurement accuracy is 0.2 rad, from Table 4.1) the threshold SIR_{th} will be selected from the condition $SIR_{th} = min(1/3, 3\sigma_{max})$. Hence, the threshold is adopted as $SIR_{th} = 0.2$.

The threshold γ_b for the LNR test can be the same value as γ_a for their consistency [23]. Also, it can be adopted from practical experience [11]. Here, the discrimination threshold $\gamma_b = 4.5$ is selected based on the evaluation of normalized residuals during normal operating conditions in this study (see Figure 5.1-Figure 5.2 from the previous section).

Table 5.3: Threshold settings for Method 1, 2, and 3.

Method	Threshold values			
	γ_a	ζ	SIR_{th}	γ_b
Method 1	4.5	3.2	-	-
Method 2	4.5	3.2	0.2	-
Method 3	4.5	-	-	4.5

5.2.2. UNEXPECTED SUDDEN LOAD CHANGE

In order to prove the capacity of the ADDI module against the unexpected sudden changes of states, several test cases of a single sudden load change were applied at different locations and with different intensities (50% and 100% reduction of the nominal power of the load or wind turbine (WT) attached to the bus) by using the RSCAD software. Table 5.4 compares the results of the three ADDI methods to detect and distinguish the sudden load change (from bad data) and identify the most likely location. The findings reveal that all Method 1, 2, and 3 are able to recognize the sudden load change precisely at the first instant of its occurrence. The values of LNI, skewness, SIR, LNR were used to compare with the threshold values depending on each method. When an LNI exceeds the threshold (γ_a = 4.5), the presence of an anomaly is detected, and the ADDI module is triggered to recognize the type of the anomaly for further actions. Concerning Method 1 and 2, as shown in Table 5.4, the skewness and SIR values are below the thresholds (ζ = 3.2 and SIR_{th} = 0.2). Hence, both methods can recognize the anomaly as the sudden load change reliably. Concerning Method 3, the sudden load change can also be discriminated (from bad data) correctly because of the lower values of LNR than the threshold (γ_b = 4.5). In addition, regardless of the method, by finding which measurement corresponds to the LNI, the PMU nearest to the event can be identified/located and reported to the system operator. For instance, as can be seen at the rows of bus 2 from Table 5.4, the measurement V_{angle} 2A is identified to have the LNI; therefore, the operator can realize that the event occurred at or near bus 2.

Further comments

After the identification stage, the proper action will be taken by switching from the EKF-FASE into the WLS-SSE, as mentioned in Section 3.3, to avoid using unreliable predictions. This is because the prediction step from the EKF still relies on the previous estimations (before the sudden change) [9], and there is a considerable difference between the states before and at the time sudden change occurs. Unlike the EKF, the newly adopted WLS filtering considers only the measurements at the present time; therefore, the WLS estimator accuracy will not be affected by the sudden load change.

Table 5.4: Results of discrimination and identification of a sudden load change event.

Bus	Nominal power	Reduction of power	LNI	Skew-ness	SIR	LNR	Identified Meas. with LNI	Mthd. 1	Mthd. 2	Mthd. 3
2	Load 7.5 MW	3.75 MW	344.22	2.54	0.01	2.09	V_{angle} 2A	✓	✓	✓
		7.5 MW	644.89	2.63	0.00	3.08	V_{angle} 2A	✓	✓	✓
3	Load 13 MW	6.5 MW	357.63	2.20	0.00	2.61	V_{angle} 3B	✓	✓	✓
		13 MW	675.22	2.19	0.00	3.19	V_{angle} 3A	✓	✓	✓
	WT 3 MW, 0.3 MVAR	3 MW, 0.3 MVAR	164.92	1.77	0.01	2.53	V_{angle} 3B	✓	✓	✓
4	Load 10.7 MW	5.35 MW	172.87	2.11	0.00	4.46	V_{angle} 4A	✓	✓	✓
		10.7 MW	502.66	2.16	0.00	4.22	V_{angle} 4C	✓	✓	✓
	WT 4 MW, 1.5 MVAR	4 MW, 1.5 MVAR	134.40	1.63	0.00	4.31	V_{angle} 4C	✓	✓	✓
5	Load 20 MW	10 MW	638.05	1.97	0.00	2.58	V_{angle} 5C	✓	✓	✓
		20 MW	940.33	2.07	0.00	3.93	V_{angle} 5A	✓	✓	✓
	WT 10.8 MW, 4 MVAR	10.8 MW, 4 MVAR	676.91	1.62	0.00	3.85	V_{angle} 5A	✓	✓	✓
6	Load 9 MW	4.5 MW	230.70	2.35	0.01	4.00	V_{angle} 6C	✓	✓	✓
		9 MW	363.45	2.39	0.00	3.66	V_{angle} 6A	✓	✓	✓

5.2.3. BAD DATA

This subsection investigated the results of anomaly detection, discrimination, and identification using Method 1, 2, and 3 against single and multiple bad data in order to analyze their capacities. First, single bad data is simulated. Then, it is followed by the multiple bad data simulation.

Several test cases of a single bad data with different magnitudes were simulated on the PMU measurements of V_{mag} and V_{angle} at bus 3 phase A and I_{mag} and I_{angle} at branch 2-3 phase A as shown in Table 5.5. The gross errors in measurements are expressed in terms of the number of measurement standard deviations (σ). The results reveal that the bad data larger than 8σ can be correctly distinguished (from sudden load change) and identified by all Method 1, 2, and 3. This is due to the three bases as the following: first, the LNI values exceed the threshold ($\gamma_a = 4.5$), indicating the presence of the anomaly. Second, regarding Method 1 and 2, the skewness and/or SIR values are higher than the adopted thresholds ($\zeta = 3.2$ and $SIR_{th} = 0.2$), revealing the characterization of bad data. Third, regarding Method 3, the LNR values exceed the threshold ($\gamma_b = 4.5$), showing the characterization of bad data. It should be highlighted that Method 1 wrongly discriminated the two cases of the bad data as the sudden load change. These are gross errors with very small magnitudes (8σ) contained in the measurements of the current magnitude and the current angle. On the contrary, Method 2 correctly recognized and identified them since the skewness values are lower than the threshold ($\zeta =$

3.2), but the SIR values are still high enough against the threshold ($SIR_{th} = 0.2$). Method 3 also correctly recognized and identified the very small bad data (8σ) because the LNR exceeds the threshold ($\gamma_b = 4.5$).

From the findings of Table 5.5, two remarks should be pointed out. First, the criteria SIR in Method 2 can help recognize bad data with very small magnitudes. Second, Method 3 can deal with very small gross errors by directly utilizing both innovations and residuals in the combined scheme. Note that, unlike Method 3, although Method 1 and 2 use only innovations, additional statistic measures are needed to be calculated (i.e., the skewness and/or the SIR) in the pre-estimation scheme.

In order to test the ADDI module against the multiple bad data, the simultaneous presence of the two bad data, as shown in Table 5.6, is simulated. The gross errors have the magnitude of 20σ on the V_{mag} measurement at bus 3 phase A and 8σ on the I_{angle} measurement at branch 2-3 phase A. From the value of LNI, skewness, SIR, LNR, it is apparent that all Method 1, 2, and 3 can recognize and identify the multiple bad data successfully. The corresponding absolute normalized innovations $|\boldsymbol{\tau}(i)|$ to the erroneous measurements were presented as the two peaks in Figure 5.15. The measurement index 49 and 103 are V_{mag} bus 3 phase A and I_{angle} branch 2-3 phase A, respectively. The ADDI module successfully identified the two peaks having the absolute normalized innovations higher than the threshold ($\gamma_a = 4.5$) for further actions.

Further comments

With regard to the countermeasures following the identification step, as noted in Section 3.3, the erroneous measurements will be rejected by substituting them with the associated forecasting measurements. The predicted values come from the process model using Holt's exponential smoothing technique based on previous data. After the countermeasures procedure, the bad data are properly removed from the measurements, and they are ready to be processed at the EKF filtering stage of SE.

Table 5.5: Results of discrimination and identification of a single bad data.

Measurements	BD (σ)	LNI	Skewness	SIR	LNR	Mthd. 1	Mthd. 2	Mthd. 3
V_{mag} 3A	20σ	16.31	6.93	0.42	10.22	✓	✓	✓
V_{mag} 3A	50σ	38.30	9.75	0.25	21.25	✓	✓	✓
V_{angle} 3A	20σ	16.54	5.89	0.45	5.87	✓	✓	✓
V_{angle} 3A	50σ	40.17	9.71	0.25	15.73	✓	✓	✓
I_{mag} 2-3A	8σ	8.50	2.72	0.38	8.19	✗	✓	✓
I_{mag} 2-3A	60σ	58.18	10.44	0.18	70.06	✓	✓	✓
I_{angle} 2-3A	8σ	7.75	2.52	0.34	7.78	✗	✓	✓
I_{angle} 2-3A	45σ	42.88	9.91	0.23	42.91	✓	✓	✓

Table 5.6: Results of the ADDI module test against multiple bad data.

Measurement	BD (σ)	$\|\boldsymbol{\tau}(i)\|$	LNI	Skewness	SIR	LNR
V_{mag} 3A	20σ	18.54	18.54	6.04	0.36	11.67
I_{angle} 2-3A	8σ	6.23				

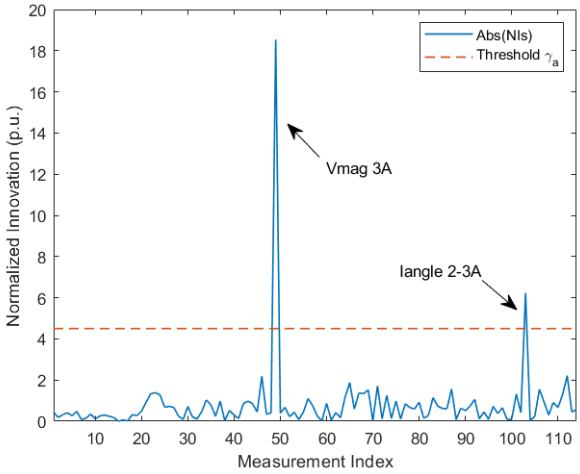

Figure 5.15: Absolute values of normalized innovations when detecting multiple bad data.

5.2.4. COMPUTATIONAL TIME

In this thesis, the power system network and the measurement devices were modeled in RSCAD/RTDS to assess the impact of the latency of the proposed algorithm. The PMU simulated by the RTDS has been set the refresh rate at 50 Hz. In general, there are two types of latencies: the computational time of the algorithm, and the time taken by the data communication system to send the PMU signals from the RTDS to Computer B [39]. Since the latency by the real-time simulation platform is not in the scope of this study, the data transmission is assumed to be ideal and has no latency. Therefore, we will focus on only the latency due to the computational time of the algorithm, which largely depends on the hardware of Computer B running this algorithm (the Computer B specification is already mentioned in Section 4.1).

Table 5.7 compares the average computational time of three algorithms under normal operations: the traditional WLS-based SSE, the basic EKF-based FASE without the ADDI, and the proposed EKF-based FASE coupled with the ADDI algorithm. The processing time starts from receiving the PMU measurements until finishing that time sample (see the flowchart in Figure 2.4 and Figure 2.5).

It is apparent that the WLS is the slowest algorithm since it needs up to four iterations to converge, whereas the EKF-based algorithms can converge within only one iteration. The computational time of the integrated ADDI into the EKF estimator is comparable to the basic EKF. A minimal time period of 3 ms is needed for the ADDI module to scan

for an anomaly (regardless of Method 1, 2, or 3). Note that the processing time of the proposed algorithm is only 13.7 ms; hence, the estimator will not miss any measurement under normal operations since the PMU streaming rate is 20 ms per sample (50 Hz).

Table 5.7: Average computation time under normal operations.

Plain WLS	EKF w/o ADDI	EKF w/ ADDI
25.3 ms	10.7 ms	13.7 ms

By conducting a number of test cases of anomalies, Table 5.8 shows the average processing times for the proposed algorithm in order to assess the computation burden between Method 1, 2, and 3. The processing time starts from the moment of receiving the PMU measurements, applying countermeasures, until the moment that the sample is finished (see the flowchart in Figure 2.5).

While the system is under sudden change, all methods execute the WLS filtering as the countermeasure, so it can be seen that the 24.1 and 27.0 ms are not much different from the plain WLS at 25.3 ms in Table 5.7. However, Method 3 consumes a bit longer time than Method 1 and 2, possibly because Method 3 has to compute both innovation and residual analysis, but Method 2 needs to compute only innovation analysis to recognize the anomaly.

In case the system is under bad data, Method 1 and 2 are about two times faster because the pre-estimation scheme can recognize the anomaly before the filtering (estimating) process. The one-iteration EKF filtering is executed after rejecting the bad data to obtain the estimated states. In contrast, Method 3 has to perform the WLS filtering first to recognize the anomaly, and the WLS consumes up to four iterations. After rejecting bad data, the EKF filtering is performed to obtain the final estimation.

Since Method 3 requires too much time for both types of anomalies, it is suggested to adopt the pre-estimation schemes either Method 1 or 2 due to the fast processing time. It should be highlighted as a significant contribution that the countermeasures for bad data can be performed in time (18.5 ms) before receiving a new measurement every 20 ms, using the EKF-FASE coupled with the ADDI module, based on the pre-estimation schemes. This study decided to adopt Method 2 over Method 1 for the main ADDI algorithm because of the good detection of some small bad data magnitudes, as shown from the results of Subsection 5.2.3.

Table 5.8: Average computational time for the proposed algorithm under the presence of anomaly.

Type of anomaly	EKF w/ ADDI	
	Method 1 and 2	Method 3
Sudden load change	24.1 ms	27.0 ms
Bad data	18.5 ms	35.6 ms

5.3. VERIFICATION OF CAPABILITY OF THE PROPOSED STATE ESTIMATION ALGORITHM TO TRACK NEW OPERATING POINTS

This section analyzes the final results after the state filtering against a sequence of anomalies: sudden load change followed by multiple bad data. The three algorithms of DSSE will be tested and compared: the traditional WLS-SSE, the EKF-FASE without the ADDI, and the EKF-FASE with the ADDI. It will be shown that the proposed EKF-FASE estimator coupled with the ADDI module has the capabilities to do the following: (i) recognizing and countering the anomaly; (ii) filtering the states properly to track the power system operating point; (iii) identifying multiple bad data then rejecting and substituting them with reliable predictions. These capabilities accomplished the main thesis objective (Objective 5); the proposed algorithm is able to online estimate the states accurately at bus 1-6 for the Enduris MV network using the PMU measurements.

The simulation in this section was carried out in real-time for a period of 7 s by adding the sequence of anomalies into a base scenario. Here, the base scenario is the quasi-steady-state operation, which has the same ramp rate of the load variation as presented in Subsection 5.1.2. Regarding the anomalies, in the beginning, the sudden load change is simulated at time 0.6 s by tripping the wind turbine of 10.8 MW at bus 5. After that, three bad data with different magnitudes were injected simultaneously between time 4-4.5 s in the following measurements: V_{mag} at bus 5 phase C, V_{angle} at bus 3 phase B, and I_{mag} at branch 4-5(1) phase C. The magnitudes of the three bad data in terms of standard deviations are 20σ, 50σ, and 60σ, respectively. The experimental results of this section are divided into two subsections as follows.

5.3.1. ANALYSIS OF PERFORMANCE INDEX J_k

Figure 5.16 compares the performance indices J_k between the three algorithms in order to analyze their filtering capabilities. Figure 5.17 shows the anomaly alarm status to show that the ADDI algorithm can classify the simulated anomalies.

At time 0.6 s and a short period after, it can be seen that the EKF coupled with ADDI estimators have identical values of J_k for every measurement to the plain WLS's. This is because the ADDI module recognized the sudden change at time 0.6 s, and the estimator switched from the EKF into the WLS filtering as the countermeasure, which became the same algorithm as the plain WLS. As shown in Figure 5.17, it is essential to notice that the alarm is still active for a short period after the moment of the actual sudden change at time 0.6 s in the power system. The reason behind this is that the LNI value was still higher than the threshold (see examples in Figure 5.18) because the process model of the EKF-FASE cannot track the system state immediately; therefore, the LNI test still triggered the ADDI algorithm for a certain time. Consequently, the WLS filtering continued to be executed until the LNI value became lower than the threshold ($\gamma_a = 4.5$) after time 1 s. After the normal operation alarm was triggered after time 1 s, the estimation algorithm switched back to the EKF filtering and again utilized the predicted states from the process model.

For the same time period from 0.6 s to 1 s, it is apparent that the EKF without the ADDI estimator has very high indices ($J_k \gg 1$) for every measurement (see the orange figures). This infers that the estimator lost the system state trajectory. But it still came

back to track the system operating point from time 1 s onwards. Unlike having the ADDI module, it can be seen that the EKF without the ADDI is likely to exhibit a longer transient period or even lose the system state tracking forever since no proper action is taken [23].

During time 4-4.5 s, it is clear that both the plain WLS and the EKF without the ADDI have similar higher indices J_k, indicating the degraded filtering performance than the prior time. This is because the erroneous measurements were not rejected; hence, they slipped into the filtering step and biased the estimation. In contrast, the EKF coupled with the ADDI exhibited the lower indices J_k, indicating the improved performance of the state filtering that effectively reduced the noises with respect to the received noisy measurements. The ADDI module detected the anomaly using the LNI test and recognized it as bad data. The multiple bad data were correctly identified as the three suspicious measurements (see the peaks in Figure 5.19) and then replaced by the corresponding forecasting measurements. As can be seen from Figure 5.17, the bad data alarm status is active from time 4 s until 4.5 s before the bad data is no longer injected. Then the system is again under normal operations.

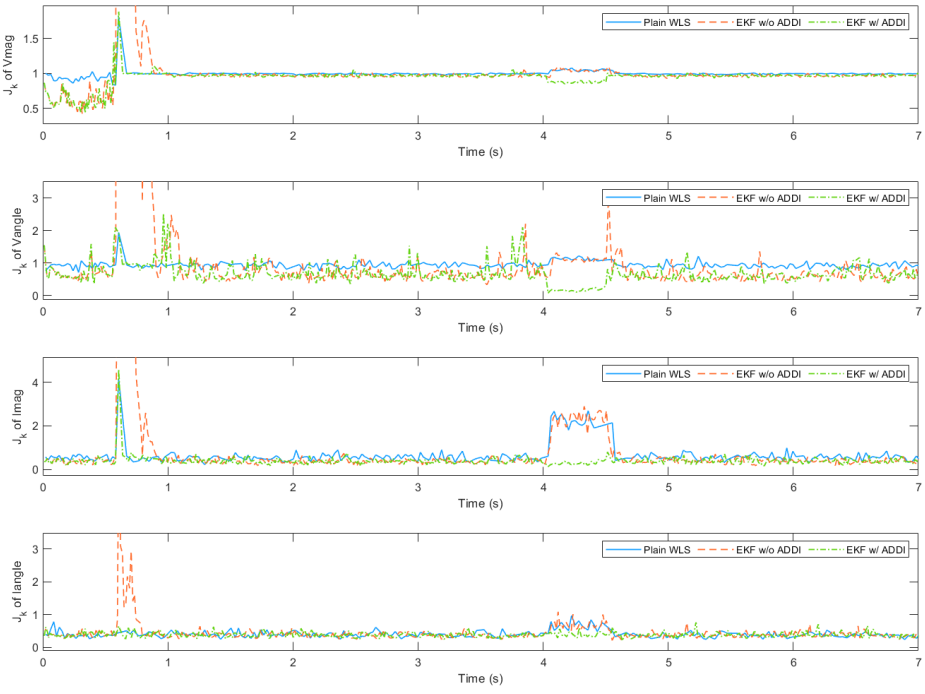

Figure 5.16: Performance indices J_k of V_{mag}, V_{angle}, I_{mag}, and I_{angle} under abnormal operating conditions.

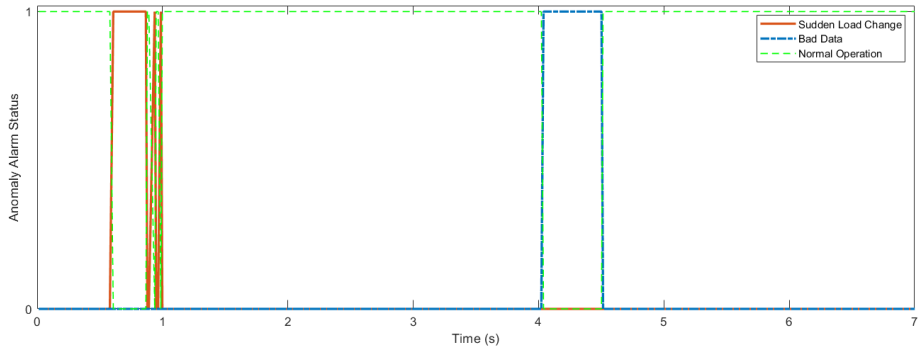

Figure 5.17: Anomaly alarm status as results of the proposed EKF-FASE estimator coupled with the ADDI module under abnormal operating conditions.

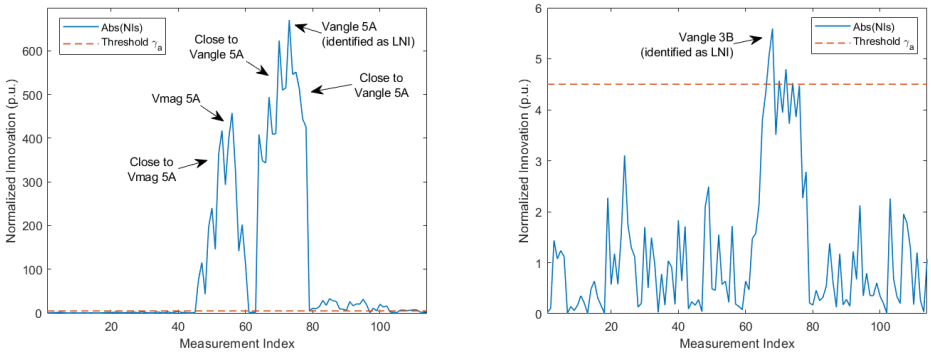

Figure 5.18: Absolute values of normalized innovations at time 0.6 s (left figure) and 1 s (right figure) when activating sudden load change alarm status.

Description: The absolute values of normalized innovations against the measurement indexes are plotted as the two snapshots: the first and the last snapshot of the sudden load change alarm status from Figure 5.17 at times 0.6 s and 1 s, respectively. The value γ_a is plotted as the dashed lines indicating the detection threshold.

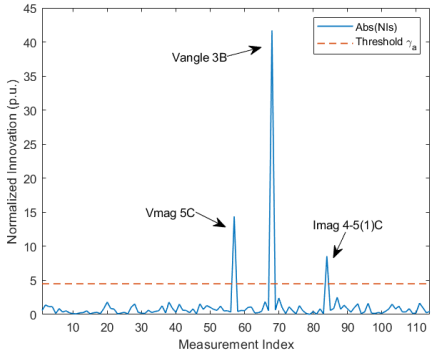

Figure 5.19: Absolute values of normalized innovations with the presence of the three bad data.

5.3.2. ANALYSIS OF PERFORMANCE INDICE MAE_k

Figure 5.20 shows the performance indices MAE_k between the three algorithms in order to prove that the proposed EKF coupled with the ADDI algorithm provides the lowest estimation error during the whole simulation time.

From time 0.6 s onwards, the EKF without the ADDI displayed very high indices MAE_k of V_{mag} and V_{angle}, indicating the loss of the system tracking for a particular period, as noted in Subsection 5.3.1. Figure 5.21 shows an example of poor predictions under sudden change; the forecasted values of V_{angle} at bus 3 phase B deviate dramatically from the actual values at around the time 0.6 s. If these unreliable predictions are taken into account in the filtering stage, the estimate will suffer from these inaccuracies. This negative impact can be seen in Figure 5.20 for the poor MAE_k values of V_{mag} and V_{angle} (orange figure) and also in Figure 5.22 for the wrong estimates of V_{angle} bus 3 phase B (orange figure). In contrast, the EKF coupled with the ADDI neglected the unreliable predictions and executed the WLS instead of the EKF filtering. Because of this countermeasure, there is no negative impact on the accuracy of the EKF estimator, resulting in good performance indices MAE_k in Figure 5.20 (green figure) and accurate estimated states in Figure 5.22 (green figure) at around the time 0.6 s against the sudden change.

Interestingly, as shown in Figure 5.20, there have been sudden growths in the indices MAE_k of V_{mag} for all algorithms since time 0.6 s. Then the indices slightly ramp up due to the gradual load variation from the quasi-steady-state operation. The possible reason behind these phenomenons is that the new system operating point had a significant difference between the new actual V_{mag} at bus 1 (the true voltage at the slack simulated from RSCAD) and the assigned constant pseudo-measurement V_{mag} at bus 1. A similar phenomenon to this case is already explained in the MAE_k results in Section 5.1.2.

Between 4-4.5 s, the EKF without the ADDI and the WLS display poor performance indices MAE_k for both V_{mag} and V_{angle} in Figure 5.20 since no action is taken to suppress the multiple bad data, as explained in the previous subsection. Figure 5.21 shows the true, predicted, and measured values of V_{angle} at bus 3 phase B to demonstrate good predictions and erroneous measurements. If the bad data is not rejected, it will get through the estimator and contaminate the filtering process, resulting in the wrong estimation, as seen in the EKF without the ADDI and the WLS in Figure 5.22 at the period 4-4.5 s. In contrast, the EKF coupled with the ADDI estimator can properly counter the multiple bad data by substituting the erroneous measurements with the corresponding forecasts to utilize the reliable predictions. This results in good performance indices MAE_k and reasonable estimates between 4-4.5 s, similar to the normal operations, as seen in Figure 5.20 (green figure) and Figure 5.22 (green figure), respectively.

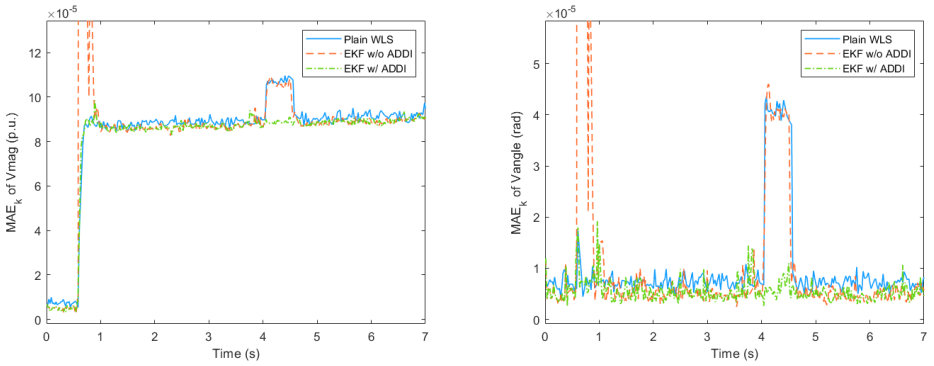

Figure 5.20: Performance indices MAE_k of V_{mag} (left figure) and V_{angle} (left figure) under abnormal operating conditions.

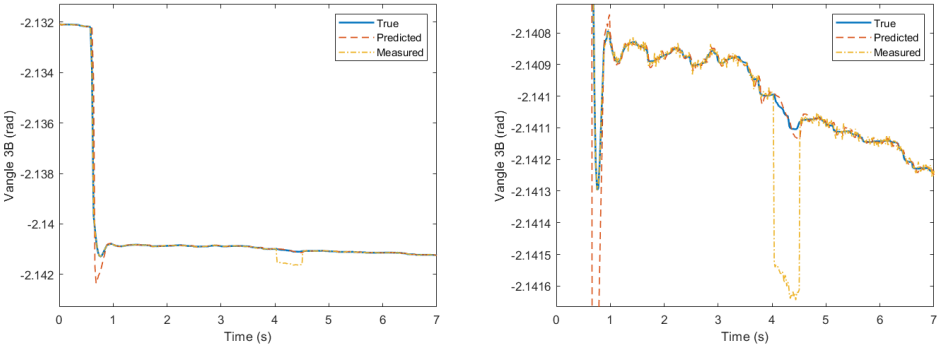

Figure 5.21: True, predicted, and measured values of V_{angle} at bus 3 phase B.
Description: The right figure focuses on a particular part of the left figure to sharpen the information.

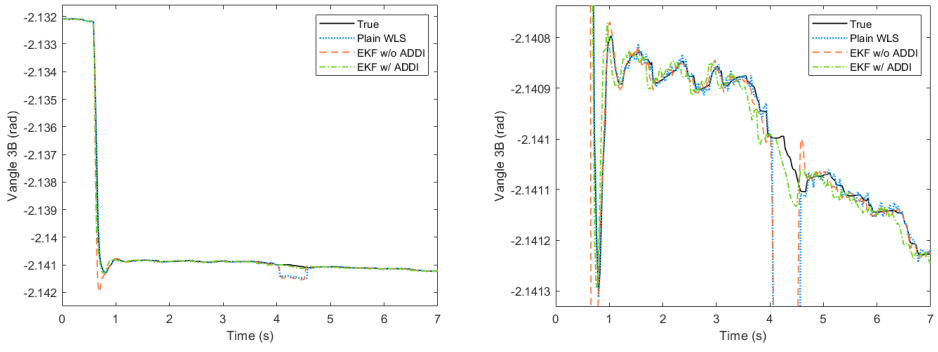

Figure 5.22: True and estimated states of V_{angle} at bus 3 phase B.
Description: The right figure focuses on a particular part of the left figure to sharpen the information.

6

CONCLUSIONS AND FUTURE WORK

6.1. CONCLUSIONS

Power systems at the distribution level are evolving, so the control and management system are needed more reliable and more accurate system monitoring on the operating conditions of the grid. In the near future, it is expected that the deployment of synchrophasor measurements will be increased in distribution grids to do fast control schemes since the modern grid topology is gradually becoming more meshed along with the high integration of distributed generation.

In this thesis, we present and analyze the implementation of DSSE algorithms on a real-life active distribution network composed of PMU devices. The measurement functions of SE are non-linear despite having the PMU measurements because some buses in the distribution network do not equip a PMU device; thus, pseudo-measurements are given to obtain full observability and for simplicity. The polar coordinates are used for both the state variables and measurements. The WLS-based SSE and EKF-based FASE estimators are studied and compared, mainly focusing on the EKF-based FASE. It is important to highlight that we experimentally validate the theoretical DSSE algorithms by fully integrating them into our real-time simulation platform to utilize real-time data from software PMUs simulated by RTDS and streamed over the internet according to IEEE Standard C37.118.2-2011. Hence, the results discussed in this thesis are from real-time state estimators using online PMU measurements.

The WLS-SSE and EKF-FASE formulations in this thesis rely on the following assumptions. First, the measurement noises are distributed in Gaussian with zero means. Second, each measurement is independent and identically distributed, so the measurement noises are uncorrelated. Third, the measurement Jacobian matrix is of full rank, so the network is observable. Fourth, the software PMUs simulated by RTDS are ideal (i.e., phasor measurements are perfectly measured), so the measurement noises are added manually in MATLAB and assumed to be very low-level noises. RTDS is used to simulate the actual Enduris MV grid in real-time and steam the PMU measurements. Meanwhile, the mathematical model of the Engurid MV grid topology as the network admittance matrix

is created in MATLAB to run SE algorithms. The model consists of three-phase series components of generic transmission lines and transformers using two-port parameters. The results of the statistical distribution of the normalized residuals from the WLS-SSE under steady-state operations confirm that the network topology model in MATLAB is reasonably matched with the actual Enduris MV grid simulated in RTDS. Objective 1 is fully accomplished at this point.

The main findings are summarized into three parts: (i) performance assessment of DSSE algorithms under normal operations, (ii) validation of the ADDI module after integrating into the EKF-FASE against anomalies, and (iii) performance assessment of DSSE algorithms under abnormal operations. Each part is explained below.

Under normal operations, i.e., steady-state and quasi-steady-state, both the WLS-FASE and EKF-FASE are successfully implemented into the real-time simulation platform. The findings show that the performance of the EKF-FASE surpasses the WLS-SSE in terms of measurement noises filtering capability and estimation accuracy. Both estimation errors are in the order of 1×10^{-6} both in p.u. and rad; thus, the difference of both estimation errors is likely insignificant. The impact of the given pseudo-measurement as a constant voltage for the slack bus is discussed. The results also point out that the average execution time for the WLS-SSE is the slowest algorithm at 25.3 ms since it needs up to four iterations to converge. In contrast, the EKF-based algorithms can converge within only one iteration. The average execution time for the basic EKF-FASE and the EKF-FASE coupled with the ADDI algorithm is 10.7 ms and 13.7 ms, respectively. This means that the ADDI module requires only 3 ms additional to scan for any anomaly and that the EKF-based algorithms are more suitable for real-time applicability. This should be highlighted as a significant contribution that the coupled EKF-FASE estimator will not miss any measurement under normal operations as the PMU streaming rate is 20 ms per sample. Objectives 2 and 3 are fully accomplished, while Objective 5 is partly accomplished at this point.

Special attention is given to the ADDI algorithm for the validation against possible disturbances in power systems and some telecommunication failures for real-life network adaptability. Three different methods of anomaly detection and discrimination (namely the conventional-, the improved-innovation analysis, and the combination of pre- and post-estimation method) are tested and compared. Then, the anomaly is identified by the traditional largest normalized innovation test. This is followed by applying countermeasures to prevent the estimation from being biased. Suppose the anomaly is characterized as a sudden change. In that case, the algorithm will switch from the EKF filtering into the WLS filtering to avoid inaccurate estimation by neglecting unreliable predictions and process only the present measurements. Otherwise, if bad data is recognized, the errors will be eliminated from the measurements by substituting them with the forecasted values and then performing the EKF filtering. By testing the ADDI module with several levels and locations of anomalies, the findings show that all three methods of anomaly detection and discrimination can correctly recognize all sudden change events and multiple bad data. Still, only the first method fails to recognize very small magnitudes of single bad data while the other methods do not. In addition, since the first and second methods are based on pre-estimation schemes that utilize innovation analysis, their average computational times are expected to be more attractive be-

cause anomalies can be processed before the estimation. In contrast, the third method should be a time-consuming algorithm because it includes the post-estimation scheme that utilizes residuals, which are obtained only after the iterative WLS filtering estimation process. As expected, the findings reveal that the average computational time interval from the moment of start receiving PMU measurements until the moment after applying countermeasures is 18.5 ms under bad data and 24.1 ms under sudden change for the pre-estimation schemes. In comparison, those for the third method are 35.6 ms and 27.0 ms, respectively. This thesis has underlined the importance of the pre-estimation scheme for the ADDI module (coupling with the EKF-FASE) that it is feasible to follow the high-speed refresh rate of PMUs at 20 ms under abnormal operations, particularly the bad data. Objective 4 is fully accomplished at this point.

Under abnormal operations, an outage of 10.8 MW wind turbine is simulated. Following this, multiple bad data is injected into the PMU measurements. The results reveal that the proposed EKF-FASE coupled with the ADDI algorithm performs well, by far better than the estimators without the ADDI module. The estimation errors are in the order of 1×10^{-5} in p.u. and 1×10^{-6} in rad during the whole simulation. These voltage magnitude and phase errors are abided by the synchrophasor standard IEEE Std C37.118-2005, allowing 1% vectorial error in phasor estimation, i.e., a maximum deviation of 1% in amplitude estimation or a maximum deviation of 1 crad (0.01 rad) for phase angle. Objective 5 is fully accomplished at this point.

In conclusion, the necessity of using the ADDI module against possible disturbances in real-life networks has been pointed out. This thesis also validates that the proposed algorithm can accurately estimate the states under both normal and abnormal operations and continuously track the new system operating point of the active distribution system in real-time.

6.2. FUTURE WORK

This study is the first step towards advanced active distribution system monitoring using Kalman filter-based SE algorithms to process online phasor measurements. Several possible directions can be developed and extended for future research. We made some suggestions that are listed in order of priority, as shown below.

- A missing point in this thesis is that there is no consistency checking between the time frame of the SE algorithm and the current time-stamped PMU data received from the data acquisition. It is suggested to develop an extra algorithm that checks the time consistency between the two and ensures that the SE algorithm will not miss any measurement, possibly by creating a buffer memory to store some data if some measurements are lost.

- Regarding the measurement uncertainty, since we assumed a very low noise level added to ideal PMU measurements from RTDS, future work can include higher measurement noises according to the class of sensors that interface the network voltage and current signals with a PMU to be more practical.

- With regard to the measurement functions, they can be improved to be linear functions by using only rectangular coordinates, i.e., measurements and states are in

the form of rectangular voltages and currents. The power injection/flow measurements also have to be converted into the current injection/flow. If the linear measurement functions are accomplished, less execution time of the SE algorithm is expected since the measurement Jacobian matrix is constant, and no need to calculate it every iteration or every time sample. Also, the estimation accuracy will increase since the linear Jacobian matrix is not an approximation anymore.

- On the issues of the ADDI module, since the considered anomalies in this study are limited to bad data and sudden load change, our pre-estimation schemes based on the innovation analysis are sufficient to distinguish between the two, as shown in the results. However, suppose more complicated anomalies like sudden topology change, incorrect topology information, or errors contained in network parameters are taken into account. In that case, only innovation analysis is not sufficient anymore; thus, the information of residuals is also needed since it represents the consistency level between the present measurements and the topology network. After that, the topology error identification method can be developed to check any inconsistencies and then fix the suspected parameters systematically to eliminate the anomaly.

- Concerning the measurement noise covariance matrix, correlation among measurements can arise when considering a larger distribution network with fewer PMU devices and more pseudo-measurements since loads can present similarity, and the weather conditions can also affect the correlation of pseudo-measurements based on their locations. Hence, including possible correlations into the measurement noise covariance matrix can significantly increase the estimation accuracy.

A

APPENDIX

A.1. PARAMETERS OF THE ENDURIS MV DISTRIBUTION GRID

The original parameters of the Enduris MV distribution grid are shown in Reference [61] using PowerFactory software. Here, this appendix section shows the modeling parameters of the grid in RSCAD software. The 150 kV transmission line and 50 kV cable parameters are shown in Table A.1 and Table A.2, respectively. The number 1 denotes the positive sequence, and the number 0 denotes the zero sequence. For example, R1 denotes the positive sequence of resistance. The transformer parameters are shown in Table A.3. Note that the three-winding transformers are simplified into two-winding transformer modeling (see the schematic in Figure 4.2), and the transformer magnetizing admittances are neglected for simplicity.

Remark: The SE topology model in MATLAB utilizes the parameters only for the 150 kV transmission lines, 50 kV cables, and 150/52.5 (HV/MV) transformers. The other MV/MV and MV/LV transformer parameters are not utilized in the SE model in MATLAB. This is because the thesis's main objective is to estimate states at only 150 kV and 50 kV substations; thus, the states at 10 kV and 0.4 kV are not considered.

Table A.1: Parameters of 150 kV Transmission Lines from RSCAD Software.

Transmission line name	R1 (Ω/km)	X1 (Ω/km)	R0 (Ω/km)	X0 (Ω/km)	C1_shunt (μF/km)	C0_shunt (μF/km)	Length (km)
Wit Gsp 150 -Wap 150w	0.0657	0.2932	0.2234	0.7727	0.0124	0.00536	7.8
Wit Wap 150w -Kng 150w	0.0657	0.2932	0.2234	0.7727	0.0124	0.00536	5.2
Wit Kng 150w -Kng 151	0.0714	0.2791	0.2393	0.7316	0.0487	0.04274	1.17

A

Table A.2: Parameters of 50 kV Cables from RSCAD Software.

Cable name	R1 (Ω/km)	X1 (Ω/km)	R0 (Ω/km)	X0 (Ω/km)	C1_shunt (μF/km)	C0_shunt (μF/km)	Length (km)
Tln-Kng	0.1508	0.1223	0.9313	0.3489	0.3464	0.3464	12.17
Otl-Tln	0.1293	0.1228	0.5446	0.2482	0.3464	0.3464	15.313
Zrz-Otl 2	0.0350	0.1590	0.2100	0.3975	0.2100	0.2100	9.804
Zrz-Otl 1	0.1153	0.1234	0.5426	0.2305	0.3464	0.3621	9.804
Gse-Zrz 1	0.1508	0.1223	0.9313	0.3489	0.3464	0.3464	19.77
Gse-Zrz 2	0.1508	0.1223	0.9313	0.3489	0.3464	0.3464	19.77
Wit Gsp-Gse	0.0967	0.3037	0.2858	0.6294	0.1945	0.1909	2.48
Zwart Gsp-Gse	0.0967	0.3037	0.2858	0.6294	0.1945	0.1909	2.48

Table A.3: Parameters of HV/MV, MV/MV, and MV/LV Transformers from RSCAD Software.

Transformer name	Rated voltage	S (MVA)	Positive sequence impedance		Zero sequence impedance	Vector group
			Short circuit voltage uk (%)	Copper losses (kW)	Short circuit voltage uk0 (%)	
151 Gsp	150/52.5	60	12.7	246.9	12.05	YNy0
152 Gsp	150/52.5	60	12.7	246.9	12.05	YNy0
153 Gsp	154.5/11.1	40	20.2	140.60	19.19	YNd11
151 Kng	150/52.5	60	12.28	172.1	11.66	Yyn0
51 Kng	52/11.1	40	20.05	158	19.17	Yd11
51 Tln	52.5/11.1	28	12.27	112.6	11.68	YNd11
51 Otl	52.5/11.1	40	20	90	18.93	YNd11
51 Zrz	52.5/11.1	27	16.5	105.5	11.28	Yd11
51 Gse	52.5/11.1	40	20	90	18.93	YNd11
Gsp-WT	10.6/0.4	4	6	4.0	3	Dyn5
Tln-WT	10.6/0.4	5.6	6	5.6	3	Dyn5
Otl-WT	10.6/0.4	5.6	6	5.6	3	Dyn5
Zrz-WT	10.6/0.4	5.6	6	5.6	3	Dyn5

REFERENCES

[1] M. Ahmad, *Power System State Estimation*. Boston : Artech House, 2013.

[2] M. E. El-Hawary, Ed., *Advances in Electric Power and Energy*. Wiley, Dec. 2020, ISBN: 9781119480402. DOI: 10.1002/9781119480402.

[3] A. Phadke and J. Thorp, *Synchronized Phasor Measurements and Their Applications*. Boston, MA: Springer US, 2008, ISBN: 978-0-387-76535-8. DOI: 10.1007/978-0-387-76537-2.

[4] S. Nuthalapati, Ed., *Power System Grid Operation Using Synchrophasor Technology*. Cham: Springer International Publishing, 2019, ISBN: 978-3-319-89377-8. DOI: 10.1007/978-3-319-89378-5.

[5] A. Monticelli, "Electric power system state estimation," *Proceedings of the IEEE*, vol. 88, no. 2, pp. 262–282, 2000. DOI: 10.1109/5.824004.

[6] J. Liu, J. Tang, F. Ponci, A. Monti, C. Muscas, and P. A. Pegoraro, "Trade-Offs in PMU Deployment for State Estimation in Active Distribution Grids," *IEEE Transactions on Smart Grid*, vol. 3, no. 2, pp. 915–924, 2012. DOI: 10.1109/TSG.2012.2191578.

[7] F. Milano, Ed., *Advances in Power System Modelling, Control and Stability Analysis*. Institution of Engineering and Technology, 2016.

[8] Z. Huang, K. Schneider, and J. Nieplocha, "Feasibility studies of applying Kalman Filter techniques to power system dynamic state estimation," in *2007 International Power Engineering Conference (IPEC 2007)*, 2007, pp. 376–382.

[9] V. Terzija, "Unscented Kalman filter for power system dynamic state estimation," English, *IET Generation, Transmission & Distribution*, vol. 5, no. 1, pp. 29–37, Jan. 2011, ISSN: 1751-8687. [Online]. Available: https://digital-library.theiet.org/content/journals/10.1049/iet-gtd.2010.0210.

[10] L. Zanni, "Power-System State Estimation based on PMUs Static and Dynamic Approaches - from Theory to Real Implementation," p. 189, 2017. DOI: 10.5075/epfl-thesis-7665. [Online]. Available: http://infoscience.epfl.ch/record/228451.

[11] M. Brown Do Coutto Filho, J. C. de Souza, and R. Freund, "Forecasting-Aided State Estimation—Part II: Implementation," *Power Systems, IEEE Transactions on*, vol. 24, pp. 1678–1685, Sep. 2009. DOI: 10.1109/TPWRS.2009.2030297.

[12] F. C. Schweppe and J. Wildes, "Power System Static-State Estimation, Part I: Exact Model," *IEEE Transactions on Power Apparatus and Systems*, vol. PAS-89, no. 1, pp. 120–125, 1970. DOI: 10.1109/TPAS.1970.292678.

[13] F. C. Schweppe and D. B. Rom, "Power System Static-State Estimation, Part II: Approximate Model," *IEEE Transactions on Power Apparatus and Systems*, vol. PAS-89, no. 1, pp. 125–130, 1970. DOI: 10.1109/TPAS.1970.292679.

[14] F. C. Schweppe, "Power System Static-State Estimation, Part III: Implementation," *IEEE Transactions on Power Apparatus and Systems*, vol. PAS-89, no. 1, pp. 130–135, 1970. DOI: 10.1109/TPAS.1970.292680.

[15] A. Abur and A. Gomez-Exposito, *Power System State Estimation: Theory and Implementation*. Sep. 2004, vol. 24, ISBN: 0-8247-5570-7. DOI: 10.1201/9780203913673.

[16] A. Monticelli, *State estimation in electric power systems : a generalized approach*. Boston : Kluwer Academic Publishers, [1999] ©1999. [Online]. Available: https://search.library.wisc.edu/catalog/999936050502121.

[17] R. E. Kálmán, "A new approach to linear filtering and prediction problems," 1960.

[18] A. S. Debs and R. E. Larson, "A Dynamic Estimator for Tracking the State of a Power System," *IEEE Transactions on Power Apparatus and Systems*, vol. PAS-89, no. 7, pp. 1670–1678, 1970. DOI: 10.1109/TPAS.1970.292822.

[19] K. Nishiya, J. Hasegawa, and T. Koike, "Dynamic state estimation including anomaly detection and identification for power systems," *IEE Proceedings C (Generation, Transmission and Distribution)*, vol. 129, no. 5, pp. 192–198, Sep. 1982.

[20] K.-I. Nishiya, H. Takagi, J. Hasegawa, and T. Koike, "Dynamic state estimation for electric power systems—introduction of a trend factor and detection of innovation processes," *Electrical Engineering in Japan*, vol. 96, no. 5, pp. 79–87, 1976. DOI: https://doi.org/10.1002/eej.4390960511. [Online]. Available: https://onlinelibrary.wiley.com/doi/abs/10.1002/eej.4390960511.

[21] ——, "Dynamic state estimation including detection of innovation process for electric power systems," *Electrical Engineering in Japan*, vol. 98, no. 1, pp. 52–61, 1978. DOI: https://doi.org/10.1002/eej.4390980108. [Online]. Available: https://onlinelibrary.wiley.com/doi/abs/10.1002/eej.4390980108.

[22] A.M. Leite da Silva, M.B. Do Coutto Filho, and J.F. de Queiroz, "State forecasting in electric power systems," *IEE Proceedings C (Generation, Transmission and Distribution)*, vol. 130, no. 5, pp. 237–244, Sep. 1983.

[23] A. M. L. da Silva, M. B. Do Coutto Filho, and J. M. C. Cantera, "An Efficient Dynamic State Estimation Algorithm including Bad Data Processing," *IEEE Transactions on Power Systems*, vol. 2, no. 4, pp. 1050–1058, 1987. DOI: 10.1109/TPWRS.1987.4335300.

[24] M.B. Do Coutto Filho, A.M. Leite da Silva, J.M.C. Calvo Cantera, and R.A. da Silva, "Information debugging for real-time power systems monitoring," *IEE Proceedings C (Generation, Transmission and Distribution)*, vol. 136, no. 3, pp. 145–152, May 1989.

[25] M. B. Do Coutto Filho and J. C. de Souza, "Forecasting-Aided State Estimation—Part I: Panorama," *IEEE Transactions on Power Systems*, vol. 24, no. 4, pp. 1667–1677, 2009. DOI: 10.1109/TPWRS.2009.2030295.

[26] A. G. Phadke, J. S. Thorp, R. F. Nuqui, and M. Zhou, "Recent developments in state estimation with phasor measurements," in *2009 IEEE/PES Power Systems Conference and Exposition*, 2009, pp. 1–7. DOI: 10.1109/PSCE.2009.4839954.

[27] M. Rice and G. T. Heydt, "Phasor Measurement Unit Data in Power System State Estimation," Power Systems Engineering Research Center, Tech. Rep., Jan. 2005.

[28] A. Monti, F. Ponci, and C. Muscas, "Phasor measurement units and wide area monitoring systems," 2016.

[29] M. Zhou, V. A. Centeno, J. S. Thorp, and A. G. Phadke, "An Alternative for Including Phasor Measurements in State Estimators," *IEEE Transactions on Power Systems*, vol. 21, no. 4, pp. 1930–1937, 2006. DOI: 10.1109/TPWRS.2006.881112.

[30] T. Yang, H. Sun, and A. Bose, "Transition to a Two-Level Linear State Estimator—Part I: Architecture," *IEEE Transactions on Power Systems*, vol. 26, no. 1, pp. 46–53, 2011. DOI: 10.1109/TPWRS.2010.2050078.

[31] ——, "Transition to a Two-Level Linear State Estimator—Part II: Algorithm," *IEEE Transactions on Power Systems*, vol. 26, no. 1, pp. 54–62, 2011. DOI: 10.1109/TPWRS.2010.2050077.

[32] N. M. Manousakis, G. N. Korres, J. N. Aliprantis, G. P. Vavourakis, and G.-C. J. Makrinas, "A two-stage state estimator for power systems with PMU and SCADA measurements," in *2013 IEEE Grenoble Conference*, 2013, pp. 1–6. DOI: 10.1109/PTC.2013.6652238.

[33] M. Glavic and T. Van Cutsem, "Tracking network state from combined SCADA and synchronized phasor measurements," in *2013 IREP Symposium Bulk Power System Dynamics and Control - IX Optimization, Security and Control of the Emerging Power Grid*, 2013, pp. 1–10. DOI: 10.1109/IREP.2013.6629376.

[34] M. Göl and A. Abur, "A Hybrid State Estimator For Systems With Limited Number of PMUs," *IEEE Transactions on Power Systems*, vol. 30, no. 3, pp. 1511–1517, 2015. DOI: 10.1109/TPWRS.2014.2344012.

[35] G. B. Denegri, M. Invernizzi, and F. Milano, "A security oriented approach to PMU positioning for advanced monitoring of a transmission grid," in *Proceedings. International Conference on Power System Technology*, vol. 2, 2002, pp. 798–803. DOI: 10.1109/ICPST.2002.1047509.

[36] A. G. Phadke, J. S. Thorp, and K. J. Karimi, "State Estimlatjon with Phasor Measurements," *IEEE Transactions on Power Systems*, vol. 1, no. 1, pp. 233–238, 1986. DOI: 10.1109/TPWRS.1986.4334878.

[37] A. Abur, "Impact of phasor measurements on state estimation," in *2009 International Conference on Electrical and Electronics Engineering - ELECO 2009*, 2009, pp. I-3-I–7. DOI: 10.1109/ELECO.2009.5355207.

[38] M. Pau, P. A. Pegoraro, and S. Sulis, "Efficient Branch-Current-Based Distribution System State Estimation Including Synchronized Measurements," *IEEE Transactions on Instrumentation and Measurement*, vol. 62, no. 9, pp. 2419–2429, 2013. DOI: 10.1109/TIM.2013.2272397.

[39] M. U. Usman and M. O. Faruque, "Validation of a PMU based fault location identification method for smart distribution network with photovoltaics using real-time data," *IET Generation, Transmission & Distribution*, vol. 12, Oct. 2018. DOI: 10.1049/iet-gtd.2018.6245.

[40] D. Della Giustina, M. Pau, P. A. Pegoraro, F. Ponci, and S. Sulis, "Electrical distribution system state estimation: measurement issues and challenges," *IEEE Instrumentation Measurement Magazine*, vol. 17, no. 6, pp. 36–42, 2014. DOI: 10.1109/MIM.2014.6968929.

[41] G. Svenda, V. C. Strezoski, and S. Kanjuh, "Real-life distribution state estimation integrated in the distribution management system," *International Transactions on Electrical Energy Systems*, vol. 27, 2017.

[42] M. Bazrafshan and N. Gatsis, "Comprehensive Modeling of Three-Phase Distribution Systems via the Bus Admittance Matrix," *IEEE Transactions on Power Systems*, vol. 33, no. 2, pp. 2015–2029, 2018. DOI: 10.1109/TPWRS.2017.2728618.

[43] P. Xiao, D. C. Yu, and W. Yan, "A unified three-phase transformer model for distribution load flow calculations," *IEEE Transactions on Power Systems*, vol. 21, pp. 153–159, 2006.

[44] "IEEE Standard for Synchrophasor Data Transfer for Power Systems," *IEEE Std C37.118.2-2011 (Revision of IEEE Std C37.118-2005)*, pp. 1–53, 2011. DOI: 10.1109/IEEESTD.2011.6111222.

[45] A. J. Wood, Bruce F. Wollenberg, and Gerald B. Sheblé, *Power generation, operation, and control*. Hoboken, New Jersey: Wiley-Interscience, 2014.

[46] J. Zhao, A. K. Singh, A. S. Mir, A. Taha, A. Abur, A. Gomez-Exposito, A. P. Meliopoulos, B. C. Pal, I. Kamwa, J. Qi, L. Mili, M. A. Mohd Ariff, M. Netto, M. Glavic, S. Yu, S. Wang, T. Bi, T. Van Cutsem, V. Terzija, and Z. Huang, "Power system dynamic state and parameter estimation-transition to power electronics-dominated clean energy systems: IEEE task force on power system dynamic state and parameter estimation," Oct. 2021.

[47] J. Zhao and L. Mili, "A Robust Generalized-Maximum Likelihood Unscented Kalman Filter for Power System Dynamic State Estimation," *IEEE Journal of Selected Topics in Signal Processing*, vol. 12, no. 4, pp. 578–592, 2018. DOI: 10.1109/JSTSP.2018.2827261.

[48] D. Ćetenović, A. Ranković, J. Zhao, Z. Jin, J. Wu, and V. Terzija, "An adaptive method for tuning process noise covariance matrix in EKF-based three-phase distribution system state estimation," *International Journal of Electrical Power & Energy Systems*, vol. 132, p. 107 192, 2021, ISSN: 0142-0615. DOI: https://doi.org/10.1016/j.ijepes.2021.107192. [Online]. Available: https://www.sciencedirect.com/science/article/pii/S0142061521004312.

[49] S. Akhlaghi, N. Zhou, and Z. Huang, "Adaptive adjustment of noise covariance in Kalman filter for dynamic state estimation," in *2017 IEEE Power Energy Society General Meeting*, 2017, pp. 1–5. DOI: 10.1109/PESGM.2017.8273755.

[50] J. Zhang, G. Welch, G. Bishop, and Z. Huang, "A Two-Stage Kalman Filter Approach for Robust and Real-Time Power System State Estimation," *IEEE Transactions on Sustainable Energy*, vol. 5, pp. 629–636, 2014.

[51] L. Zanni, J.-Y. Le Boudec, R. Cherkaoui, and M. Paolone, "A Prediction-Error Covariance Estimator for Adaptive Kalman Filtering in Step-Varying Processes: Application to Power-System State Estimation," *IEEE Transactions on Control Systems Technology*, vol. 25, no. 5, pp. 1683–1697, 2017. DOI: 10.1109/TCST.2016.2628716.

[52] W. H. Kersting, *Distribution System Modeling and Analysis*. CRC Press, Aug. 2001, ISBN: 9780429125904. DOI: 10.1201/9781420041736.

[53] A. Ranković, B. M. Maksimović, and A. T. Sarić, "A three-phase state estimation in active distribution networks," *International Journal of Electrical Power & Energy Systems*, vol. 54, pp. 154–162, 2014, ISSN: 0142-0615. DOI: https://doi.org/10.1016/j.ijepes.2013.07.001. [Online]. Available: https://www.sciencedirect.com/science/article/pii/S0142061513002986.

[54] Shahid Jaman, "Implementation of Forecasting-Aided State Estimation," Ph.D. dissertation, Universidad de Oviedo, Sep. 2017.

[55] Z. Jin, S. Chakrabarti, J. Yu, L. Ding, and V. Terzija, "An improved algorithm for cubature Kalman filter based forecasting-aided state estimation and anomaly detection," *International Transactions on Electrical Energy Systems*, vol. 31, no. 5, e12714, 2021. DOI: https://doi.org/10.1002/2050-7038.12714. [Online]. Available: https://onlinelibrary.wiley.com/doi/abs/10.1002/2050-7038.12714.

[56] D. M. Falcao, P. A. Cooke, and A. Brameller, "Power System Tracking State Estimation and Bad Data Processing," *IEEE Transactions on Power Apparatus and Systems*, vol. PAS-101, no. 2, pp. 325–333, 1982. DOI: 10.1109/TPAS.1982.317110.

[57] S. J. Geetha, A. Meghwani, S. Chakrabarti, K. Rajawat, and V. Terzija, "Spoofing attack on synchrophasor GPS clock: Impact and detection in power system state estimation," *International Journal of Electrical Power & Energy Systems*, vol. 134, p. 107 396, 2022, ISSN: 0142-0615. DOI: https://doi.org/10.1016/j.ijepes.2021.107396. [Online]. Available: https://www.sciencedirect.com/science/article/pii/S0142061521006359.

[58] D. S. Ouellette, M. D. Desjardine, and R. Kuffel, "Using a real time digital simulator with phasor measurement unit technology," in *11th IET International Conference on Developments in Power Systems Protection (DPSP 2012)*, 2012, pp. 1–6. DOI: 10.1049/cp.2012.0034.

[59] "IEEE Standard for a Precision Clock Synchronization Protocol for Networked Measurement and Control Systems," *IEEE Std 1588-2008 (Revision of IEEE Std 1588-2002)*, pp. 1–269, 2008. DOI: 10.1109/IEEESTD.2008.4579760.

[60] M. Naglic, M. Popov, M. A. M. M. van der Meijden, and V. Terzija, "Synchro-Measurement Application Development Framework: An IEEE Standard C37.118.2-2011 Supported MATLAB Library," *IEEE Transactions on Instrumentation and Measurement*, vol. 67, no. 8, pp. 1804–1814, 2018. DOI: 10.1109/TIM.2018.2807000.

[61] N. Save, *Phasor Measurement Unit (PMU) based power system analysis of MV distribution grid*. Delft, Sep. 2016.

[62] N. D. Hatziargyriou, Ed., *Microgrids : architectures and control*. Wiley-IEEE Press, 2014.

[63] I. Cobelo, A. Shafiu, N. Jenkins, and G. Strbac, "State estimation of networks with distributed generation," *European Transactions on Electrical Power*, vol. 17, pp. 21–36, 2007.

[64] "IEEE Standard for Synchrophasors for Power Systems," *IEEE Std C37.118-2005 (Revision of IEEE Std 1344-1995)*, pp. 1–65, 2006. DOI: 10.1109/IEEESTD.2006.99376.

[65] M. Pau, P. A. Pegoraro, and S. Sulis, "Efficient Branch-Current-Based Distribution System State Estimation Including Synchronized Measurements," *Instrumentation and Measurement, IEEE Transactions on*, vol. 62, pp. 2419–2429, Oct. 2013. DOI: 10.1109/TIM.2013.2272397.

[66] M. Huang, Z. Wei, J. Zhao, R. A. Jabr, M. Pau, and G. Sun, "Robust Ensemble Kalman Filter for Medium-Voltage Distribution System State Estimation," *IEEE Transactions on Instrumentation and Measurement*, vol. 69, no. 7, pp. 4114–4124, 2020. DOI: 10.1109/TIM.2019.2945743.

[67] X. Kong, Y. Chen, C. Yong, X. Ma, and J. Kong, "Stepwise robust distribution system state estimation considering PMU measurement," *Journal of Renewable and Sustainable Energy*, vol. 11, no. 2, Mar. 2019, ISSN: 1941-7012. DOI: 10.1063/1.5064532.

[68] A. Dubey, S. Chakrabarti, and V. Terzija, "SCADA and PMU Measurement Based Methods for Robust Hybrid State Estimation," *Electric Power Components and Systems*, vol. 47, no. 9-10, Jun. 2019, ISSN: 1532-5008. DOI: 10.1080/15325008.2019.1627606.

[69] D. H. Foster, *A Concise Guide to Communication in Science and Engineering*, English. United Kingdom: Oxford University Press, Nov. 2017, ISBN: 9780198704249.

[70] *MATLAB version 9.8.0.1359463 (R2020a) Update 1*, Natick, Massachusetts, 2020.